NASA TECHNICAL NOTE

NASA TN D-7851

NASA TN D-7851

LOW-SPEED AERODYNAMIC CHARACTERISTICS OF A LIFTING-BODY HYPERSONIC RESEARCH AIRCRAFT CONFIGURATION

Jim A. Penland and Theodore R. Creel, Jr.

Langley Research Center
Hampton, Va. 23665

NATIONAL AERONAUTICS AND SPACE ADMINISTRATION • WASHINGTON, D. C. • FEBRUARY 1975

1. Report No.	2. Government Accession No.	3. Recipient's Catalog No.
NASA TN D-7851		

4. Title and Subtitle	5. Report Date
LOW-SPEED AERODYNAMIC CHARACTERISTICS OF A LIFTING-BODY HYPERSONIC RESEARCH AIRCRAFT CONFIGURATION	February 1975
	6. Performing Organization Code
7. Author(s)	8. Performing Organization Report No.
Jim A. Penland and Theodore R. Creel, Jr.	L-9811
	10. Work Unit No.
9. Performing Organization Name and Address	505-11-31-02
NASA Langley Research Center Hampton, Va. 23665	11. Contract or Grant No.
	13. Type of Report and Period Covered
12. Sponsoring Agency Name and Address	Technical Note
National Aeronautics and Space Administration Washington, D.C. 20546	14. Sponsoring Agency Code

15. Supplementary Notes

16. Abstract

An experimental investigation of the low-speed longitudinal, lateral, and directional stability characteristics of a lifting-body hypersonic research airplane concept was conducted in a low-speed tunnel with a 12-foot (3.66-meter) octagonal test section at the Langley Research Center. The model was tested with two sets of horizontal and vertical tip controls having different planform areas, a center vertical tail and two sets of canard controls having trapezoidal and delta planforms, and retracted and deployed engine modules and canopy. This investigation was conducted at a dynamic pressure of 239.4 Pa (5 psf) (Mach number of 0.06) and a Reynolds number of 2×10^6 based on the fuselage length. The tests were conducted through an angle-of-attack range of 0° to 30° and through horizontal-tail deflections of 10° to -30°.

The complete configuration exhibited excessive positive static longitudinal stability about the design center-of-gravity location. However, the configuration was unstable laterally at low angles of attack and unstable directionally throughout the angle-of-attack range. Longitudinal control was insufficient to trim at usable angles of attack. Experiments showed that a rearward shift of the center of gravity and the use of a center-located vertical tail would result in a stable and controllable vehicle.

17. Key Words (Suggested by Author(s))	18. Distribution Statement
Hypersonic aircraft Low-speed stability and control Lifting body Aerodynamics	Unclassified – Unlimited STAR Category 02

19. Security Classif. (of this report)	20. Security Classif. (of this page)	21. No. of Pages	22. Price*
Unclassified	Unclassified	69	$4.25

*For sale by the National Technical Information Service, Springfield, Virginia 22151

LOW-SPEED AERODYNAMIC CHARACTERISTICS OF A LIFTING-BODY HYPERSONIC RESEARCH AIRCRAFT CONFIGURATION

By Jim A. Penland and Theodore R. Creel, Jr.
Langley Research Center

SUMMARY

An experimental investigation of the low-speed longitudinal, lateral, and directional stability characteristics of a lifting-body hypersonic research airplane concept was conducted in a low-speed tunnel with a 12-foot (3.66-meter) octagonal test section at the Langley Research Center. The model was tested with two sets of horizontal and vertical tip controls having different planform areas, a center vertical tail and two sets of canard controls having trapezoidal and delta planforms, and retracted and deployed engine modules and canopy. This investigation was conducted at a dynamic pressure of 239.4 Pa (5 psf) (Mach number of 0.06) and a Reynolds number of 2×10^6 based on the fuselage length. The tests were conducted through an angle-of-attack range of 0° to 30° and through horizontal-tail deflections of 10° to -30°.

The complete configuration exhibited excessive positive static longitudinal stability about the design center-of-gravity location. However, the configuration was unstable laterally at low angles of attack and unstable directionally throughout the angle-of-attack range. Longitudinal control was insufficient to trim at usable angles of attack. Experiments showed that a rearward shift of the center of gravity and the use of a center-located vertical tail would result in a stable and controllable vehicle.

INTRODUCTION

Under a National Aeronautics and Space Administration contract (refs. 1 to 4), McDonnell Aircraft Company identified the required research for future hypersonic cruise aircraft, evaluated the research potential, and assessed the usefulness of several new candidate research facilities. This Hypersonic Research Facilities (HYFAC) study concluded that major advances must be made in the technological state of the art before air-breathing hypersonic aircraft employing advanced propulsion and fuel systems could be considered either feasible or practical. Recommendations were made that both ground facilities and flight vehicles be utilized in order to improve the state of the art aerodynamically, structurally, and propulsively.

One recommended flight research aircraft, a model of which is shown in figures 1 and 2, was a manned Mach 12, air-launched, rocket-boosted, all-body aerothermodynamic configuration that would operate in the true high-temperature environment. After boost, this test aircraft would cruise at a constant Mach number for up to 5 minutes, and record data throughout the flight mission. The aircraft would then decelerate to a dead-stick landing as has been customary for previous research aircraft. Reference 5 reported the aerodynamic characteristics of this all-body hypersonic research aircraft configuration at Mach 6. References 6 and 7 documented the aerodynamic characteristics of similar configurations at low speeds.

Because the proposed research aircraft will be flown to a powerless landing, the low-speed aerodynamic characteristics must be known. The purpose of this report is to document the aerodynamic characteristics of a lifting-body hypersonic research airplane at a dynamic pressure of 239.4 Pa (5 psf) (Mach number of 0.06) and a Reynolds number of 2×10^6 based on the fuselage length.

COEFFICIENTS AND SYMBOLS

The results of the tests are presented as standard coefficients of forces and moments. The longitudinal data are referred to the stability-axis system; the lateral-directional data are referred to the body-axis system. The axis systems are illustrated in figure 3, and the design center of gravity, located at 63.6 percent body length, was used as the moment reference. Values are given in both SI and U.S. Customary Units. The measurements and calculations were made in U.S. Customary Units.

A_r reference area, planform area including small horizontal tails, 0.325 m^2 (504.18 in^2)

b wing span, including small horizontal tails, 0.602 m (23.72 in.)

C_D drag coefficient, $\frac{F'_D}{q_\infty A_r}$

$C_{D,o}$ drag coefficient at $C_L = 0$

C_L lift coefficient, $\frac{F_L}{q_\infty A_r}$

C_{L_α} rate of change of lift coefficient with angle of attack per deg, $\alpha = 0^o$

C_l rolling-moment coefficient, $\frac{M_X}{q_\infty A_r b}$

C_{l_β} rate of change of rolling-moment coefficient with angle of sideslip per deg

C_m pitching-moment coefficient, $\frac{M_Y}{q_\infty A_r l}$

C_{m_α} rate of change of pitching-moment coefficient with angle of attack per deg, $\alpha = 0^o$

$C_{m,o}$ pitching-moment coefficient at $\alpha = 0^o$

$\frac{\partial C_m}{\partial C_L}$ rate of change of pitching-moment coefficient with lift coefficient, longitudinal stability

C_n yawing-moment coefficient, $\frac{M_Z}{q_\infty A_r b}$

C_{n_β} rate of change of yawing-moment coefficient with angle of sideslip per deg

C_Y side-force coefficient, $\frac{F_Y}{q_\infty A_r}$

C_{Y_β} rate of change of side-force coefficient with angle of sideslip per deg

c wing chord

$c_{r,exp}$ exposed root chord

F_A axial force along X-axis; positive direction, -X

$F'_D = F_N \sin \alpha + F_A \cos \alpha$

$F_L = F_N \cos \alpha - F_A \sin \alpha$

F_N normal force along Z-axis; positive direction, -Z

F_Y side force along Y-axis; positive direction, +Y

L/D lift-drag ratio, $\frac{C_L}{C_D}$

l reference length (length of sharp nosed body), 1.528 m (60.15 in.)

M Mach number

M_X, M_Y, M_Z moments about X-, Y-, and Z-axes

q_∞ free-stream dynamic pressure

X, Y, Z reference axes

x distance, theoretical nose to body station

z distance vertical from horizontal center line

α angle of attack, deg

β angle of sideslip, deg

δ angle of control deflection, positive deflection when trailing edge is down, deg

Subscripts:

C both canards deflected

H both elevons deflected

s stability-axis system

t trim condition, $C_m = 0$

Model nomenclature:

B body or fuselage

C_1 small trapezoidal canards

C_2 small delta-planform canards

C_3 large trapezoidal canards

C_4 large delta-planform canards

C_P deployed canopy

E_o open flow-through engine

E_R retracted engine

H_1 small horizontal tails

H_2 large horizontal tails

V_1 small twin vertical tails

V_2 large twin vertical tails

V_3 center vertical tail

MODELS

A photograph of the 0.062-scale model installed in the Langley 12-foot low-speed tunnel is shown in figure 1. Detailed geometric characteristics of the models and the various components are shown in figure 2 and tabulated in table I. Three types of detachable vertical tails were utilized: small and large twin vertical tails (fig. 2(c)); and a center vertical tail, positioned on the top aft section of the fuselage (fig. 2(b)). Two types of horizontal tails were utilized, small and large, and are shown in figure 2(c). The scramjet engine was represented in the retracted and open positions, the latter configuration having a constant-area duct. The canopy was designed to retract into the fuselage nose with the canopy top faired in with normal fuselage contours. In the present tests the canopy was either in place or removed in order to simulate the deployed and retracted conditions, respectively.

Small and large trapezoidal and delta-planform canards, having planform areas of 2 percent and 4 percent of the reference area, were tested and were mounted as shown in figure 2(b). The small canard controls were tested at deflection angles of 0° to 15°.

It should be noted that the data presented herein for the body alone were measured on the body shown in figure 2(a) (dashed lines in the aft cross-sectional views without horizontal and vertical tails or fillets). The model was constructed of wood and fiberglass with the various removable components screwed in place and located by dowels.

APPARATUS AND TESTS

The tests were conducted in the Langley 12-foot low-speed tunnel at a Reynolds number of 2×10^6 based on the body length and a dynamic pressure of 239.4 Pa (5 psf)

(M = 0.06). A six-component strain-gage balance was installed inside the model fuselage and attached to the tunnel sting-support system. The force and moment data were measured through an angle-of-attack range of 0° to 30° and at angles of sideslip of 0°, 5°, and 10°. All joints and hinge-line cracks were sealed with plastic tape prior to each test run. Brief tests with and without fixed transition indicated no parameter variations other than a fractional percent decrease in drag. Therefore, the tests were made without fixed transition. No base-pressure corrections were made. Moments were calculated about a center of gravity located on the vehicle center line at the $x/l = 0.636$ body station measured from the theoretical sharp nose.

Because of the very low test Reynolds number of this investigation and the relatively high turbulence factor of the tunnel flow, it is not recommended that the drag data be extrapolated to flight Reynolds numbers. Lift-curve slopes, moments, and drag increments caused by component variations, however, are considered to be valid.

RESULTS AND DISCUSSION

Static Longitudinal Characteristics

Configuration buildup.- The static longitudinal characteristics of the basic body alone and the variations effected by the addition of vertical and horizontal tails, engine modules, and cockpit are presented in figure 4 through the test range of angles of attack from 0° to 30°. The body alone (B) and the models with the body and small twin vertical tails (BV_1) exhibit nonlinear lift curves throughout the test range (fig. 4(a)) as compared with the models having horizontal tails $(H_1$ or $H_2)$, engine modules $(E_O$ or $E_R)$, and deployed canopy (C_P). These models having horizontal tails, engine modules, and deployed canopy not only have greater lift but also have linear lift curves up to the region of probable flow separation on the horizontal tails at an angle of attack of about 20°. Conversely, the B and BV_1 models have more linear pitching-moment and stability curves (figs. 4(d) and 4(e)) than do the models with the added components; the models with the added components not only show a higher degree of stability up to $\alpha \approx 20^{\circ}$ but also have a slight pitch-up tendency. The addition of E_O, E_R, or C_P to the BH_1V_1 model shifted the angle of attack for $C_L = 0$ and for $C_m = 0$ but had no significant effect on the slopes C_{L_α}, C_{m_α}, and $\partial C_m/\partial C_L$. The exchange of H_2V_2 for H_1V_1 resulted in a marked improvement in the aforementioned stability derivatives approximately proportional to the planform areas involved. This improvement with the use of H_2V_2 was about 1.5 times the gain resulting from the use of H_1V_1 on model B, that is, the ratio of the areas of H_2V_2 to H_1V_1. With the exception of the $BH_1V_1E_RC_P$ test, the drag and lift-drag ratio results of the configuration buildup were as expected: an improvement in L/D with the addition of H_1 and a decrease with the addition of E_O, E_R, and/or C_P.

Drag due to lift.- The drag due to lift for most of the configurations just discussed is presented in figure 5. Again the B and BV_1 models exhibit the most linear of the curves shown. It should be observed that although model B had the lowest $C_{D,o}$ (drag at $C_L = 0$), it also had the highest slope $\partial C_D/\partial C_L^2$ (drag-rise factor) and, therefore, the greater drag due to lift. The addition of V_1 slightly increased $C_{D,o}$ but decreased the drag-rise factor; this was possibly caused by the end-plate effects of the outboard-located vertical tails. The addition of H_1 appears to have had a negligible effect on $C_{D,o}$ but greatly decreased the drag-rise factor and had a nonlinearizing effect on the curve. The $C_{D,o}$ was significantly increased by the addition of E_R and C_P, but, at the higher values of C_L^2, the curve is generally similar to that shown for the BH_1V_1 model. The addition of the larger H_2 and V_2 again increased the $C_{D,o}$ and further decreased the drag-rise factor as expected.

Center vertical tail.- Tests using a center vertical tail were conducted primarily to compare the directional-stability characteristics with those of the twin outboard tails; these characteristics are discussed in the section entitled "Static Lateral-Directional Characteristics." However, such tests automatically produce longitudinal data. (See fig. 6.) The addition of V_3 to the basic $BH_1V_1E_RC_P$ model resulted in a decrease in C_L and L/D, an increase in C_D, a small positive increment of pitching moment, and no change in C_{m_α} or in the longitudinal stability $\partial C_m/\partial C_L$. Tests with a C_1 canard in conjunction with V_3 were made to determine whether any interference could be caused by the wake or vorticular flow impinging on the center vertical tail. The use of the small trapezoidal canards (C_1) longitudinally resulted in a small increase in C_L approximately equal to the loss incurred by the use of V_3, a further increase in drag, no change in L/D, and an additional positive increment in pitching moment with only a negligible change in C_{m_α} and $\partial C_m/\partial C_L$.

Large vertical and horizontal tails.- Figure 7 presents a partial configuration buildup utilizing available data on the large vertical and horizontal tails. The most notable effect of the addition of $V_2E_RC_P$ to the body alone (B) was the reversal of the curvature of the lift, pitch, and stability curves. (See figs. 7(a), 7(d), and 7(e).) The installation of H_2 greatly increased the lift-curve slope C_{L_α} and increased negatively the slope of the pitching-moment curve C_{m_α} in the angle-of-attack range up to about 20°. There was little change in the stability $\partial C_m/\partial C_L$ at low lift coefficients corresponding to $\alpha = 0^\circ$ to 5°, but the curve was made almost linear, a condition which extended the region of positive longitudinal stability to a lift coefficient of about 0.56, corresponding to $\alpha = 20^\circ$.

Canards.- The results of the longitudinal tests on the four canard shapes, described in the section "Models," are presented in figures 8, 9, and 10. Figure 8 presents the results for the basic complete model $BH_1V_1E_RC_P$ and for this model equipped with each

of the four canards at $\delta_C = 0^o$ and $\delta_{H_1} = 0^o$. Figures 9 and 10 present results of tests of canards C_1 and C_2, respectively, with δ_{C_1} and $\delta_{C_2} = 0^o$, 5^o, 10^o, and 15^o, and $\delta_{H_1} = 0^o$.

An inspection of these results shows that all canards tested, regardless of the deflection angle, were relatively ineffective in producing lift, pitch, or an improved lift-drag ratio. The $C_{m,o}$ was increased less than 0.01 and the trim angle of attack was increased less than 4^o for the large trapezoidal canards, the most efficient subsonic design tested. This apparent lack of overall measured effectiveness is, of course, partly caused by the inherent low efficiency associated with the low Reynolds number of the tests. This apparent lack is also caused by the center-of-gravity location of the configuration which yields a longitudinal static margin of 15.6 percent body length. A rearward shift of the center of gravity of 13 percent body length would make possible trim by undeflected canards alone up to almost $C_{L,t} = 0.2$ for the small trapezoidal canard and would provide neutral stability to $C_{L,t} = 0.25$ for the small delta canard.

Longitudinal control characteristics.- The longitudinal characteristics of the complete model $BH_1V_1E_RC_P$ are presented in figure 11 for elevon deflections of 10^o to -30^o through an angle-of-attack range of 0^o to 30^o. All parameters show an orderly variation with control deflection at low angles of attack. An inspection of the lift curves shows indications of separation occurring at a local flow deflection over the controls of about 20^o; that is, $\alpha = 10^o$ plus $\delta_{H_1} = 10^o$, $\alpha = 15^o$ plus $\delta_{H_1} = 5^o$, and so forth. Figures 11(d) and 11(e) show the model to be exceedingly stable and to have insufficient elevon control power. With a $\delta_{H_1} = -30^o$ and the design center-of-gravity location at 0.636ℓ, the model could trim only to an angle of attack of 13^o corresponding to a $C_{L,t}$ of 0.125. An estimate of the trim capability with an aft-shifted center of gravity was made by rotating the axes in figure 11(e); the rotations are shown as heavy dashed lines. By moving the center of gravity aft about 7.4 percent body length to the 0.71ℓ body station, the -30^o elevon deflection trims the model to $\alpha = 30^o$ at a $C_{L,t}$ of 0.47 and still retains a degree of longitudinal stability. Such a move of the center of gravity, while appearing to solve the longitudinal trim problem, further aggravates a directional-stability deficiency.

The effects of increasing the horizontal-tail area by 100 percent and the vertical-tail area by 50 percent on the longitudinal control capabilities are shown in figure 12 for model $BH_2V_2E_RC_P$. This increase in control area markedly increased the lift-curve slope, the drag, and the longitudinal stability, and decreased the lift-drag ratio, as compared with the small-tail model of figure 11. This increase in lift may be attributed to both the increase in model planform area and the increase in planform aspect ratio. The drag rise is primarily caused by the increased area of the 5^o toed-in vertical tails, but is also caused by the increased wetted area of the enlarged horizontal tails. The increased tail-surface area resulted in an even more stable configuration than the small-tail model

when the 0.636ℓ center-of-gravity location was used as a common reference. The trim capability was identical with that of the model equipped with the small horizontal and vertical tails; again the model could only trim to $\alpha = 13^{\circ}$ and a $C_{L,t}$ of 0.125. In this instance the required rearward shift of the center of gravity was about 9.4 percent body length to a new center of gravity at 0.73ℓ, to trim with $\delta_{H_1} = -30^{\circ}$ (fig. 12(e)). Because of the excessively large center-of-gravity shifts required for a reasonable trim range of the angle of attack, trim plots were considered to be unnecessary for the presentation of results and, therefore, were omitted.

Static Lateral-Directional Characteristics

The coefficients of side force, rolling-moment, and yawing moment for the basic $BH_1V_1E_RC_P$ model are presented in figure 13 with angle of attack for various fixed angles of sidelip. At $\beta = 0^{\circ}$, the magnitude of the parameters is small and thereby indicates little or no asymmetry in the model construction or in the flow angularity in the tunnel. The positive values of rolling moment at low angles of attack for both positive values of the sideslip angle provide a measure of undesirable negative dihedral effect; at higher angles of attack the model exhibits the desired negative roll with positive sideslip angle or positive dihedral effect. Yawing moments are negative throughout the angle-of-attack range for both sideslip angles. This condition results in a directionally unstable configuration, which, when coupled with the negative dihedral effect at low angles of attack, probably causes dynamic instability through that region. It should be noted that there is apparent blanketing of the downstream vertical tail by the body cross flow, as evidenced by the similarity of the yawing moments produced by the 5° and 10° sideslip angles.

Figure 14 shows the variation of the coefficients of side force, rolling moment, and yawing moment with sideslip angle at $\alpha = 0^{\circ}$ for the basic model $BH_1V_1E_RC_P$. The importance of this figure is that it shows all parameters to be approximately linear with sideslip angle. It was assumed that these lateral and directional parameters were linear with sideslip angle at all angles of attack and that the slopes obtained from data on various configurations, measured at 0° and 5° sideslip angles, were valid. The results of the tests reduced in this manner are presented in figures 15 to 18 for various model configurations.

Configuration buildup.- The static lateral and directional stability characteristics are presented in figure 15 for the body alone with a systematic buildup of components to the complete basic configuration. Except at the lower angles of attack, all configurations show positive dihedral effect $-C_{\ell_\beta}$ up to $\alpha = 25^{\circ}$. All configurations are unstable directionally throughout the angle-of-attack range and this instability increases at angles above 16°. It should be noted that the addition of the vertical tails to the basic body improved the directional stability as expected, but the addition of the horizontal tails

adversely affected the conditions. The addition of the retracted engine, which was located near the center of gravity, had no effect on the directional stability, but the canopy further increased the instability.

Enlarged vertical and horizontal tail.- Figure 16 presents a comparison of the lateral-directional stability of the model with the small and large vertical tails. The installation of the enlarged horizontal and vertical tails in place of the small surfaces had a pronounced and desirable effect on the stability characteristics. The low angle-of-attack, negative dihedral-effect region was reduced to neutral and the configuration was now directionally stable up to $\alpha = 20^{\circ}$. The model without the horizontal tails was directionally stable to $\alpha = 25^{\circ}$, but with their addition the model became unstable at $\alpha = 20^{\circ}$, the instability probably caused by a blanketing of the vertical-tail surfaces.

Center vertical tail.- Figure 17 presents a comparison of the lateral-directional stability of the basic configuration with and without the center vertical tail and with the small trapezoidal canards. The addition of the center vertical tail to the basic model greatly improved both the lateral and directional stability. The model exhibits positive dihedral effect throughout the angle-of-attack range and positive directional stability up to an angle of attack of about 23°. The addition of the small trapezoidal canards had only minor effects on the center vertical configuration.

Canards.- The effects on the lateral-directional stability of the addition of the small trapezoidal and delta canards to the basic complete configuration are presented in figure 18. These data indicate that the lateral stability was improved through the middle angle-of-attack range by the more negative values of C_{l_β}; the directional stability was improved at high angles of attack by the more positive values of C_{n_β} with the addition of the canards. This increase in directional stability accompanied by an increased negative side force was probably caused by local separation in the vicinity of the canards at the higher angles of attack or, possibly, by the vortiginous wake of the canards impinging on the aft section of the model.

Discussion of Summary Figures

As an aid to this discussion, figures 19 and 20 have been included to show graphically the change in the location of the longitudinal aerodynamic center and the directional aerodynamic center, respectively, in terms of model length for various configuration modifications. Figure 19 shows that the body alone has a favorable aerodynamic-center location and that the addition of vertical tails and horizontal tails moves the aerodynamic center further rearward. The aerodynamic center is moved to such an extent that the model is exceptionally stable, having a static margin of about 15.6 percent for the small tail model and 19 percent for the large tail model. This high degree of stability resulted in a longitudinally stiff configuration that was impossible to trim to any usable angle of

attack with the design center-of-gravity location of $0.636l$ as was discussed in the previous section.

Figure 20 shows that the directional-stability characteristics of the configurations are diametrically dissimilar to the longitudinal-stability characteristics discussed previously. The body alone is unstable and the addition of either the small vertical tails, horizontal tails, or retracted engine contributes positively by shifting the aerodynamic center rearward but not sufficiently to move the aerodynamic center behind the design center of gravity and produce a directionally stable configuration. The canopy has an adverse effect. Only by the addition of the enlarged vertical and horizontal tails or by the addition of the center vertical tail was there success in making the model statically and directionally stable. The center vertical tail is by far the more efficient stabilizing surface and has shifted the directional aerodynamic center rearward to $0.795l$, which is very close to the location of the longitudinal aerodynamic center that resulted from the addition of the small horizontal tails (fig. 19). Thus, if the center of gravity were moved rearward to the $0.71l$ body station, as suggested in the section of this paper entitled "Longitudinal control characteristics," and a center tail were installed, the configuration would possess both longitudinal and directional stability and would be longitudinally controllable to $\alpha = 30^{\circ}$. The practicality of such a large shift in the center of gravity would require a serious design study, but the addition of the rearward located center vertical tail and the required rearward movement of the main landing gear would certainly contribute to this design change.

CONCLUDING REMARKS

An experimental investigation of the low-speed longitudinal, lateral, and directional stability characteristics of a lifting-body hypersonic research airplane concept was conducted at a Reynolds number based on fuselage length of 2×10^6. The configuration was found to be longitudinally stable without controls and, with the addition of horizontal controls, to be excessively stable; this stability resulted in a longitudinally stiff vehicle that was impossible to trim to any usable angle of attack with the design center of gravity location. Conversely, the configuration was directionally unstable with and without the design vertical controls and required an additional 50-percent vertical-tail area in the form of enlarged tip fins or a center vertical tail for positive static directional stability. Therefore, both a rearward shift in design center of gravity for longitudinal control and an increase in vertical-tail size for directional stability are required for an aerodynamically viable vehicle.

Langley Research Center,
National Aeronautics and Space Administration,
Hampton, Va., November 27, 1974.

REFERENCES

1. Anon.: Hypersonic Research Facilities Study. Phase I – Preliminary Studies. Volume II, Part 1 – Research Requirements and Ground Facility Synthesis. NASA CR-114323, 1970.

2. Anon.: Hypersonic Research Facilities Study. Phase I – Preliminary Studies. Vol. II, Pt. 2 – Flight Vehicle Synthesis. NASA CR-114324, 1970.

3. Anon.: Hypersonic Research Facilities Study. Phase II – Parametric Studies. Vol. III, Pt. 2 – Flight Vehicle Synthesis. NASA CR-114326, 1970.

4. Anon.: Hypersonic Research Facilities Study. Phase III – Final Studies. Vol. IV, Pt. 1 – Flight Research Facilities. NASA CR-114327, 1970.

5. Clark, Louis E.: Hypersonic Aerodynamic Characteristics of an All-Body Research Aircraft Configuration. NASA TN D-7358, 1973.

6. Penland, Jim A.: Creel, Theodore R., Jr.; and Howard, Floyd G.: Experimental Low-Speed and Calculated High-Speed Aerodynamic Characteristics of a Hypersonic Research Airplane Concept Having a 65° Swept Delta Wing. NASA TN D-7633, 1974.

7. Creel, Theodore R., Jr.; and Penland, Jim A.: Low-Speed Aerodynamic Characteristics of a Hypersonic Research Airplane Concept Having a 70° Swept Delta Wing. NASA TM X-71974, 1974.

TABLE I.- GEOMETRIC CHARACTERISTICS OF MODEL

Body:	
Length, theoretical, m (in.)	1.528 (60.15)
Length, actual, m (in.)	1.502 (59.15)
Maximum width, m (in.)	0.394 (15.5)
Maximum height, m (in.)	0.2362 (9.3)
Base area, m^2 (in^2)	0.025 (40.12)
Nose radius, m (in.)	0.0033 (0.13)
Aspect ratios:	
Body alone	0.5336
Body and small horizontal tails	1.203
Body and large horizontal tails	1.4396
Body with small horizontal tail:	
Planform area, m^2 (in^2)	0.325 (504.18)
Span, m (in.)	0.602 (23.72)
Trapezoidal-planform canards, large:	
Area, total, m^2 (in^2)	0.0186 (28.86)
Area, exposed, m^2 (in^2)	0.013 (20.2)
Span, m (in.)	0.316 (12.43)
Aspect ratio	6
Root chord, at fuselage center line, m (in.)	0.071 (2.79)
Root chord, exposed, m (in.)	0.064 (2.52)
Tip chord, m (in.)	0.0269 (1.059)
Mean aerodynamic chord, m (in.)	0.052 (2.054)
Sweepback angles:	
Leading edge, deg	3.4
25-percent-chord line, deg	0
Trailing edge, deg	-9.5
Taper ratio	0.5
Dihedral, deg	0
Airfoil section	NACA 0012
Hinge-line location	25 percent chord
Trapezoidal-planform canards, small:	
Area, total, m^2 (in^2)	0.0093 (14.43)
Area, exposed, m^2 (in^2)	0.0065 (10.1)
Span, m (in.)	0.2357 (9.28)
Aspect ratio	6
Root chord, at fuselage center line, m (in.)	0.0526 (2.07)
Root chord, exposed, m (in.)	0.0459 (1.81)
Tip chord, m (in.)	0.0264 (1.04)
Mean aerodynamic chord, m (in.)	0.0409 (1.61)
Sweepback angles:	
Leading edge, deg	3.4
25-percent-chord line, deg	0
Trailing edge, deg	-9.5
Taper ratio	0.5
Dihedral, deg	0
Airfoil section	NACA 0012
Hinge-line location	25 percent chord

TABLE I.- GEOMETRIC CHARACTERISTICS OF MODEL – Continued

Delta-planform canards, large:	
Area, total, m^2 (in^2)	0.029 (44.8)
Area, exposed, m^2 (in^2)	0.013 (20.2)
Span, total, m (in.)	0.203 (8.00)
Aspect ratio, total	1.43
Root chord, at fuselage center line, m (in.)	0.232 (9.12)
Root chord, exposed, m (in.)	0.197 (7.75)
Mean aerodynamic chord, total, m (in.)	0.153 (6.04)
Sweepback angles:	
Leading edge, deg	65
Trailing edge, deg	-6.5
Dihedral, deg	0
Airfoil section	Circular arc
Airfoil thickness ratio	0.05
Leading-edge radius, m (in.)	0.0008 (0.032)
Delta-planform canards, small:	
Area, total, m^2 (in^2)	0.0145 (22.4)
Area, exposed, m^2 (in^2)	0.0065 (10.1)
Span, total, m (in.)	0.1600 (6.3)
Aspect ratio, total	1.76
Root chord, at fuselage center line, m (in.)	0.1803 (7.1)
Root chord, exposed, m (in.)	0.1389 (5.47)
Mean aerodynamic chord, m (in.)	0.1201 (4.73)
Sweepback angles:	
Leading edge, deg	65
Trailing edge, deg	-6.5
Dihedral, deg	0
Airfoil section	Circular arc
Airfoil thickness ratio	0.05
Leading-edge radius, m (in.)	0.0008 (0.032)
Vertical tails, twin, small:	
Area, total, m^2 (in^2)	0.0691 (107.08)
Span, m (in.)	0.1224 (4.82)
Aspect ratio	0.434
Root chord, at fuselage center line, m (in.)	0.436 (17.16)
Mean aerodynamic chord of exposed area, m (in.)	0.298 (11.72)
Sweepback angles:	
Top leading edge, deg	78
Bottom leading edge, deg	14
Trailing edge, deg	11
Airfoil section	Circular arc
Leading-edge radius, m (in.)	0.00119 (0.047)
Trailing-edge height, m (in.)	0.0016 (0.063)
Thickness ratio	0.04

TABLE I.- GEOMETRIC CHARACTERISTICS OF MODEL – Concluded

Vertical tails, twin, large:	
Area, total, m^2 (in^2)	0.1036 (160.62)
Span, m (in.)	0.181 (7.13)
Aspect ratio	0.633
Root chord, at fuselage center line, m (in.)	0.436 (17.16)
Mean aerodynamic chord of exposed area, m (in.)	0.301 (11.85)
Sweepback angles:	
Top leading edge, deg	66
Bottom leading edge, deg	14
Trailing edge, deg	11
Airfoil section	Circular arc
Leading-edge radius, m (in.)	0.00119 (0.047)
Trailing-edge height, m (in.)	0.0016 (0.063)
Thickness ratio	0.04
Center vertical tail:	
Area, total, m^2 (in^2)	0.0345 (53.54)
Span, exposed, m (in.)	0.168 (6.63)
Aspect ratio, exposed	0.821
Taper ratio, exposed	0.308
Root chord, at fuselage surface line, m (in.)	0.251 (9.9)
Tip chord, m (in.)	0.0775 (3.05)
Mean aerodynamic chord of exposed area, m (in.)	0.178 (7.008)
Sweepback angles:	
Leading edge, deg	60
Trailing edge, deg	30
Airfoil section	NACA 0004
Leading-edge radius, m (in.)	0.00119 (0.047)
Trailing-edge radius, m (in.)	0 (0)
Horizontal tails, small:	
Area, exposed, each, m^2 (in^2)	0.0145 (22.51)
Span, total, exposed, m (in.)	0.1054 (4.15)
Aspect ratio, exposed	0.76
Root chord, exposed, m (in.)	0.276 (10.85)
Mean aerodynamic chord, total, m (in.)	0.1836 (7.23)
Sweepback angles:	
Leading edge, deg	65
Trailing edge, deg	-6.5
Dihedral, deg	0
Airfoil section	Circular arc
Airfoil thickness ratio	0.03
Leading-edge radius, m (in.)	0.00119 (0.047)
Horizontal tails, large:	
Area, exposed, each, m^2 (in^2)	0.029 (45.00)
Span, total, exposed, m (in.)	0.403 (15.87)
Aspect ratio, exposed	0.76
Root chord, exposed, m (in.)	0.263 (10.34)
Mean aerodynamic chord, total, m (in.)	0.263 (10.34)
Sweepback angles:	
Leading edge, deg	65
Trailing edge, deg	-6.5
Dihedral, deg	0
Airfoil section	Circular arc
Airfoil thickness ratio	0.03
Leading-edge radius, m (in.)	0.00119 (0.047)

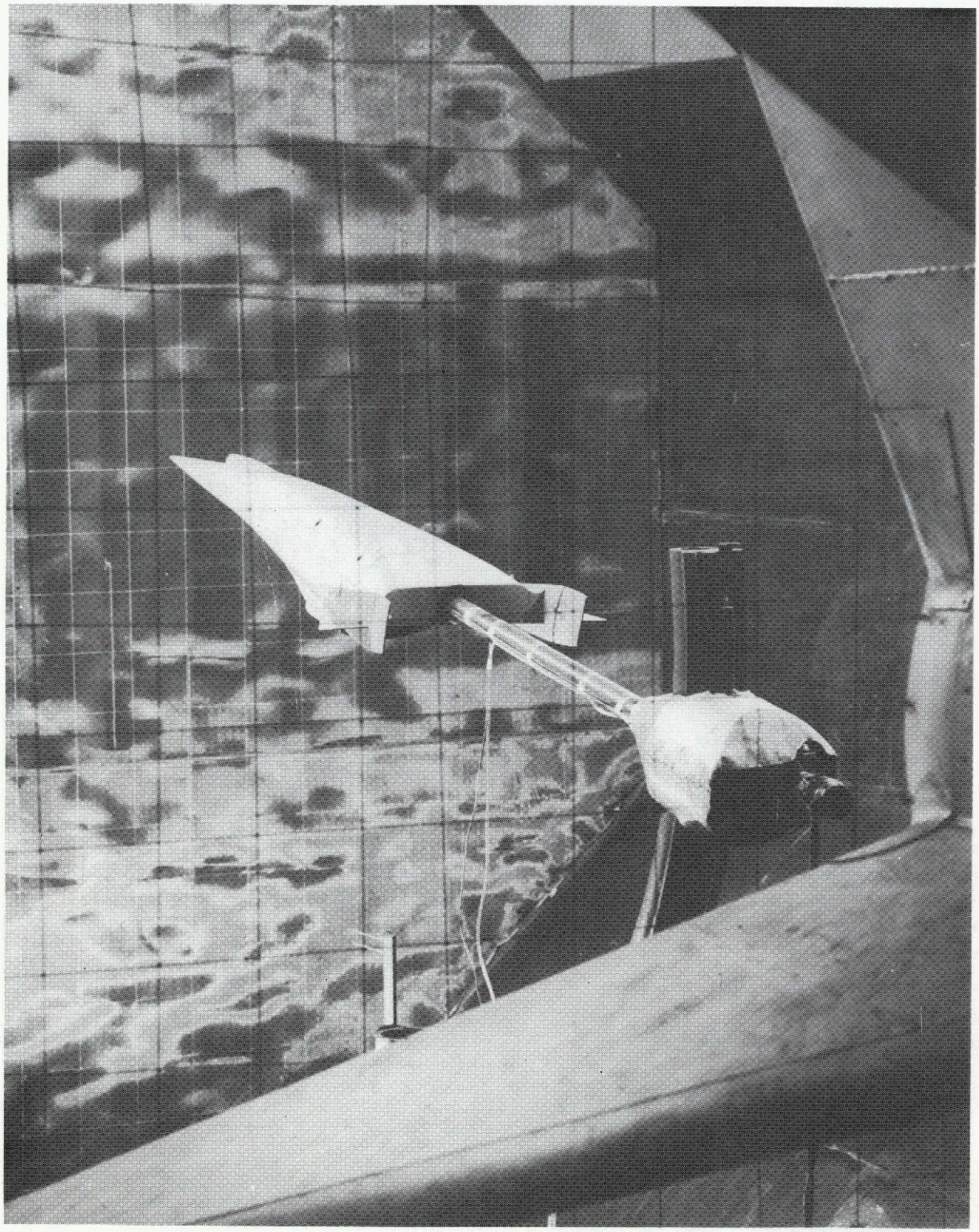

L-72-3741

Figure 1.- Photograph of model installed in tunnel.

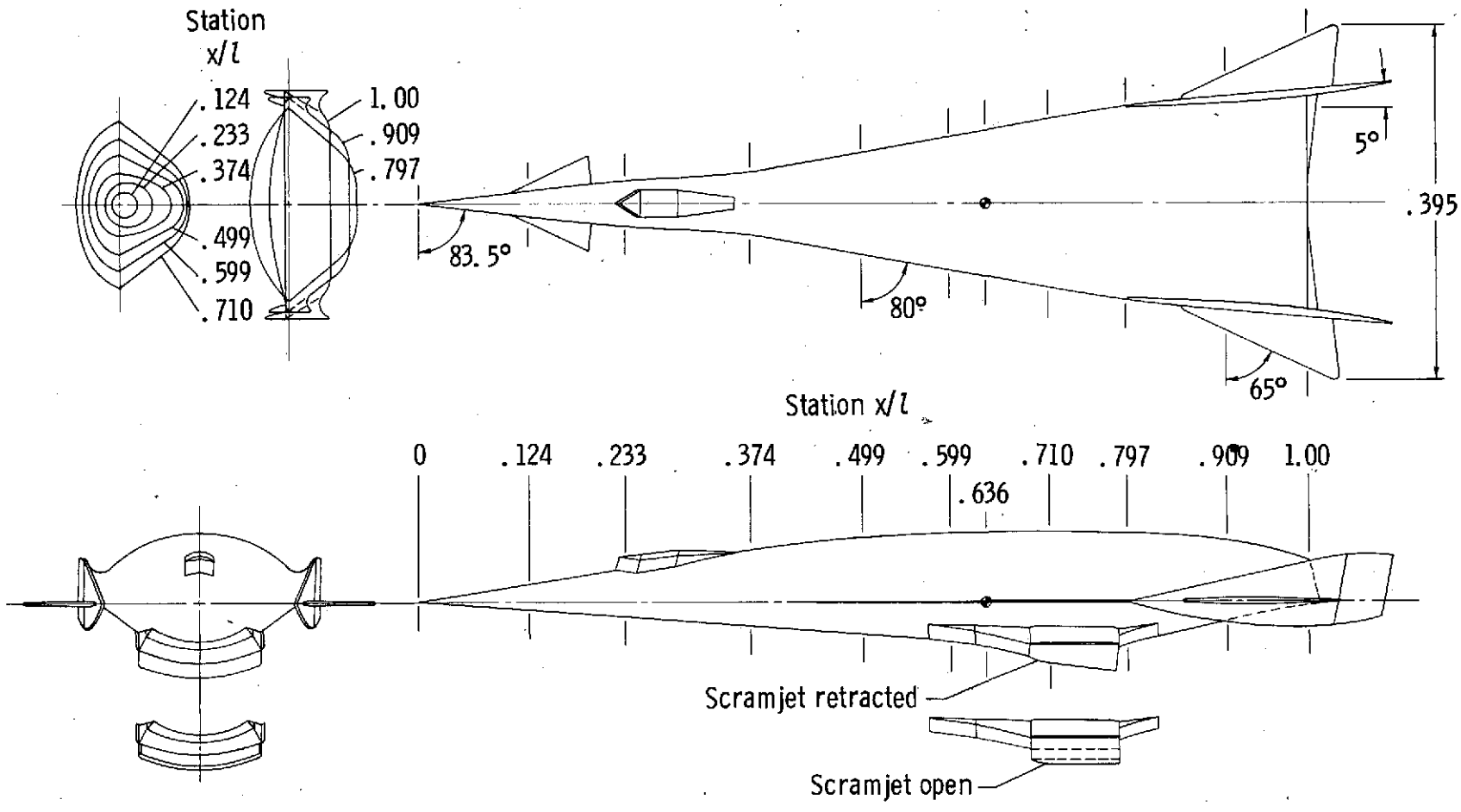

(a) Complete model.

Figure 2.- Details of wind-tunnel model. All dimensions are normalized by the fuselage length l.

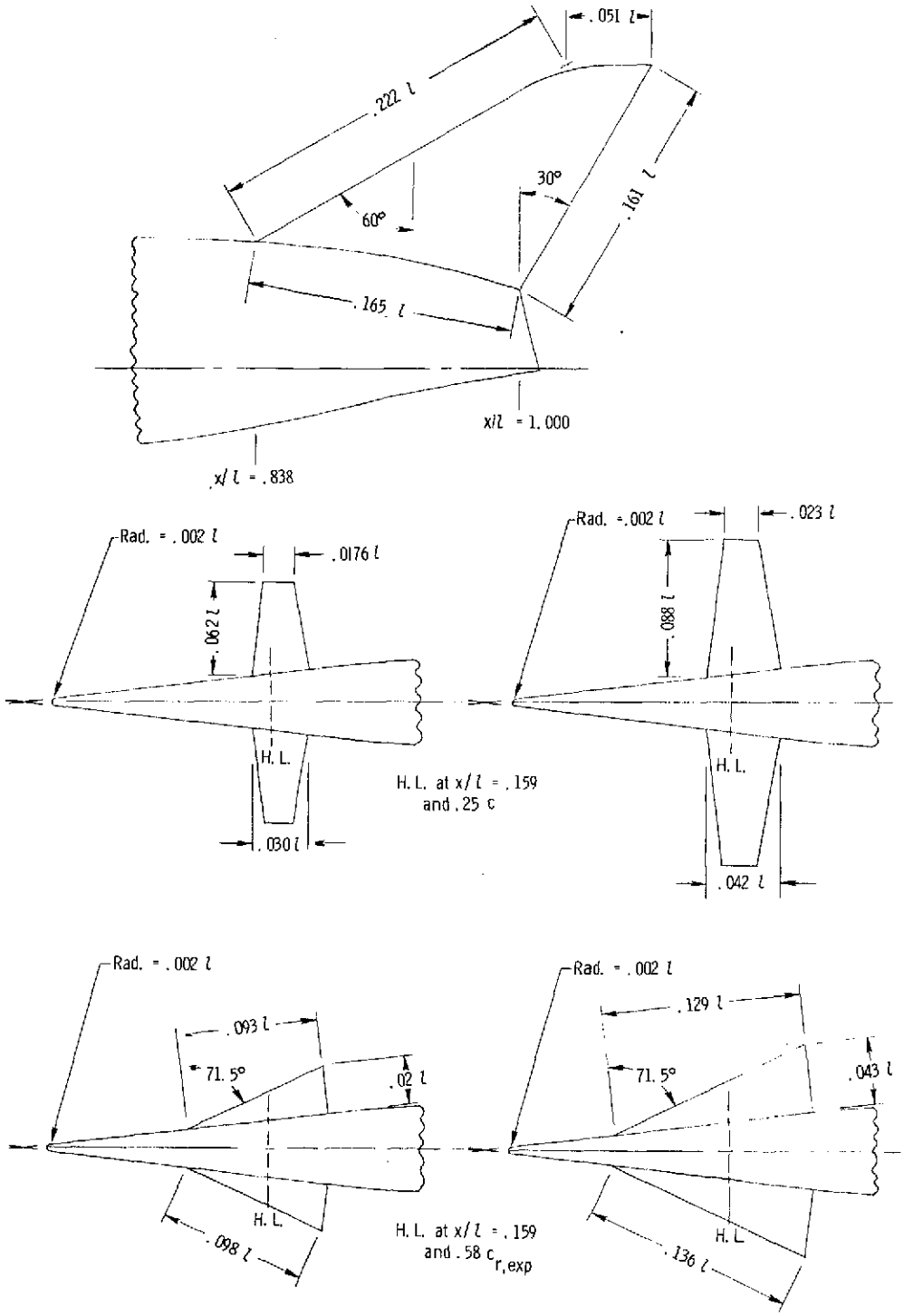

(b) Center vertical tail and small and large trapezoidal and delta canards. H.L. denotes hinge line.

Figure 2.- Continued.

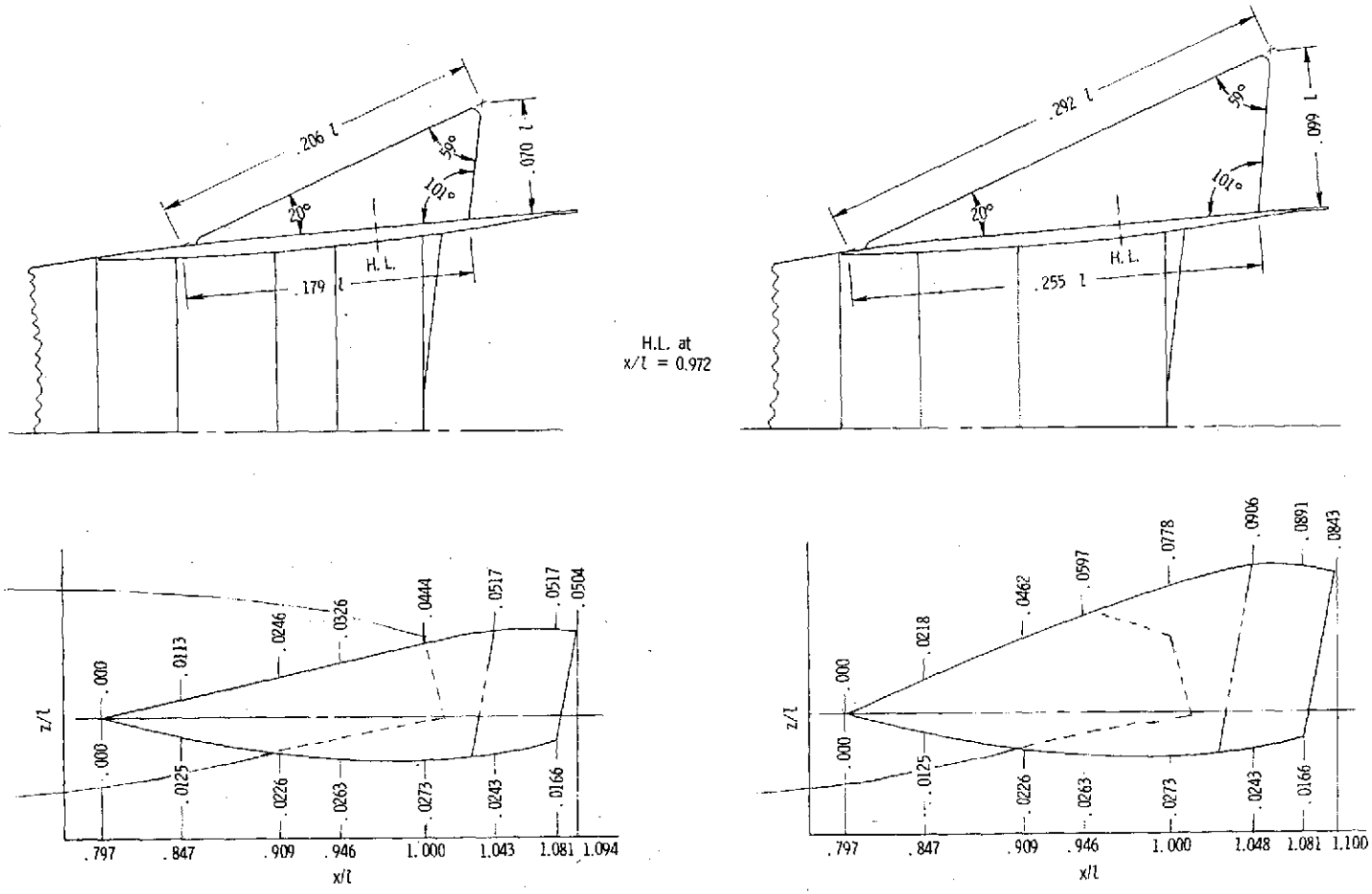

(c) Small and large horizontal and vertical tails.

Figure 2.- Concluded.

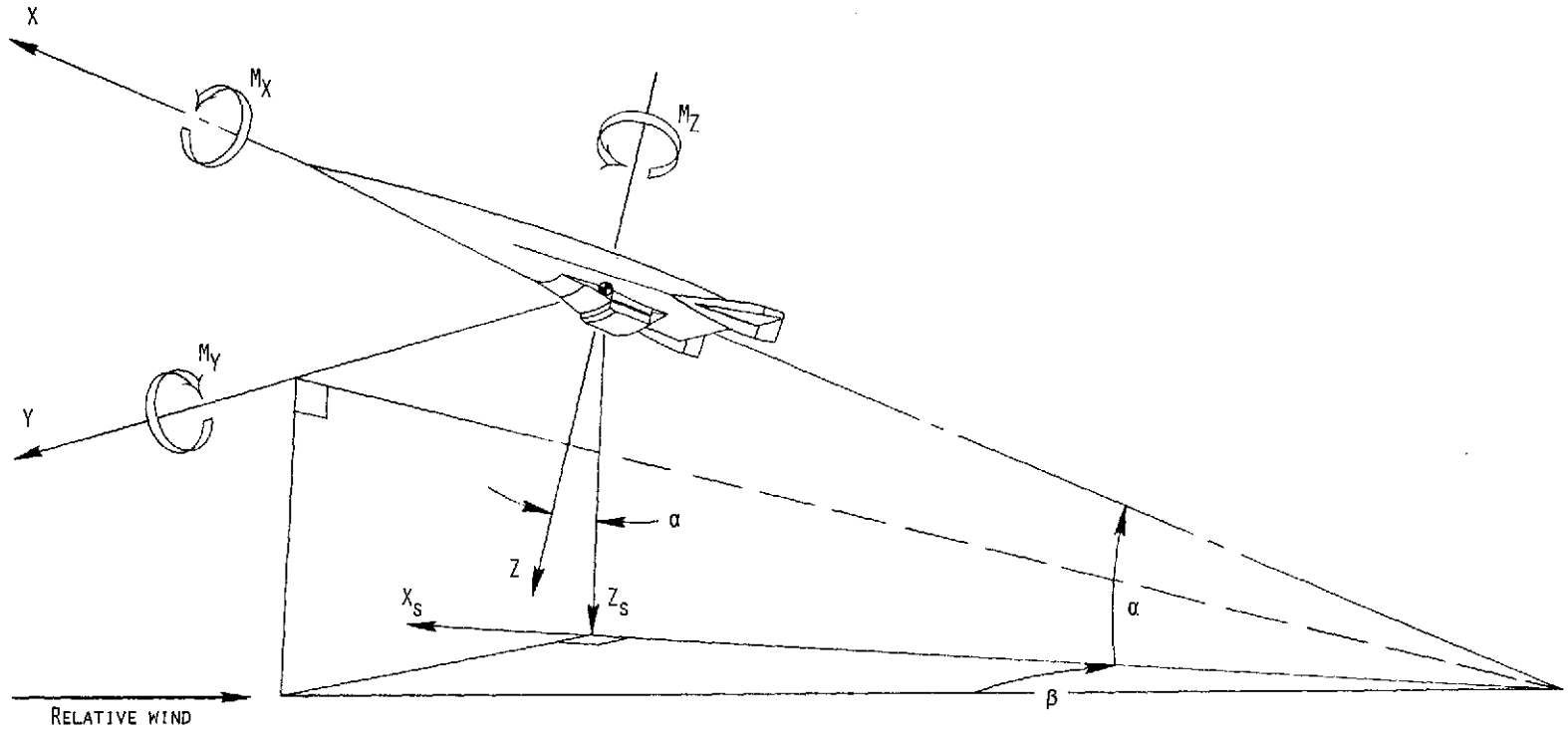

Figure 3.- Systems of reference axes; arrows indicate positive directions.

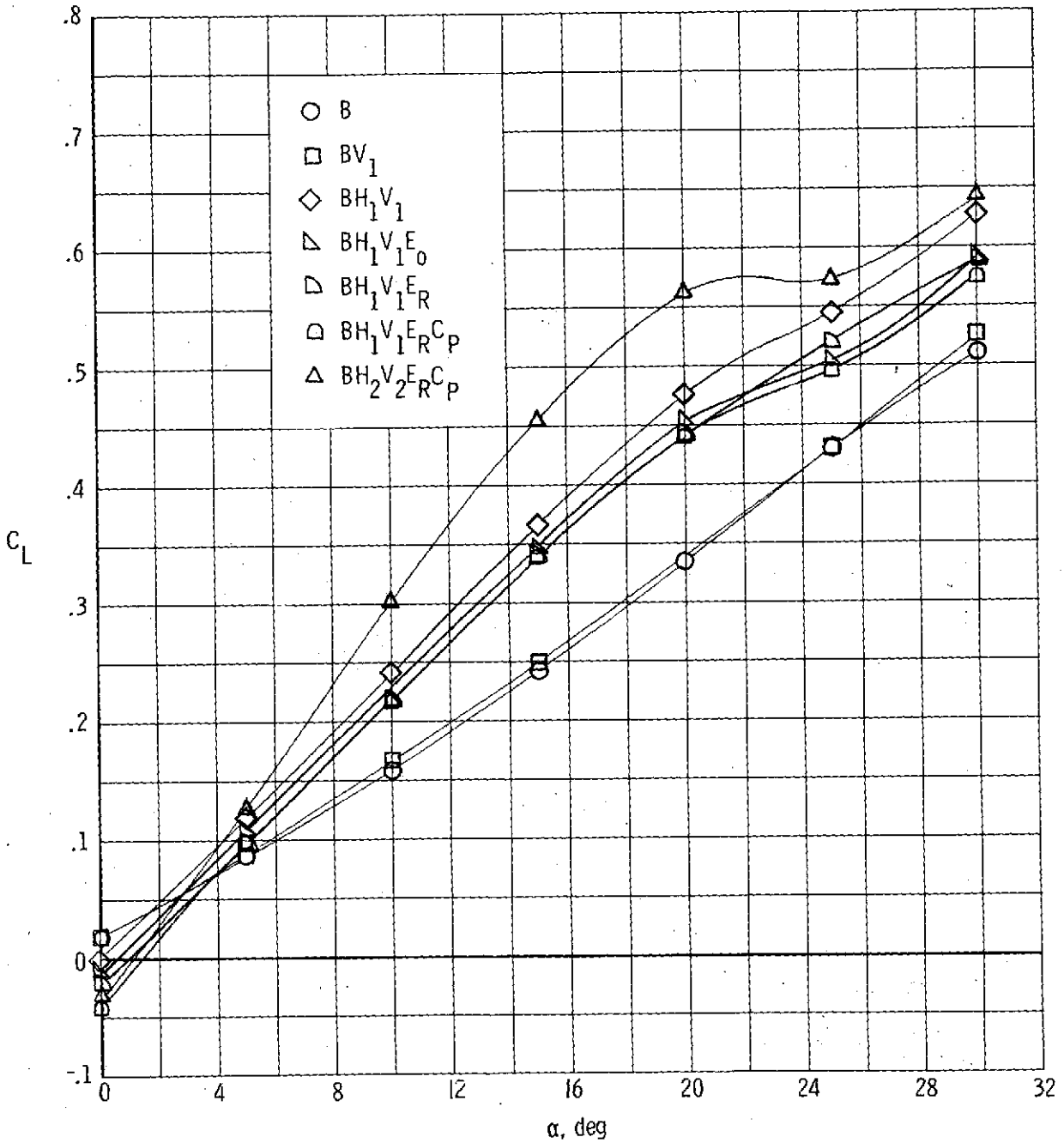

(a) Lift.

Figure 4.- Longitudinal characteristics of the body alone and the body with various horizontal and vertical tails. $\delta_H = 0^o$.

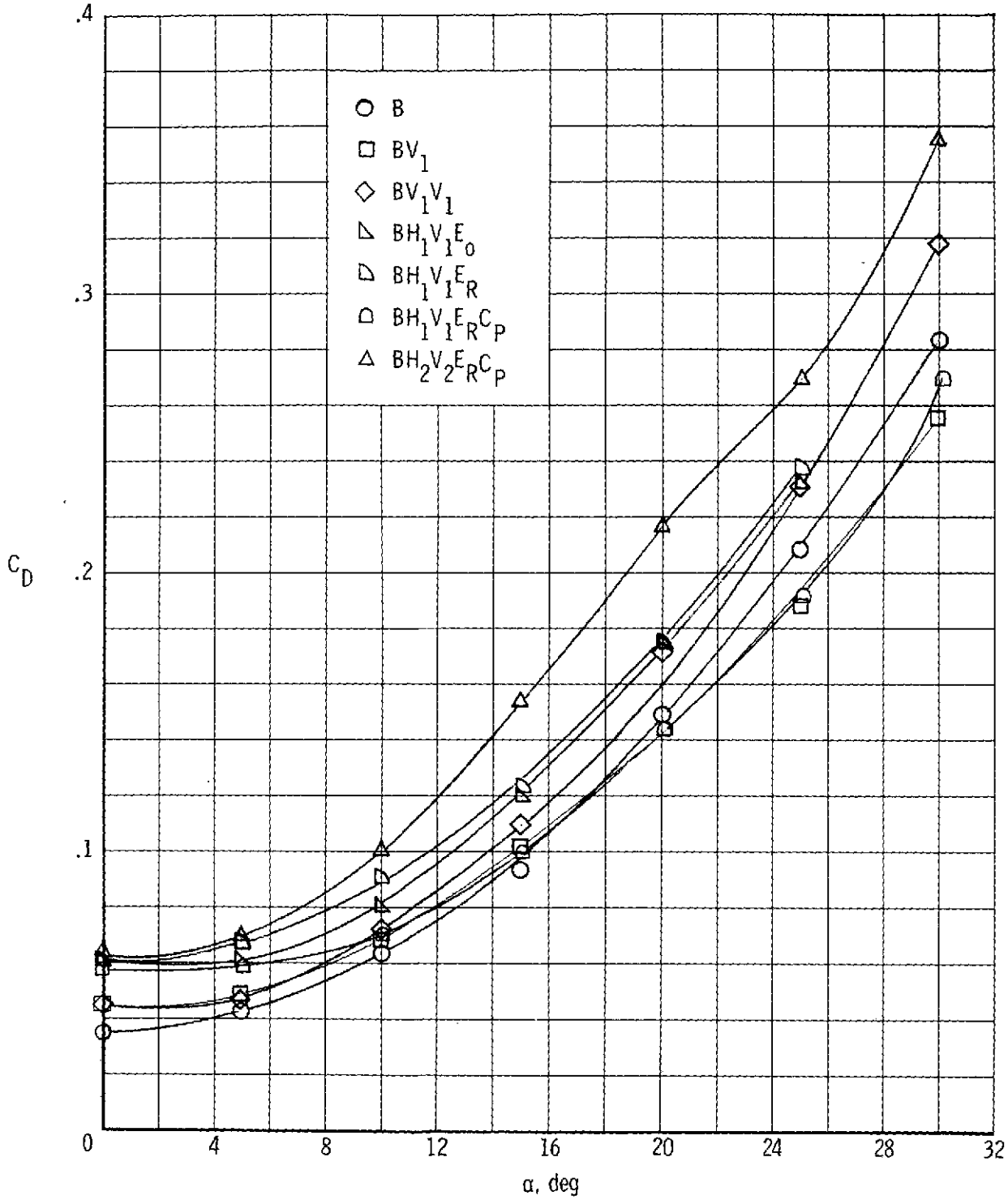

(b) Drag.

Figure 4.- Continued.

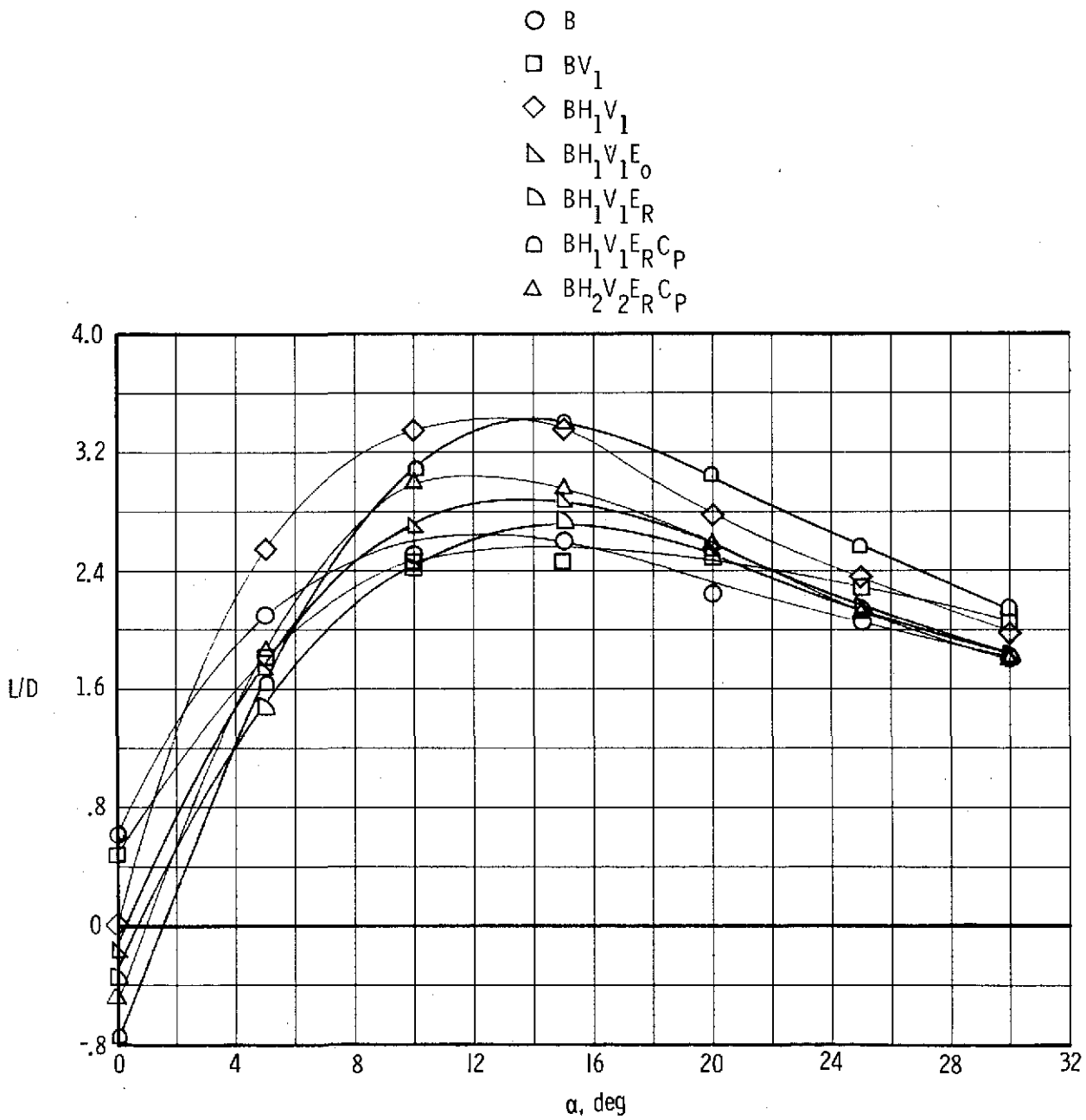

(c) Lift-drag ratio.

Figure 4.- Continued.

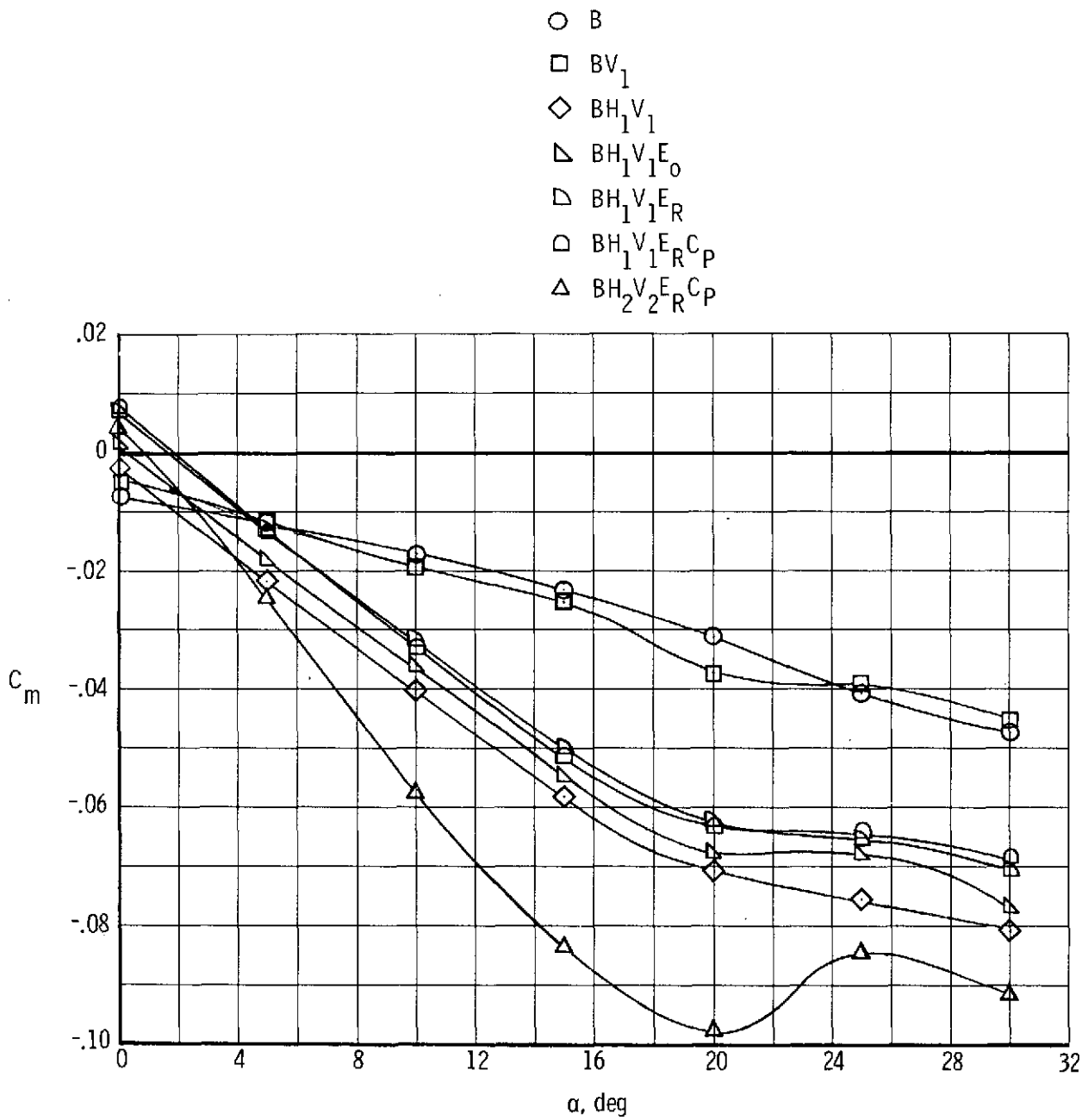

(d) Pitch.

Figure 4.- Continued.

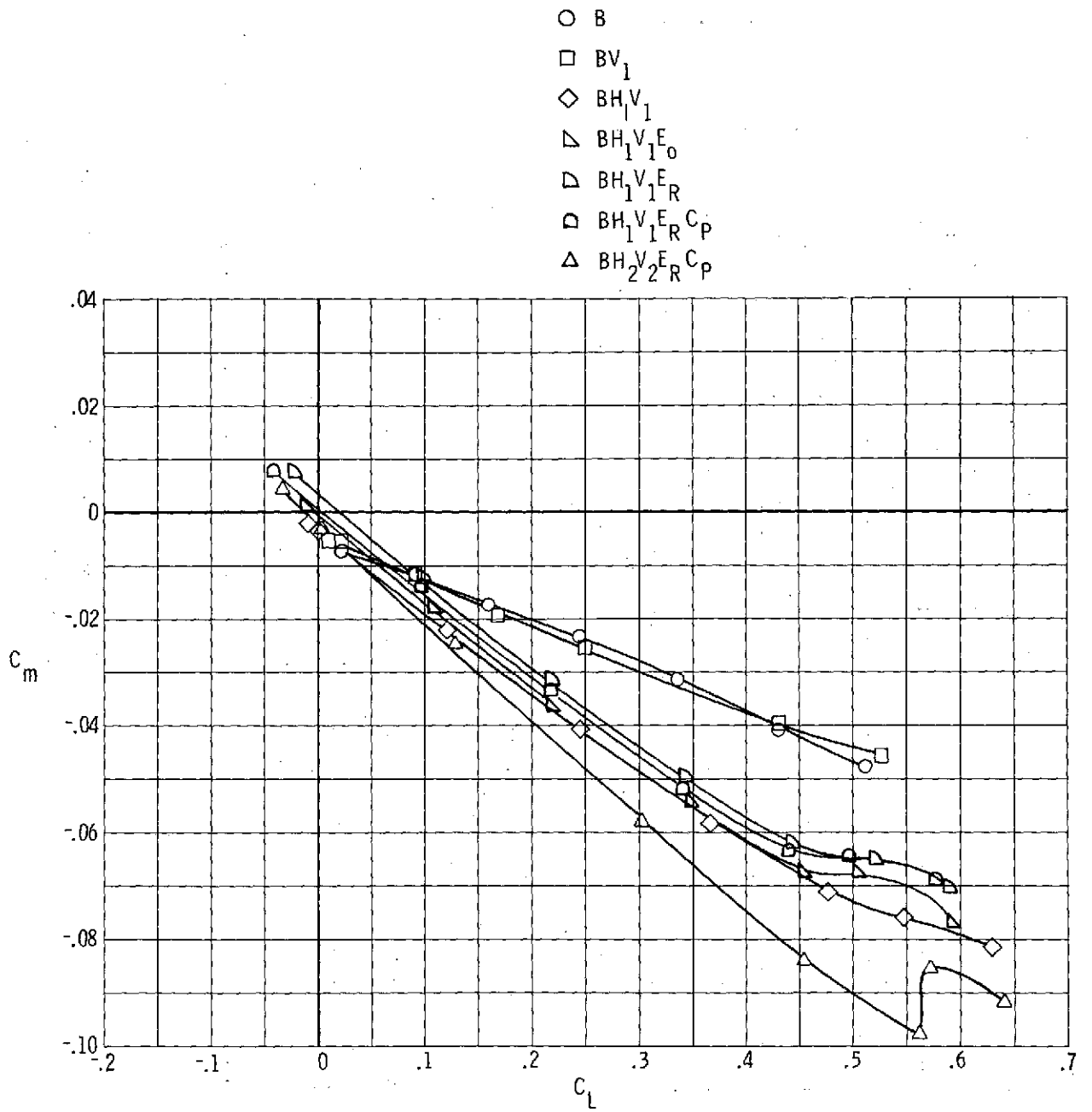

(e) Stability.

Figure 4. - Concluded.

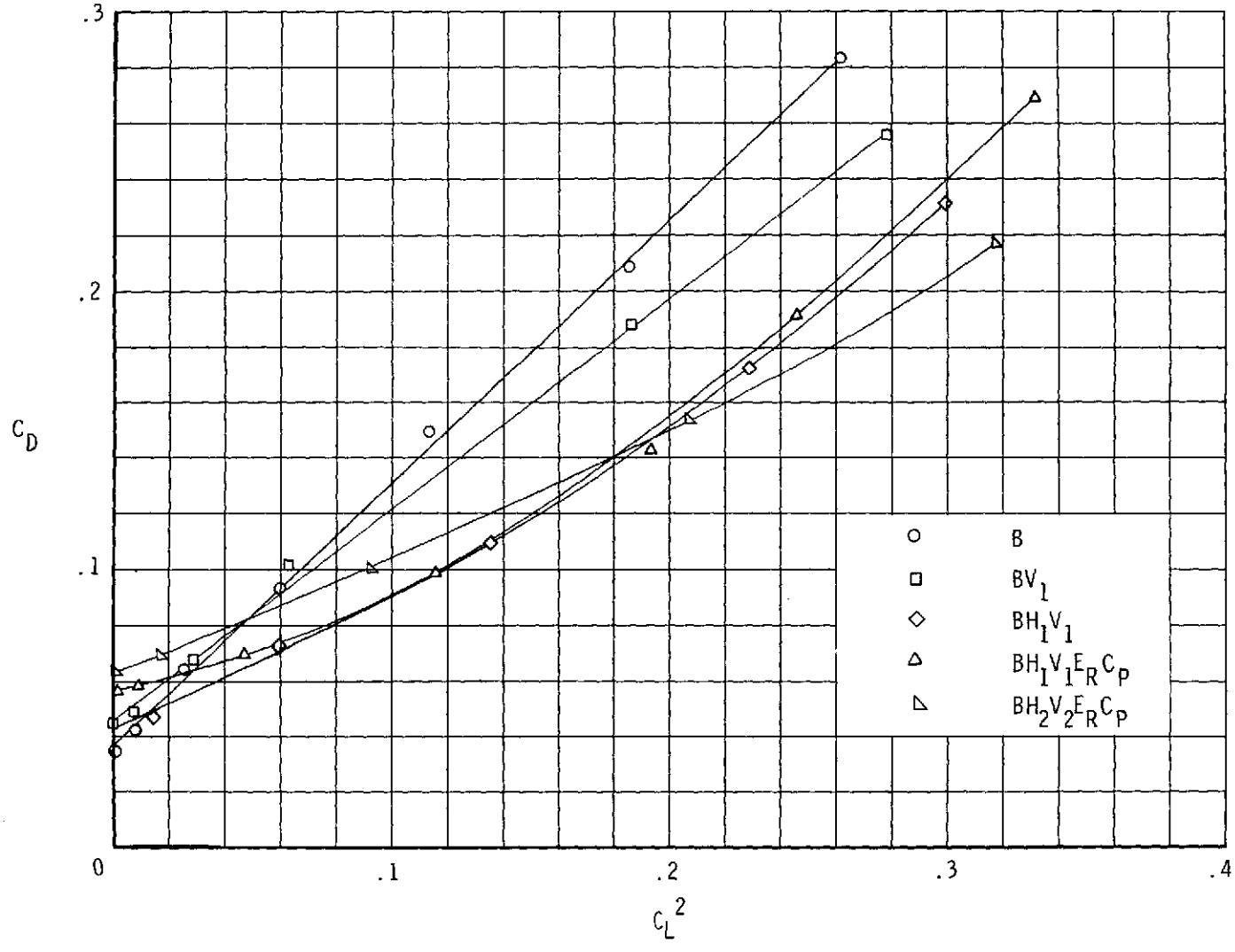

Figure 5.- The drag due to lift of the body alone and the body with vertical and horizontal tails, retracted engine, and canopy. $\delta_H = 0^o$.

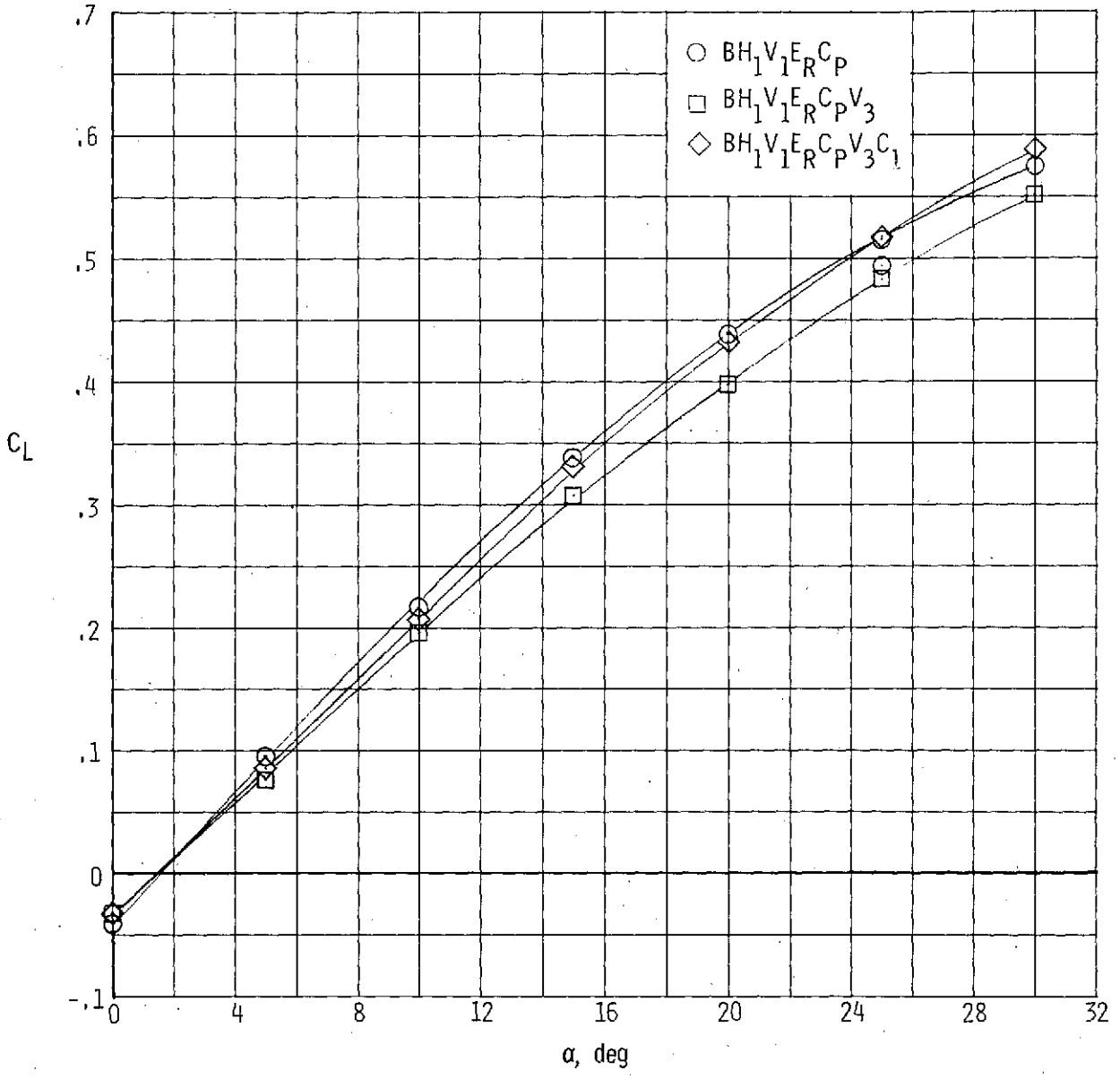

(a) Lift.

Figure 6.- Effect on longitudinal characteristics of addition of the center vertical tail and small trapezoidal canards to the $BH_1V_1E_RC_P$ configuration. $\delta_H = 0^o$.

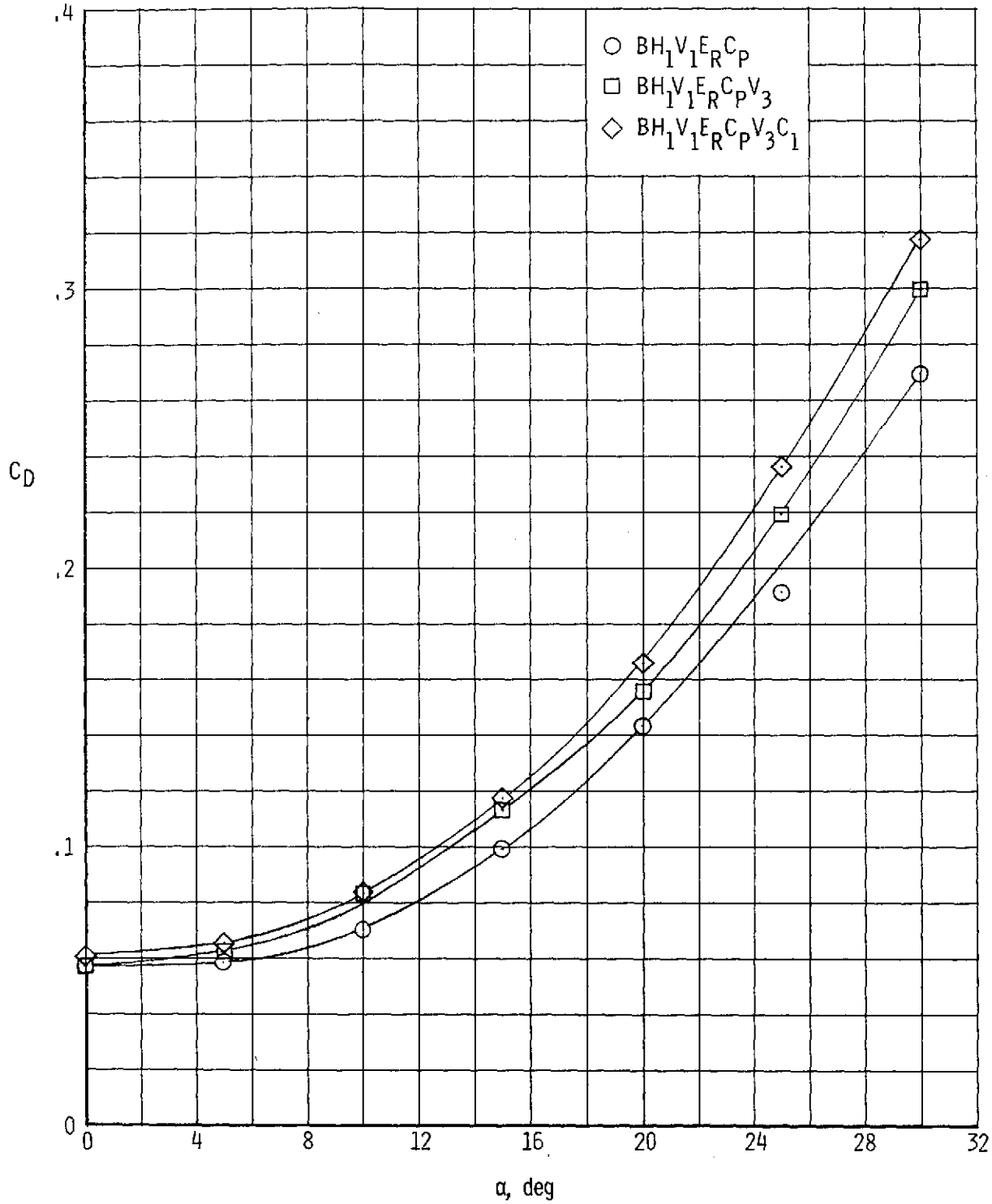

(b) Drag.

Figure 6.- Continued.

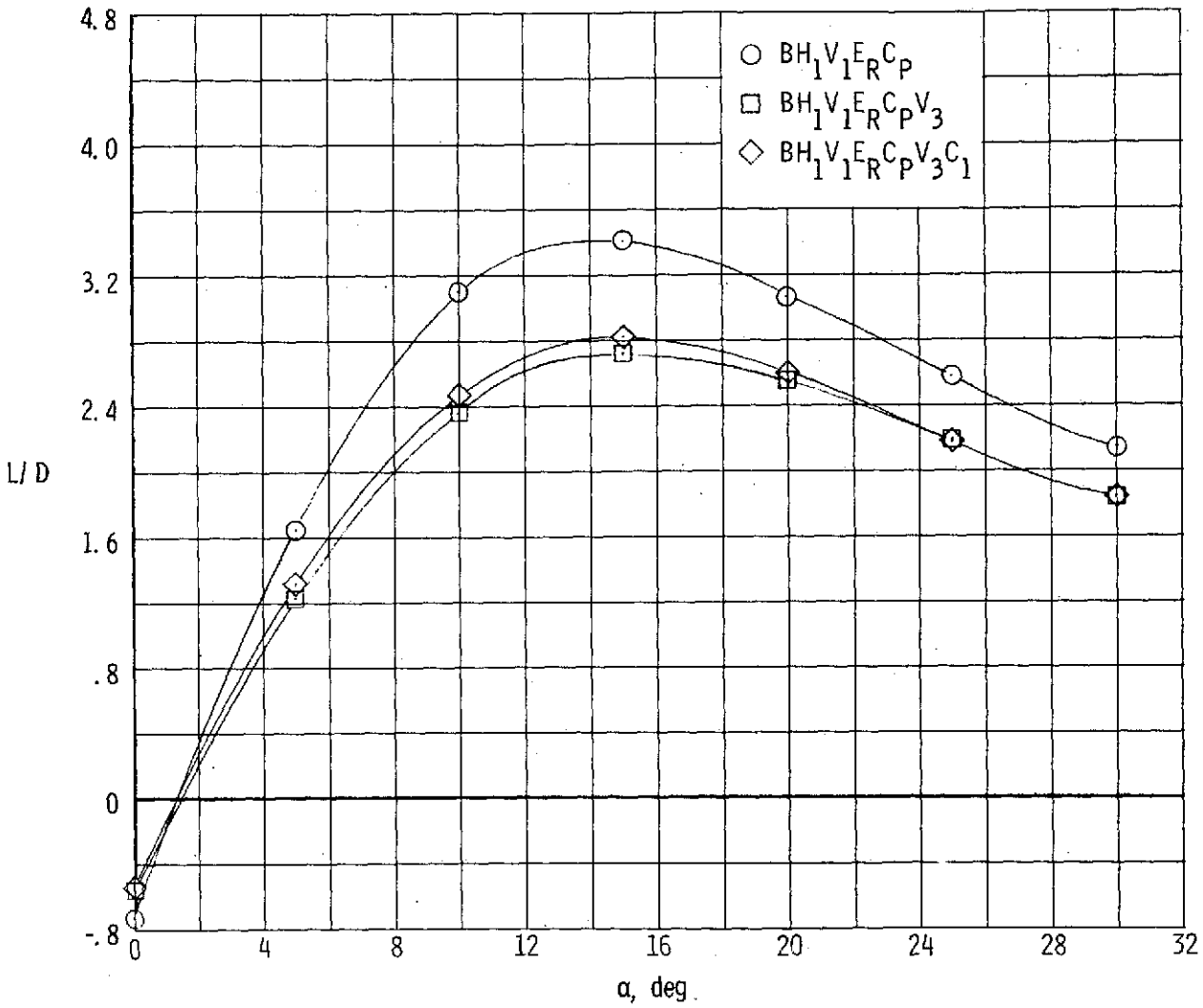

(c) Lift-drag ratio.

Figure 6.- Continued.

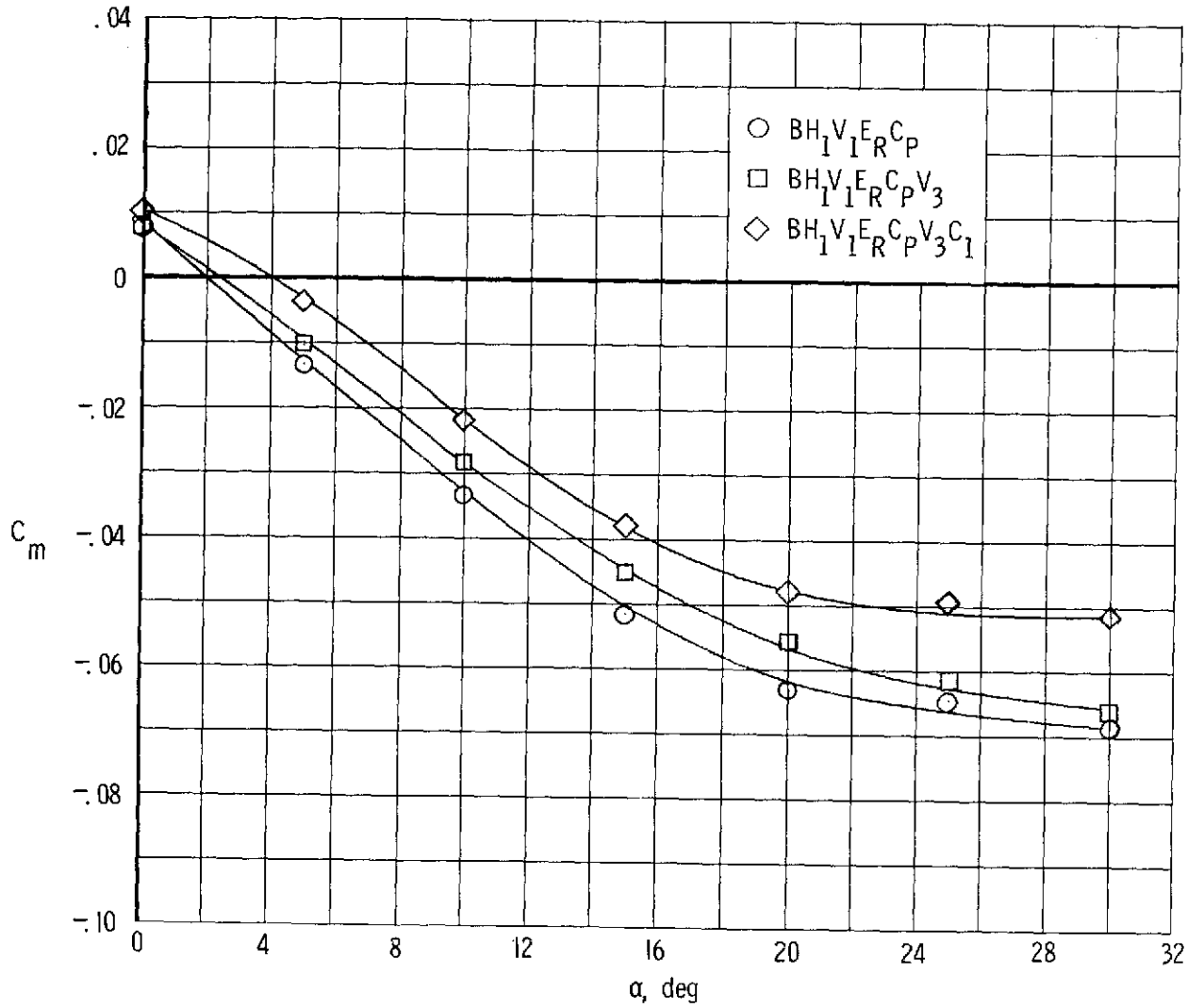

(d) Pitch.

Figure 6.- Continued.

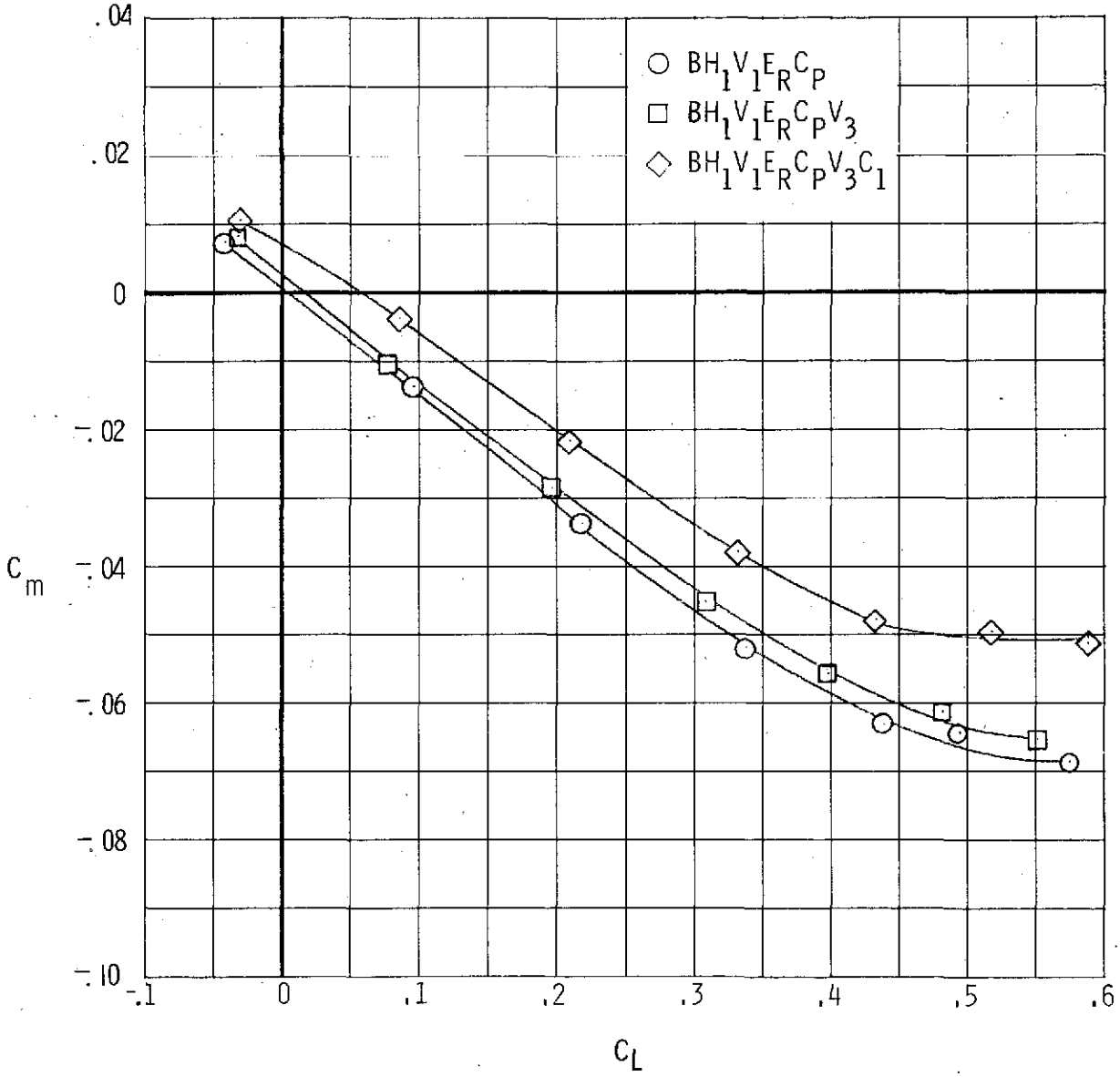

(e) Stability.

Figure 6.- Concluded.

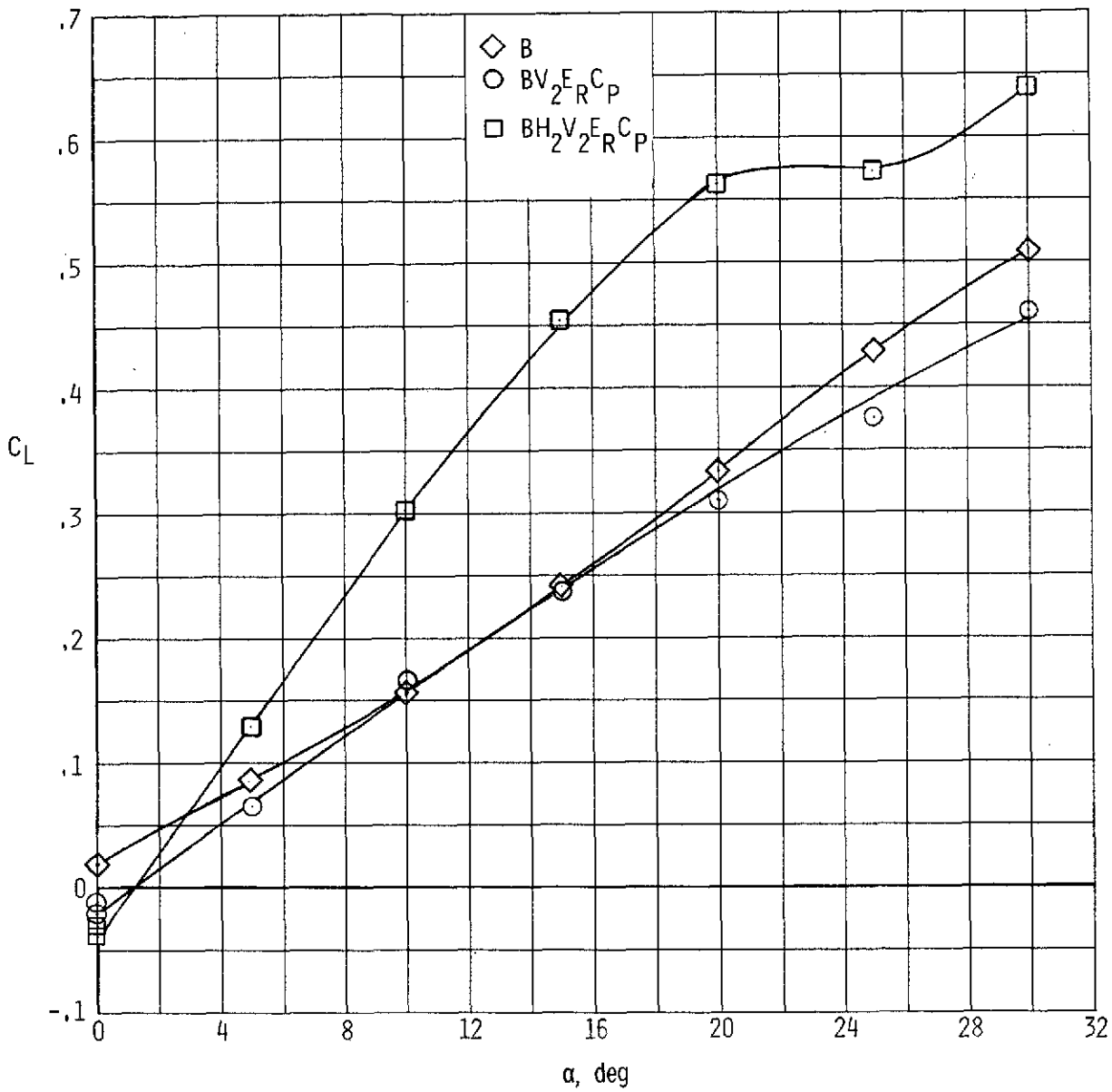

(a) Lift.

Figure 7.- Effect on longitudinal characteristics of addition of the large horizontal tail H_2 to the $BV_2E_RC_P$ configuration. $\delta_H = 0^o$.

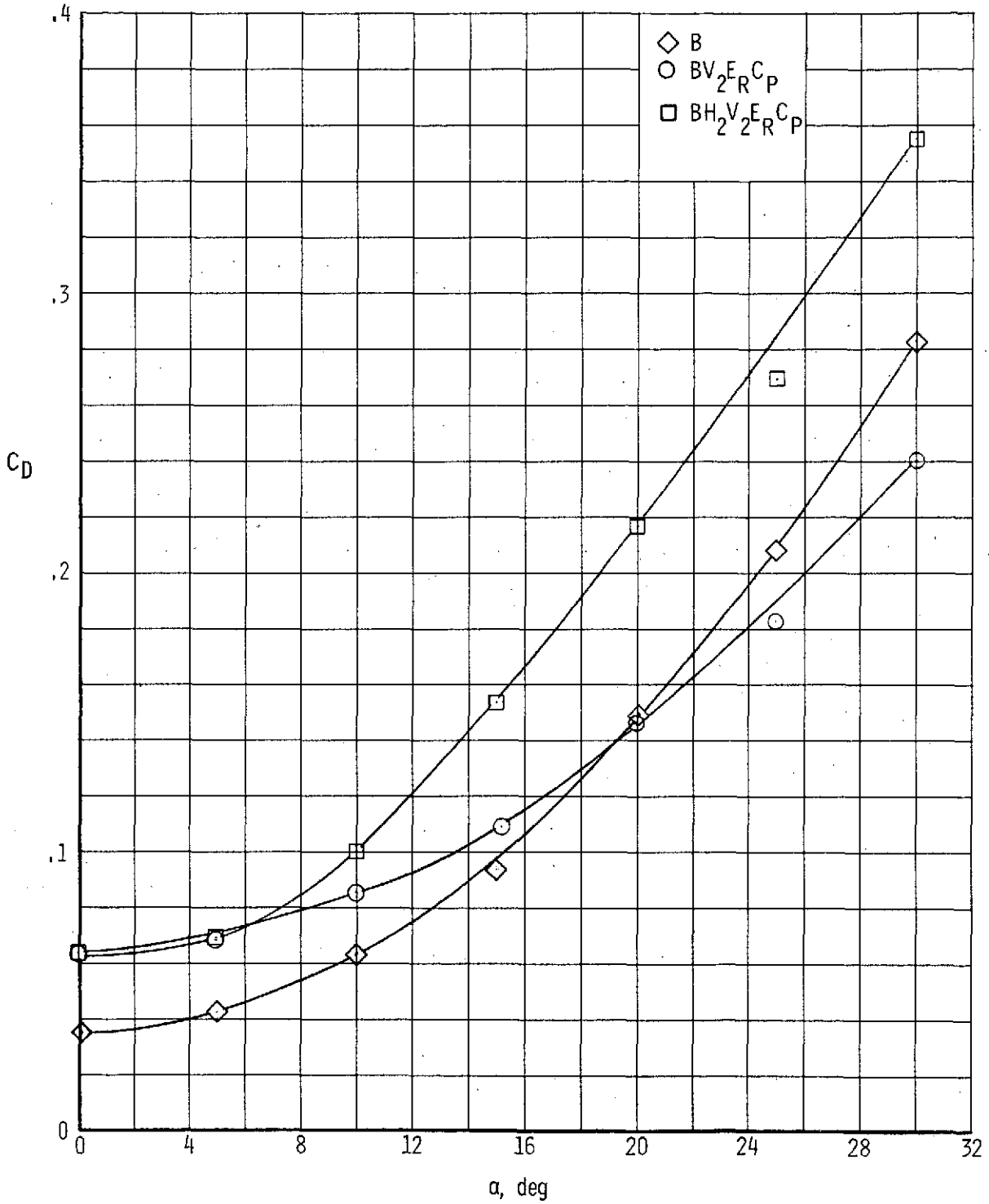

(b) Drag.

Figure 7.- Continued.

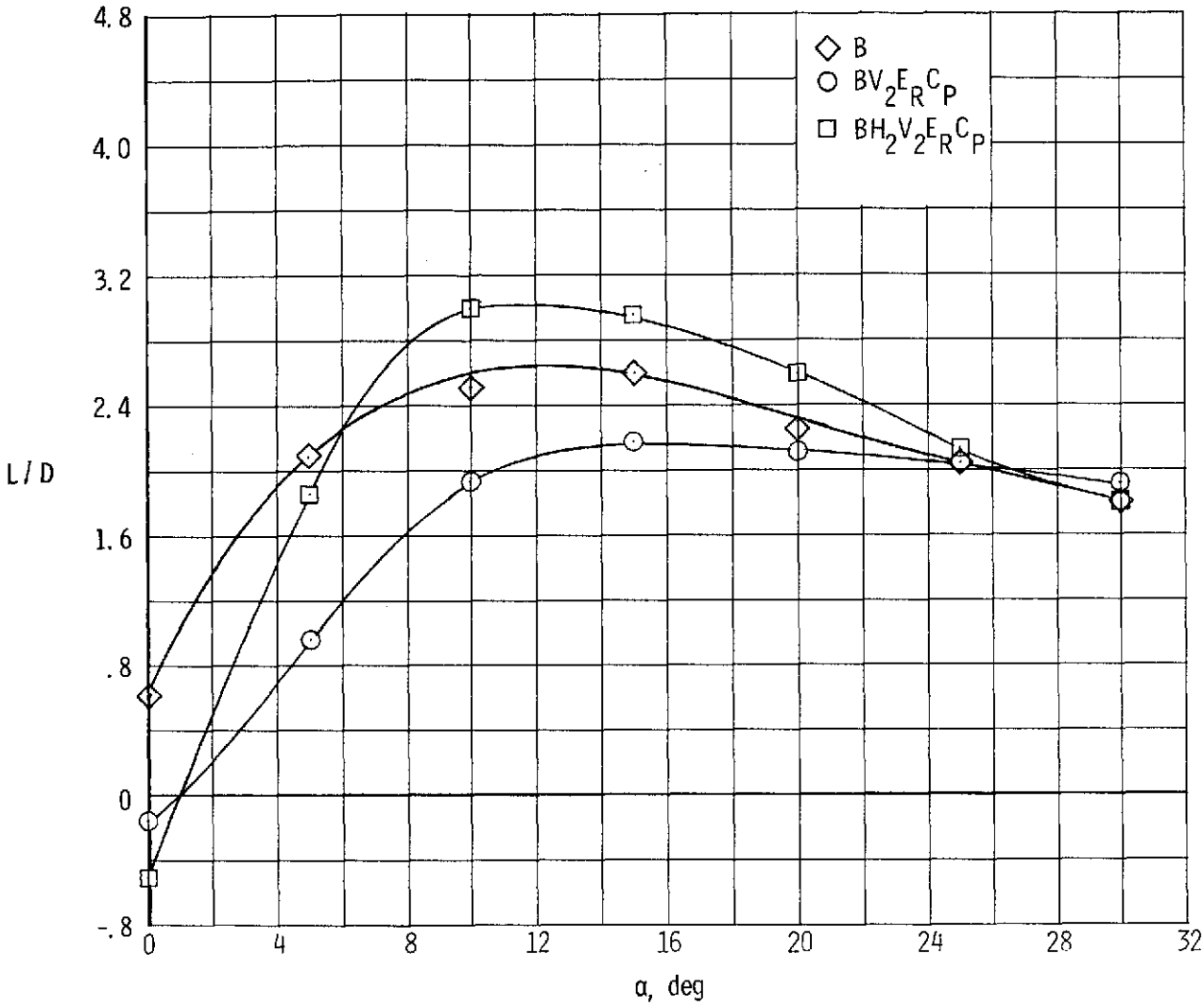

(c) Lift-drag ratio.

Figure 7.- Continued.

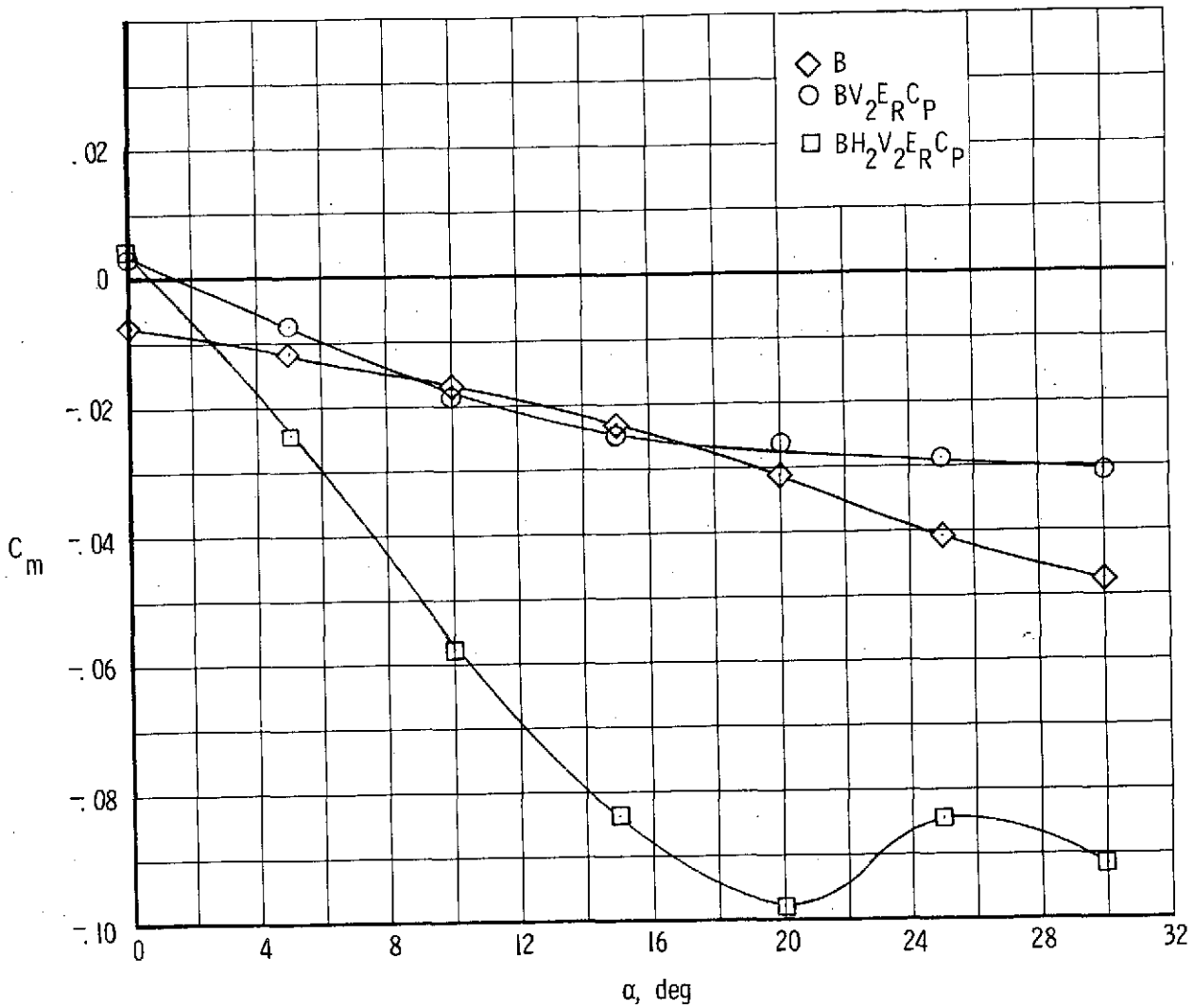

(d) Pitch.

Figure 7.- Continued.

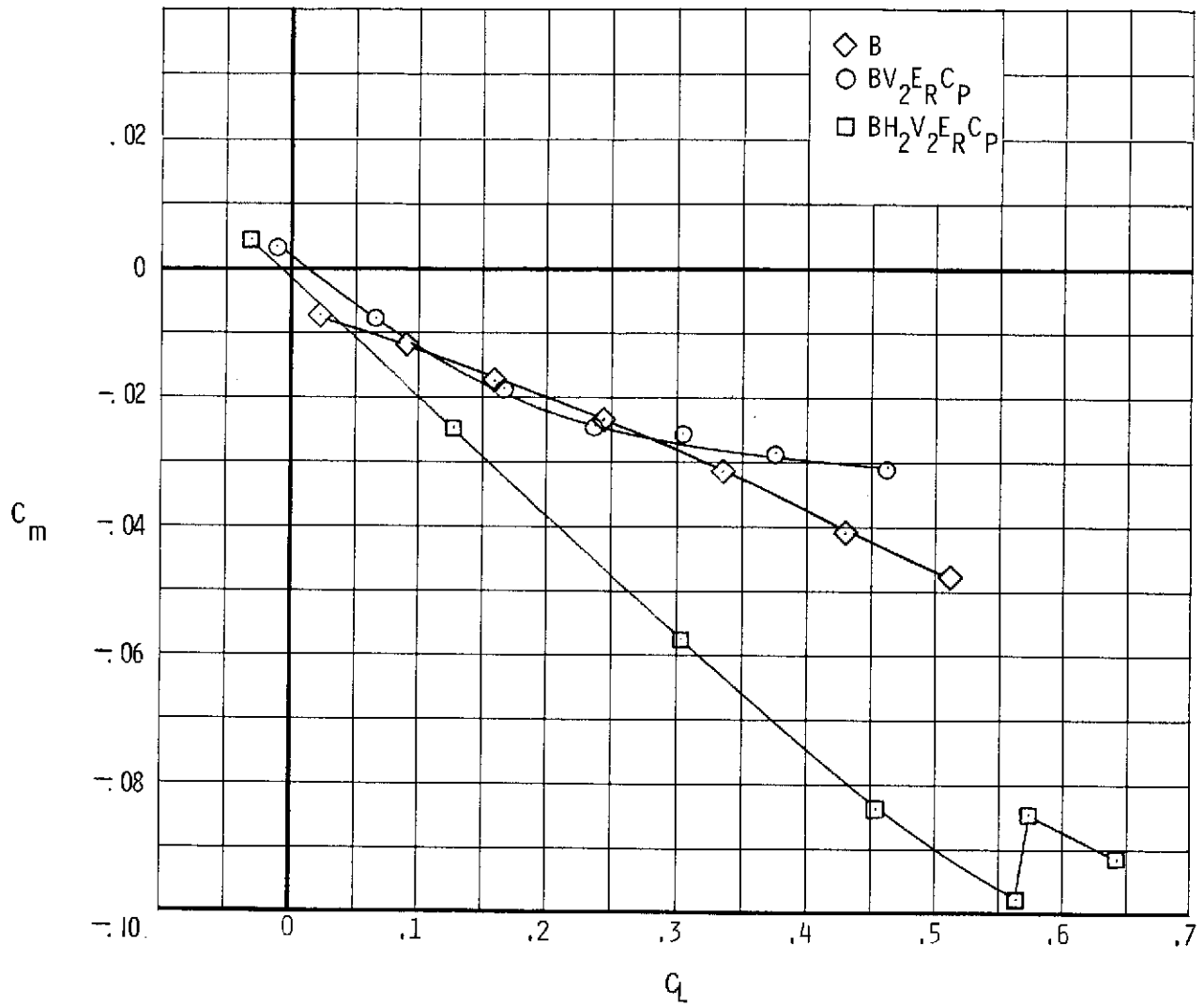

(e) Stability.

Figure 7.- Concluded.

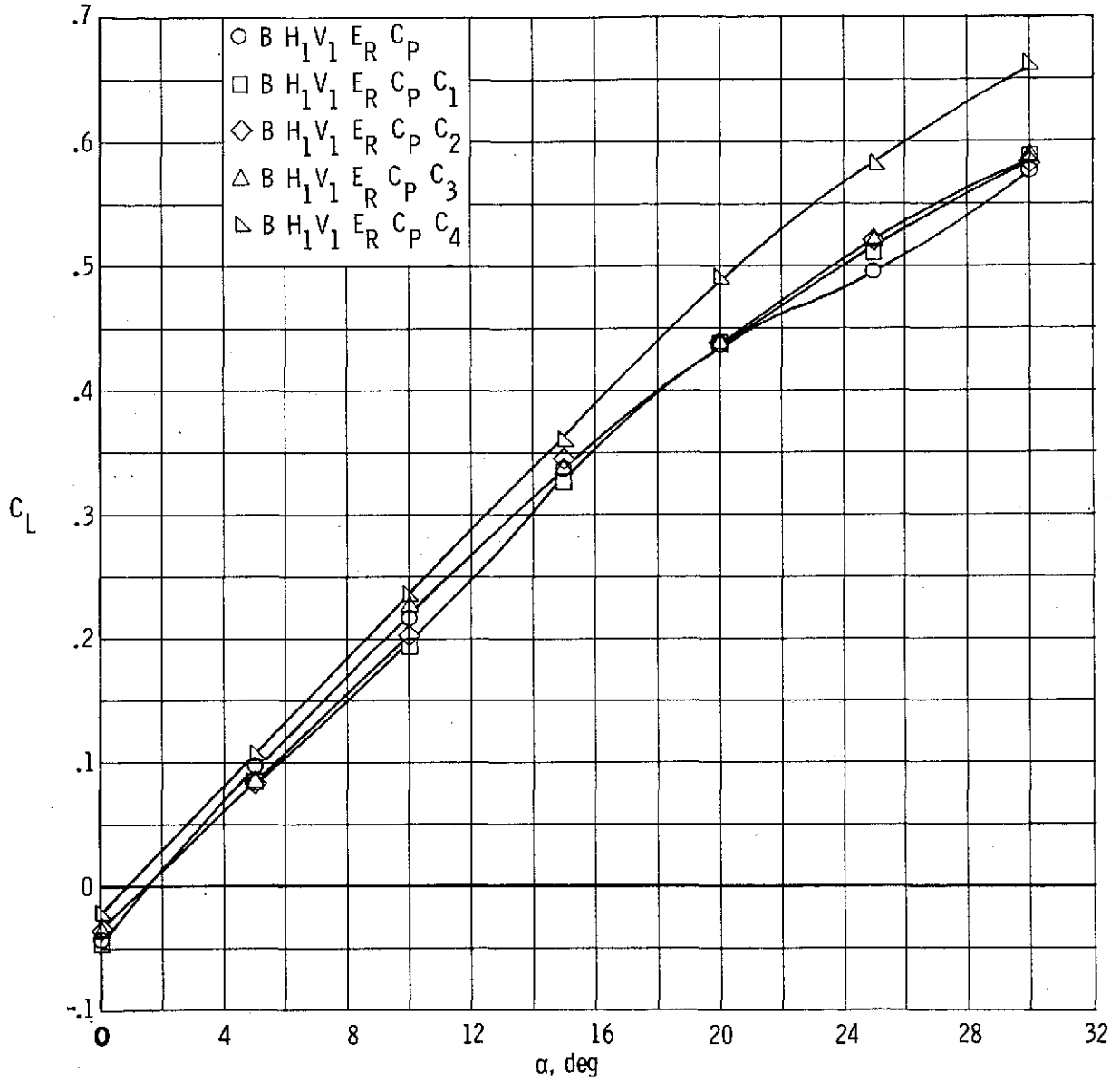

(a) Lift.

Figure 8.- Longitudinal characteristics of model $BH_1V_1E_RC_P$ (body, small tails, retracted engine, and canopy) with various canards. $\delta_C = \delta_H = 0^o$.

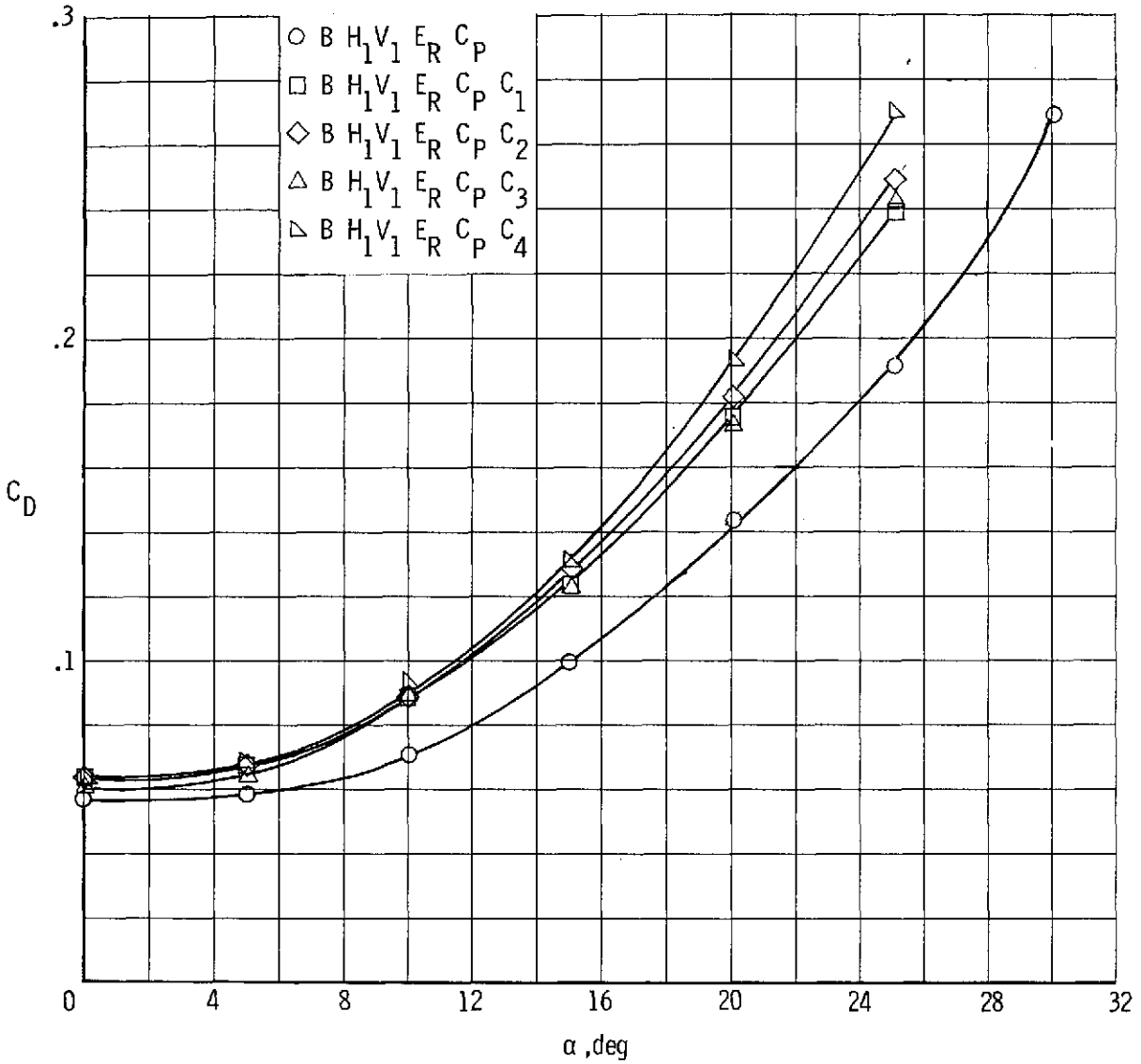

(b) Drag.

Figure 8.- Continued.

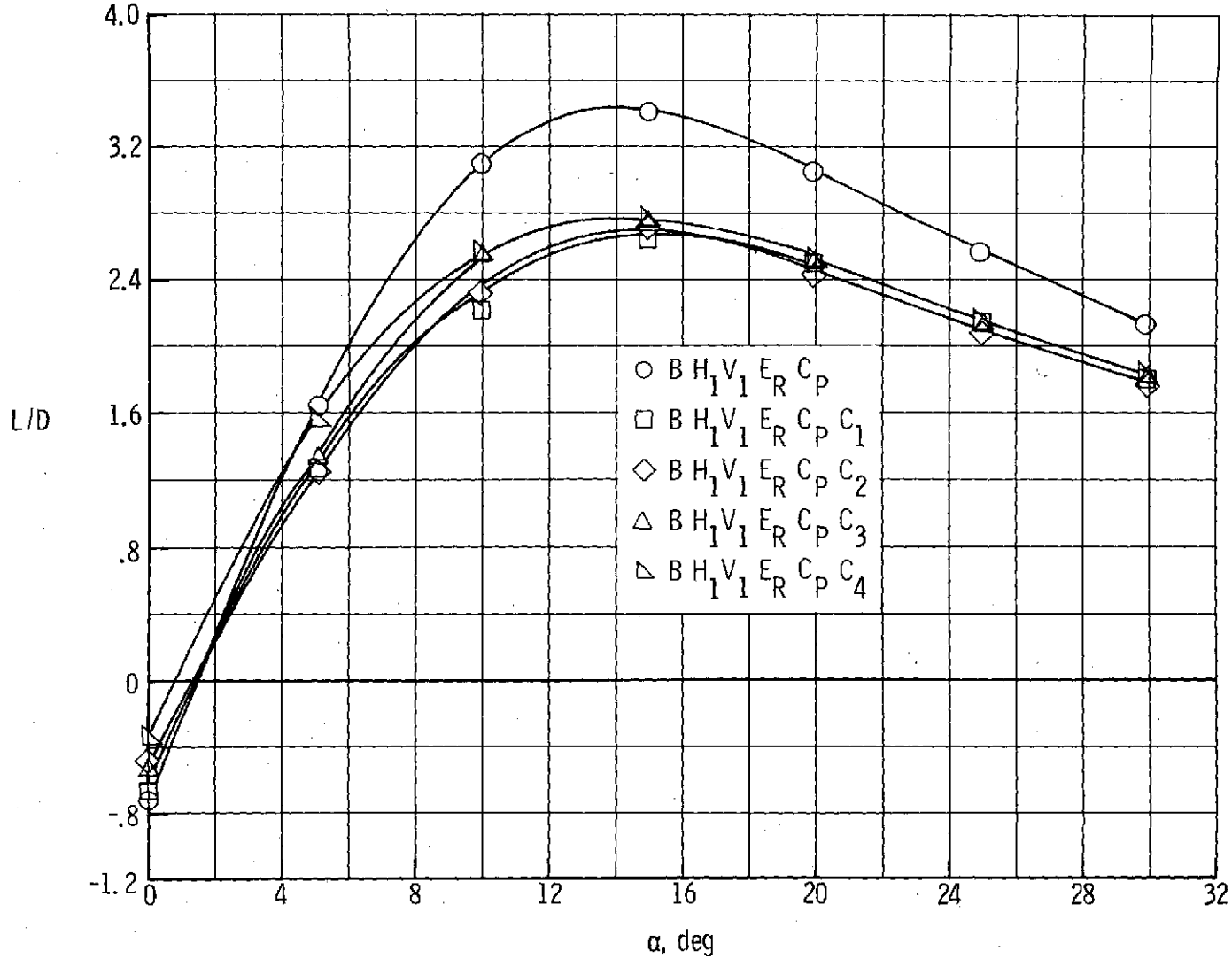

(c) Lift-drag ratio.

Figure 8. - Continued.

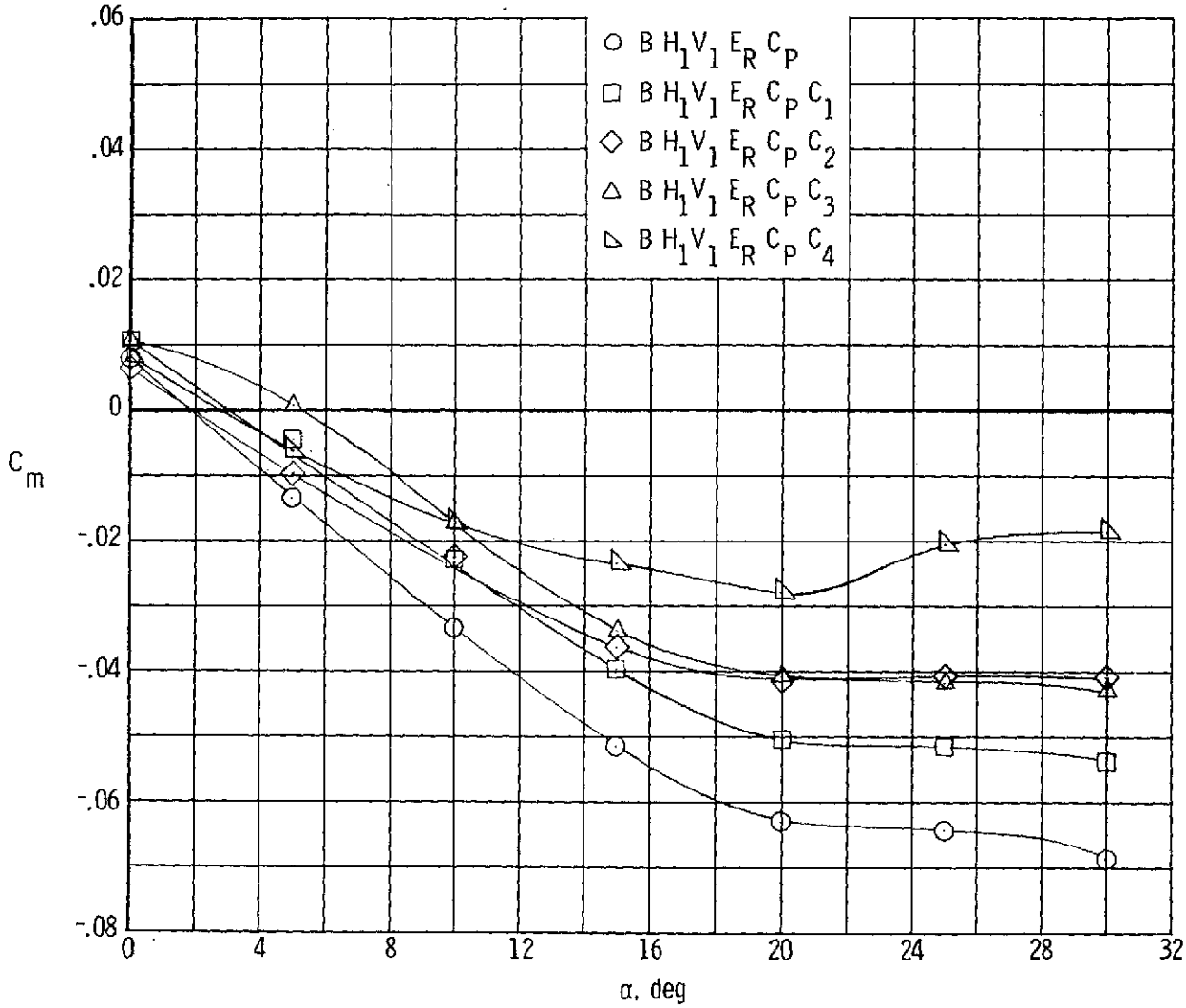

(d) Pitch.

Figure 8.- Continued.

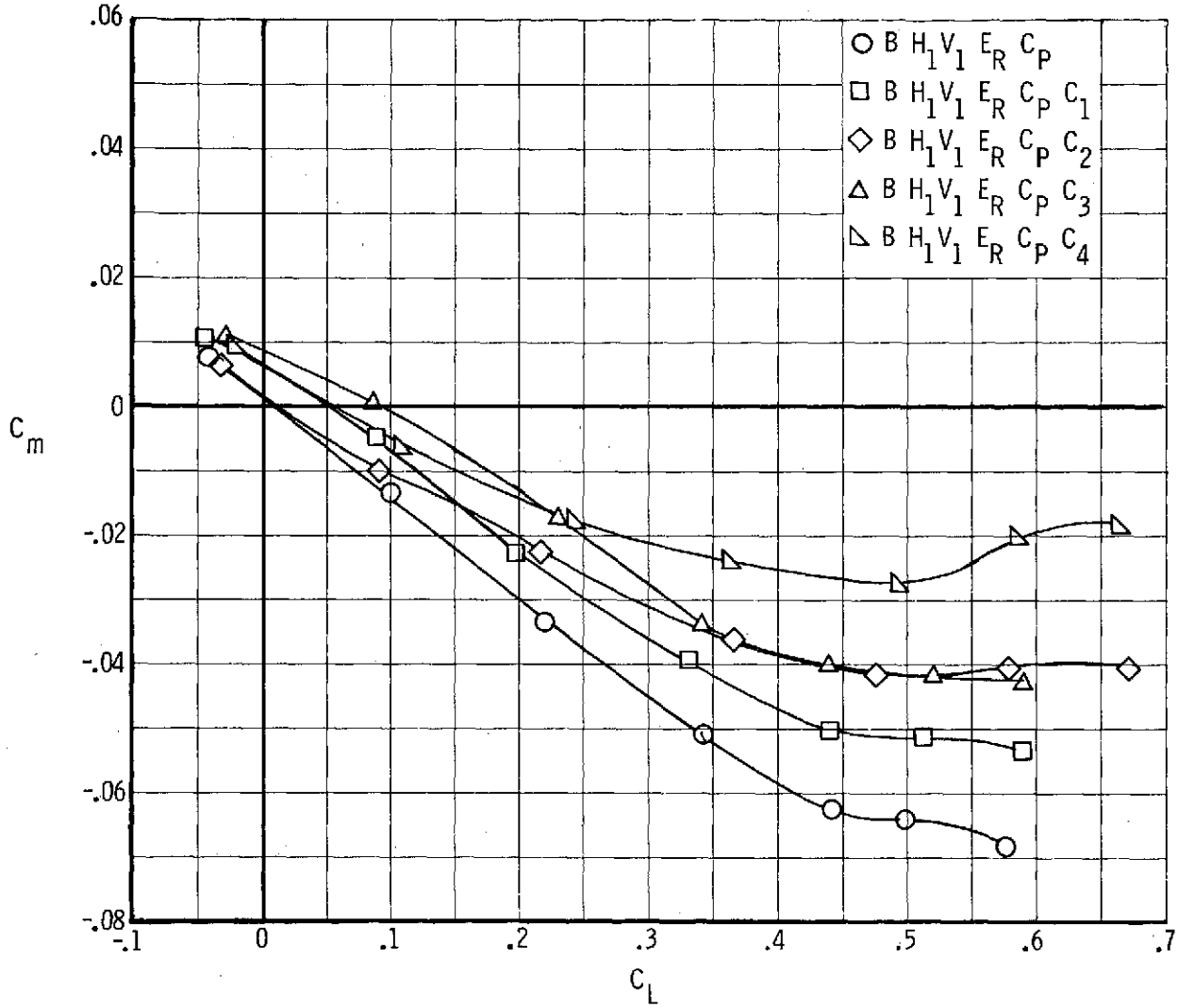

(e) Stability.

Figure 8.- Concluded.

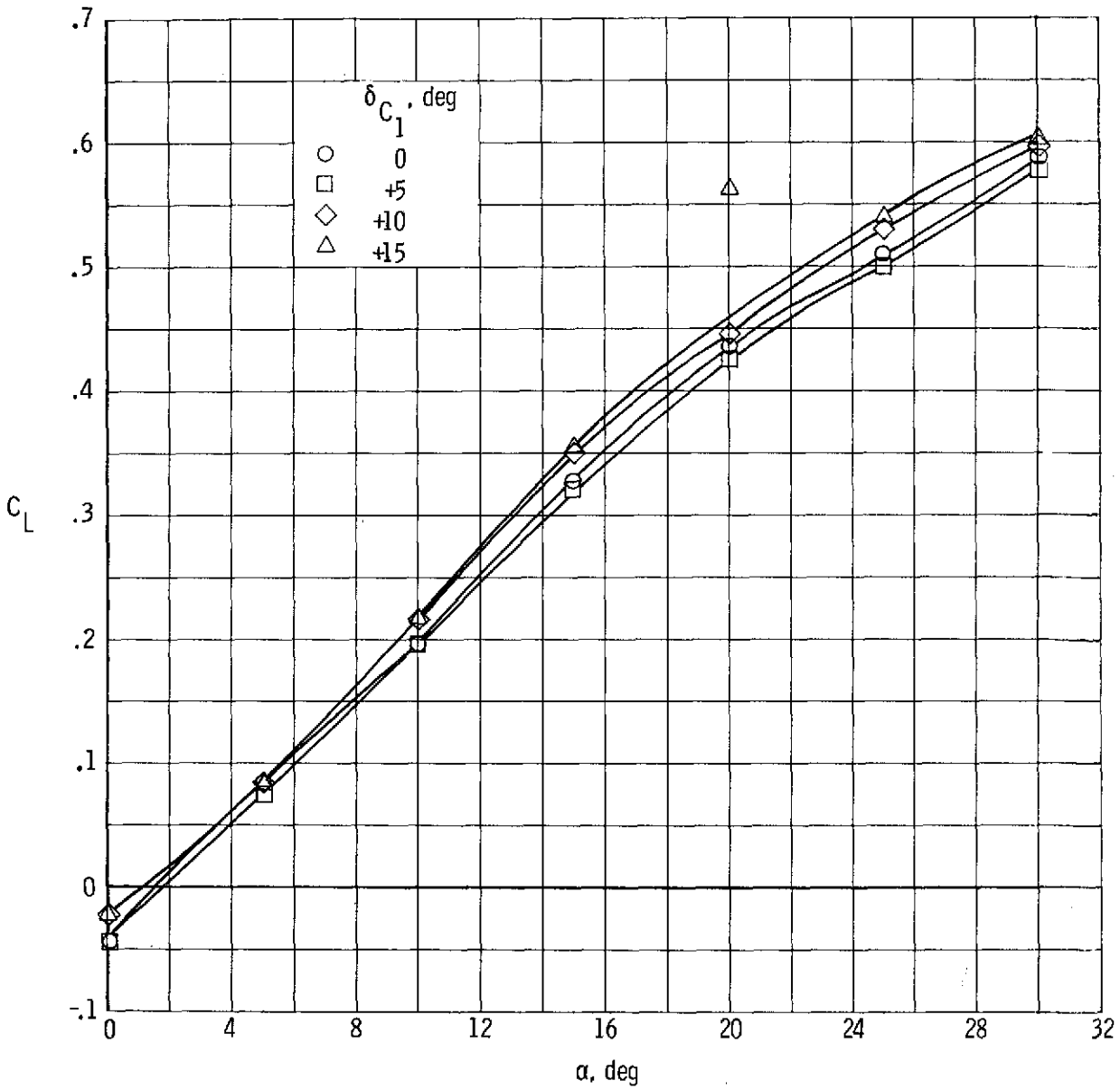

(a) Lift.

Figure 9.- Longitudinal characteristics of model $BH_1V_1E_RC_PC_1$ (body, small tails, retracted engine, canopy, and small trapezoidal canards). $\delta_{H_1} = 0^o$.

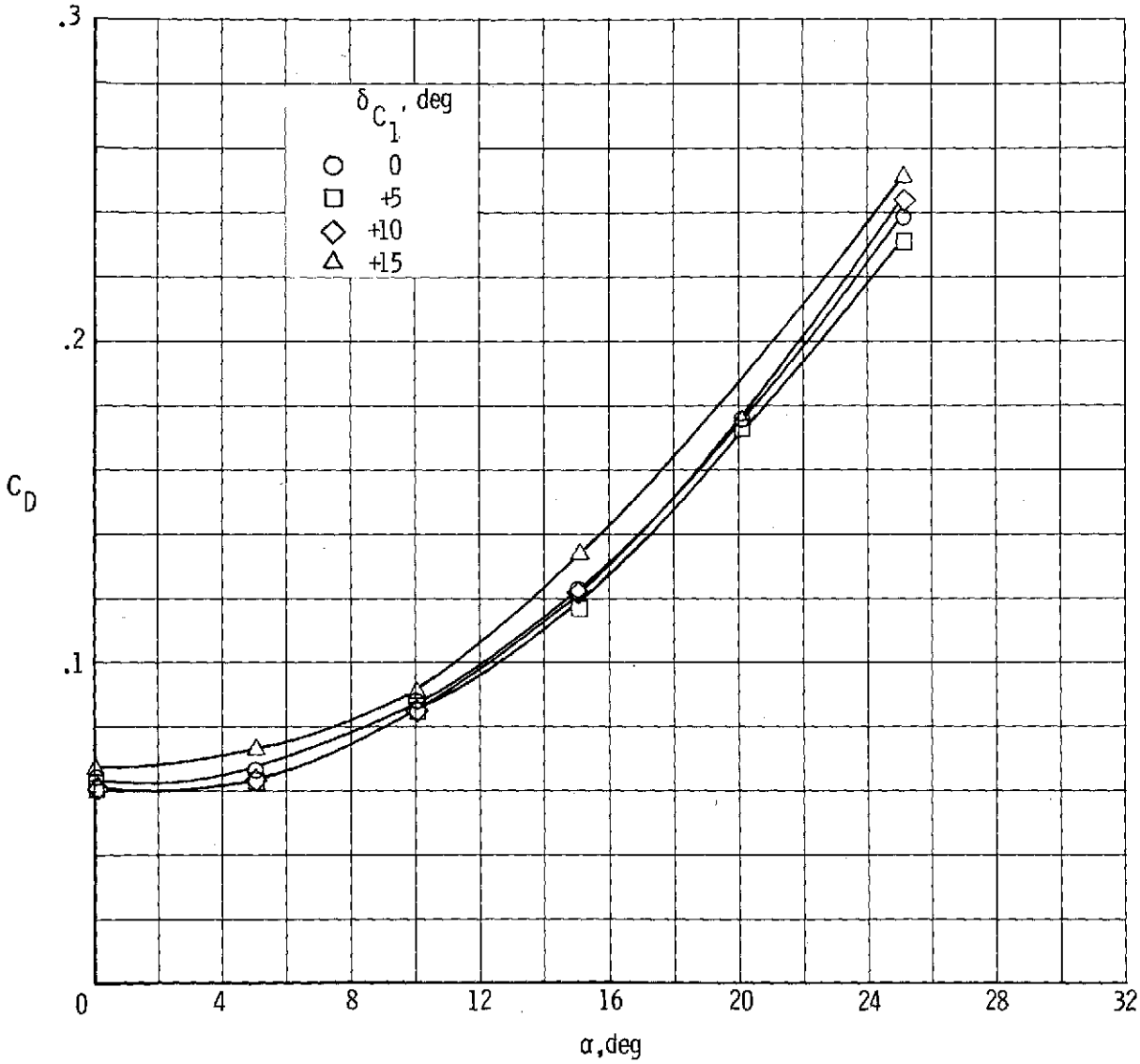

(b) Drag.

Figure 9.- Continued.

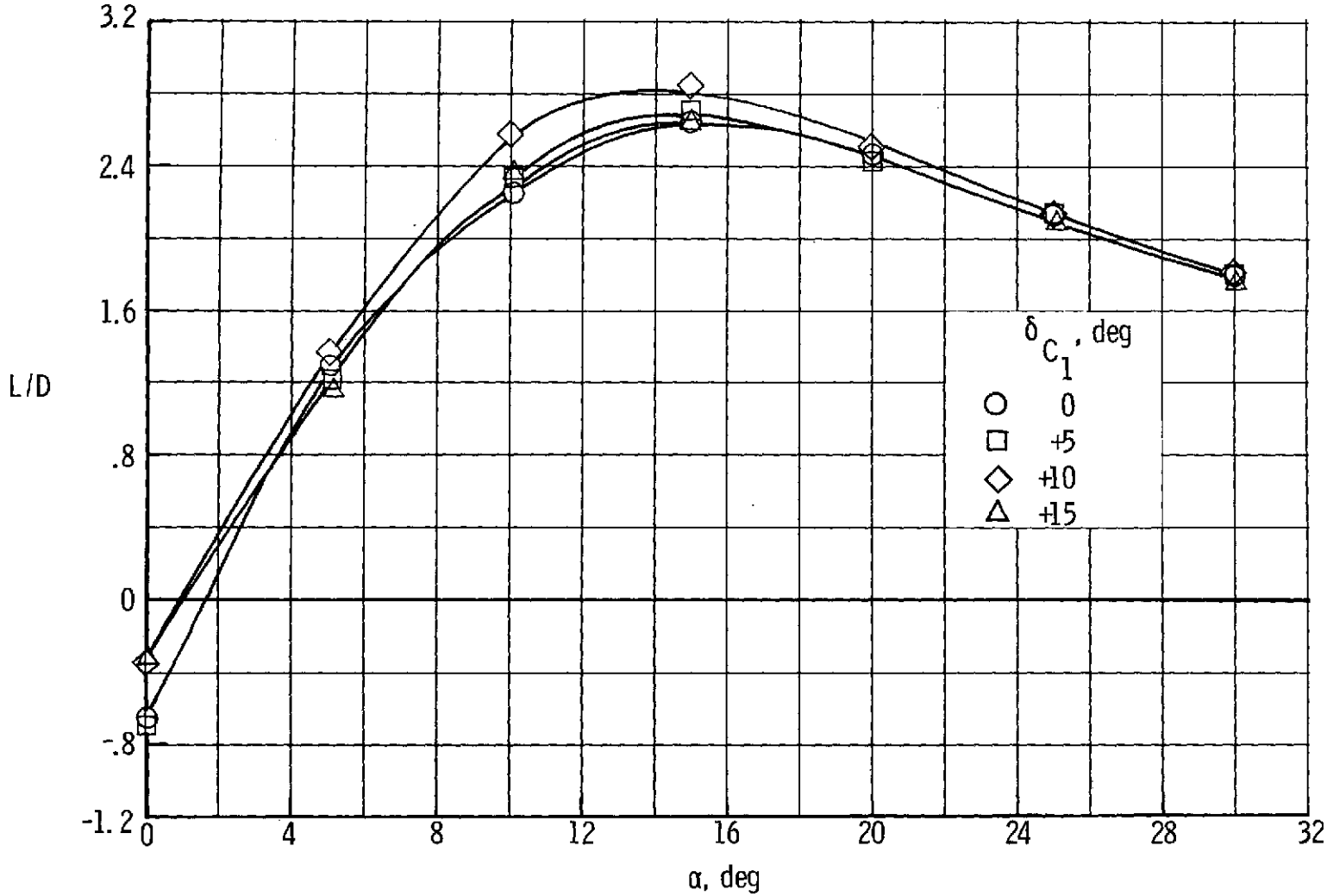

(c) Lift-drag ratio.

Figure 9.- Continued.

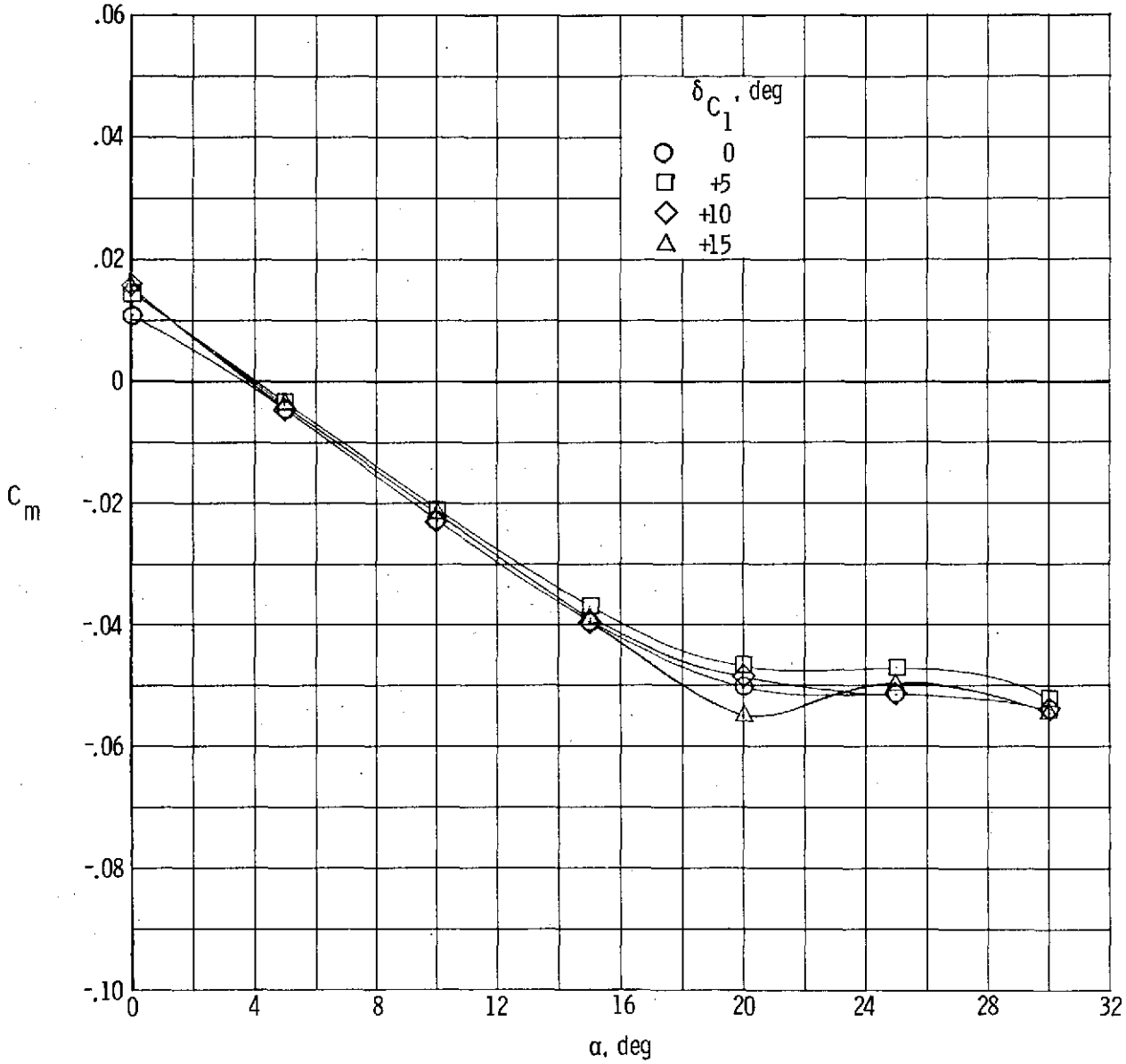

(d) Pitch.

Figure 9.- Continued.

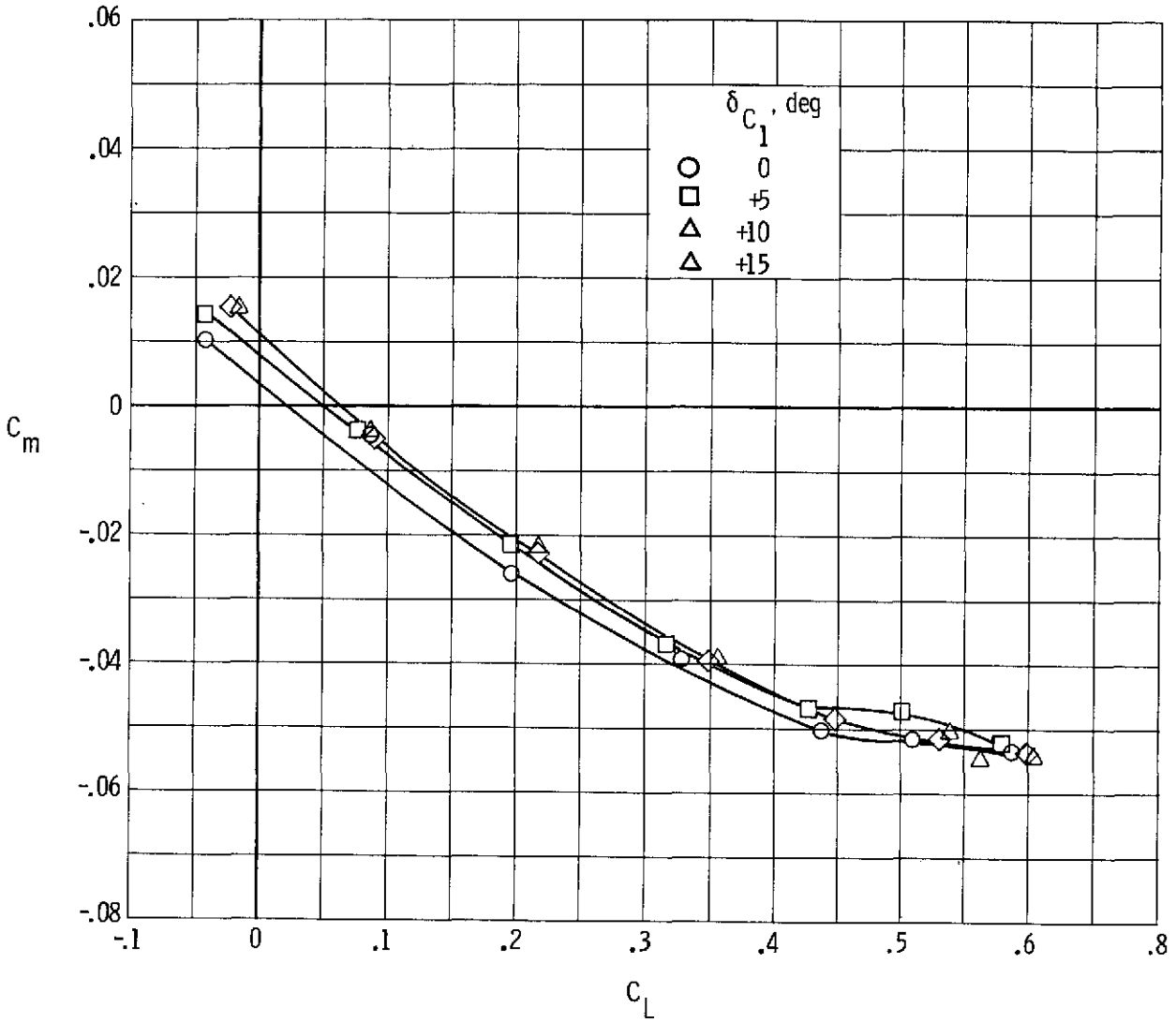

(e) Stability.

Figure 9.- Concluded.

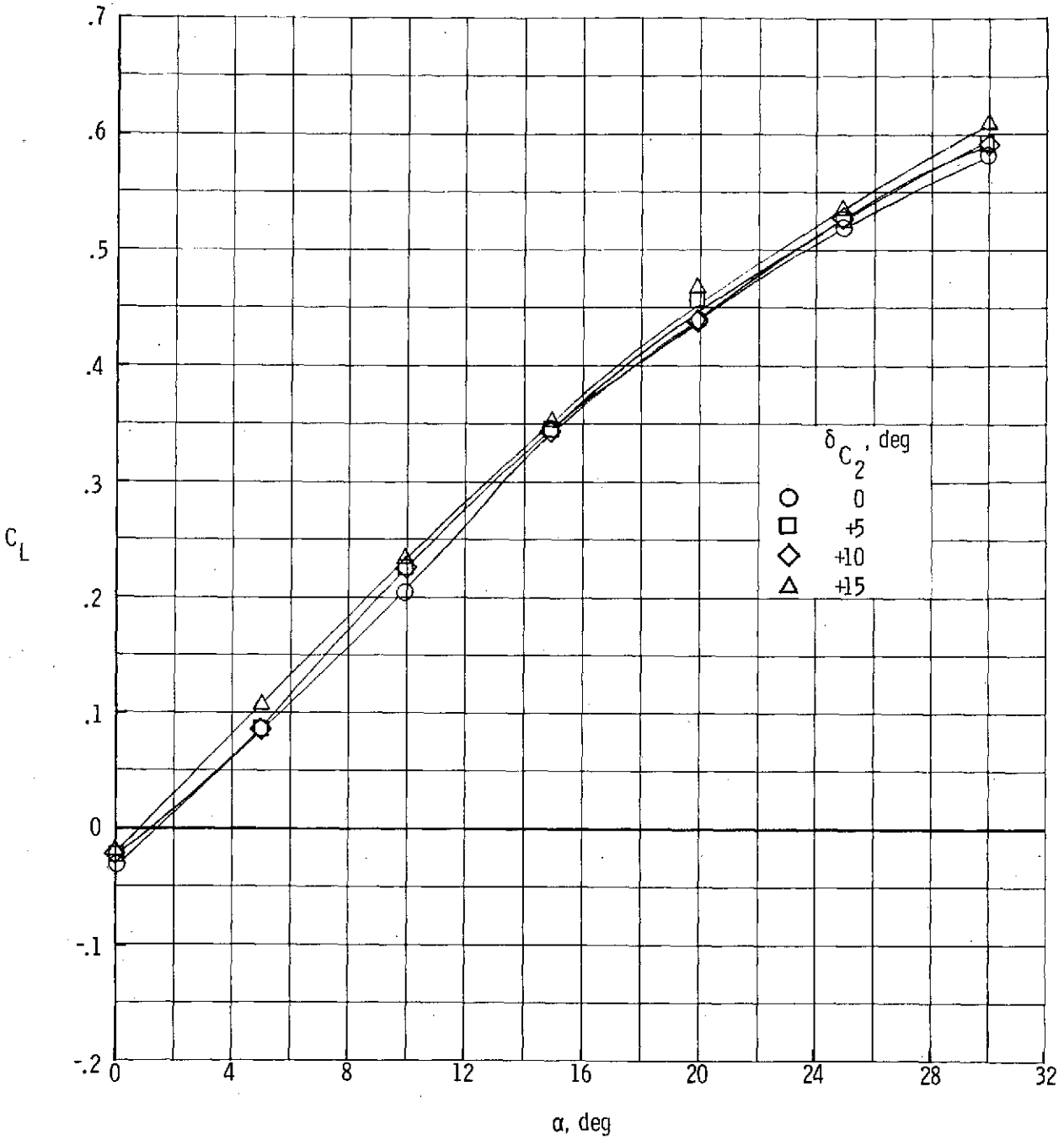

(a) Lift.

Figure 10.- Longitudinal characteristics of model $BH_1V_1E_RC_PC_2$ (body, small tails, retracted engine, canopy, and small delta canards).

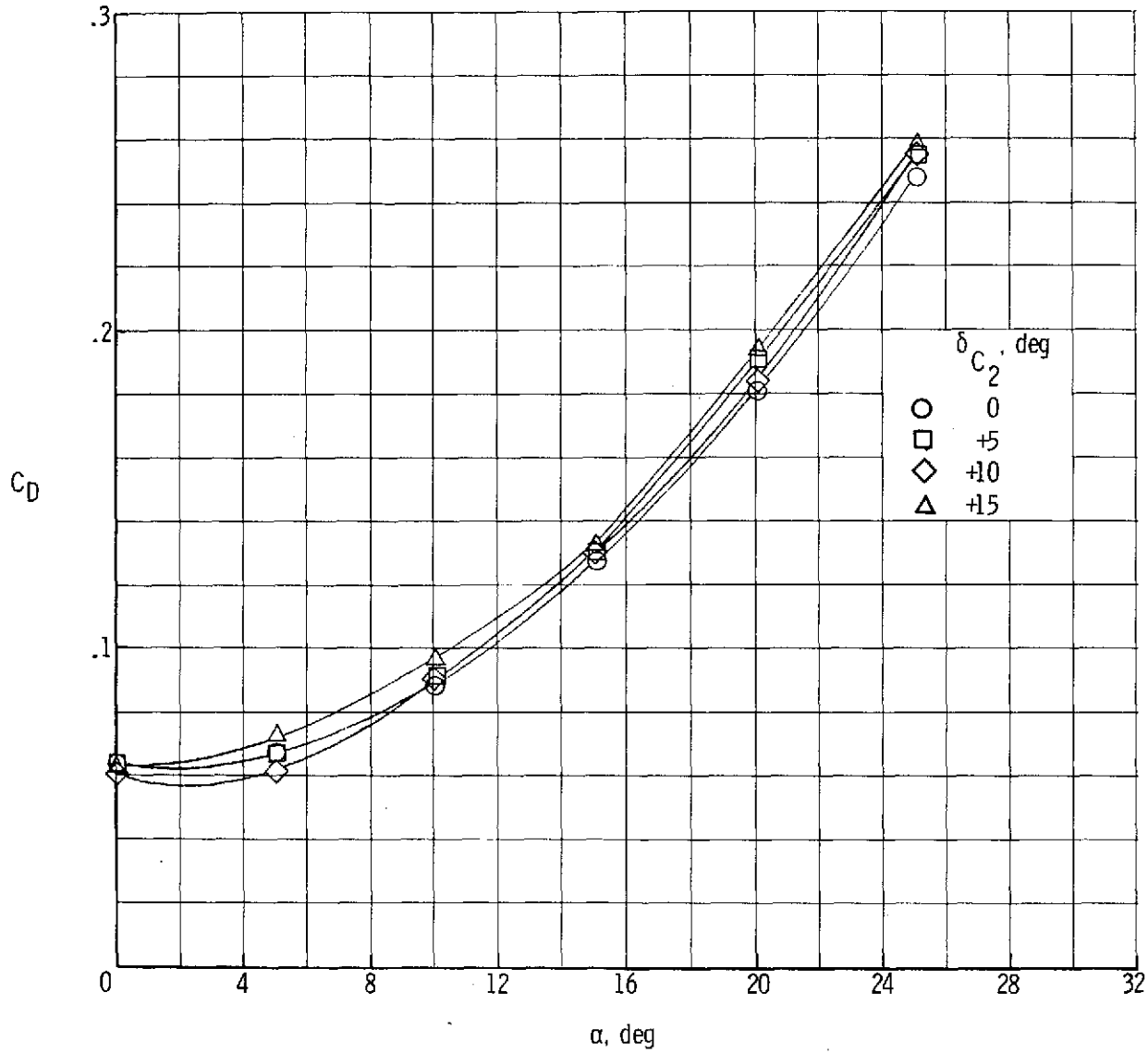

(b) Drag.

Figure 10.- Continued.

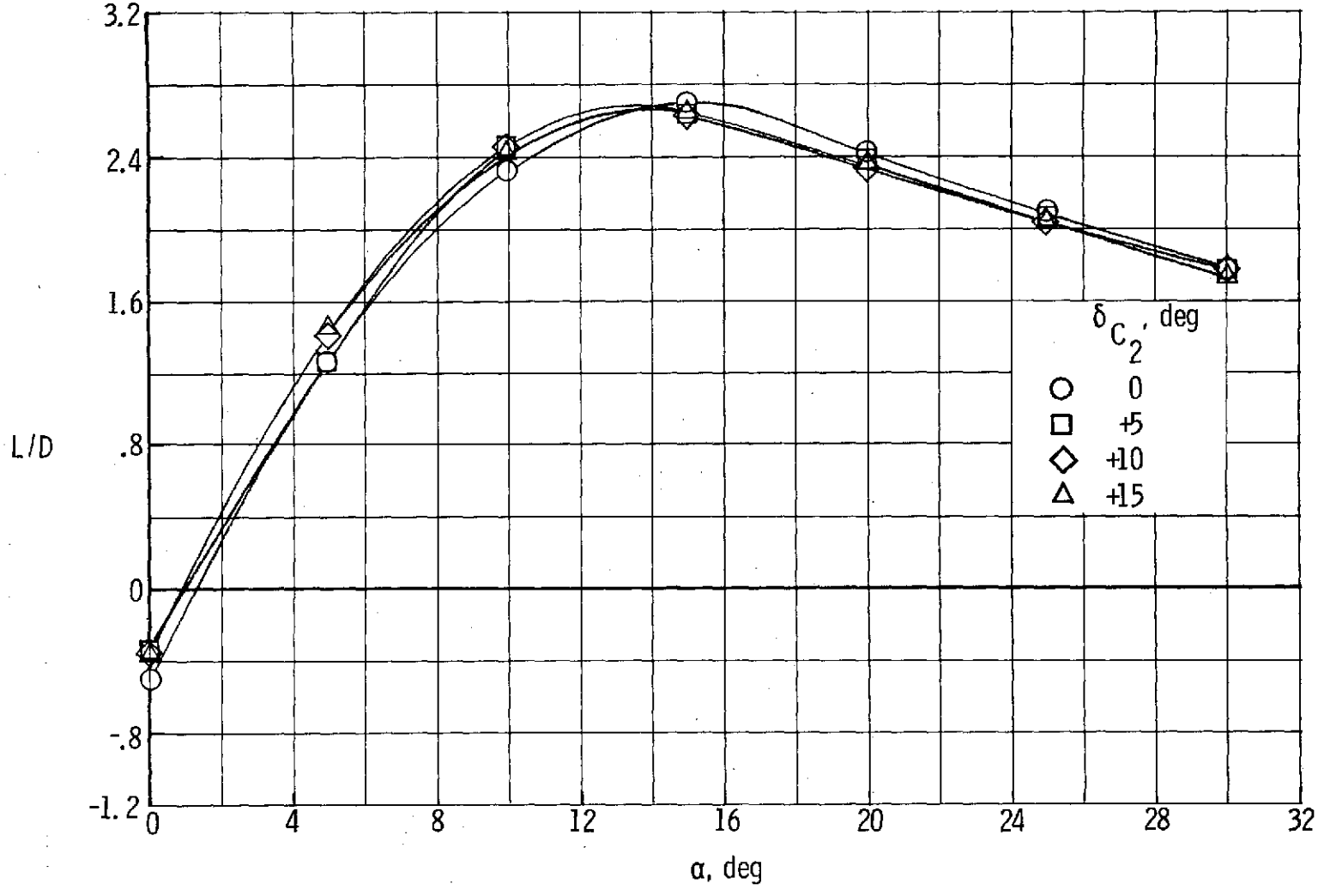

(c) Lift-drag ratio.

Figure 10.- Continued.

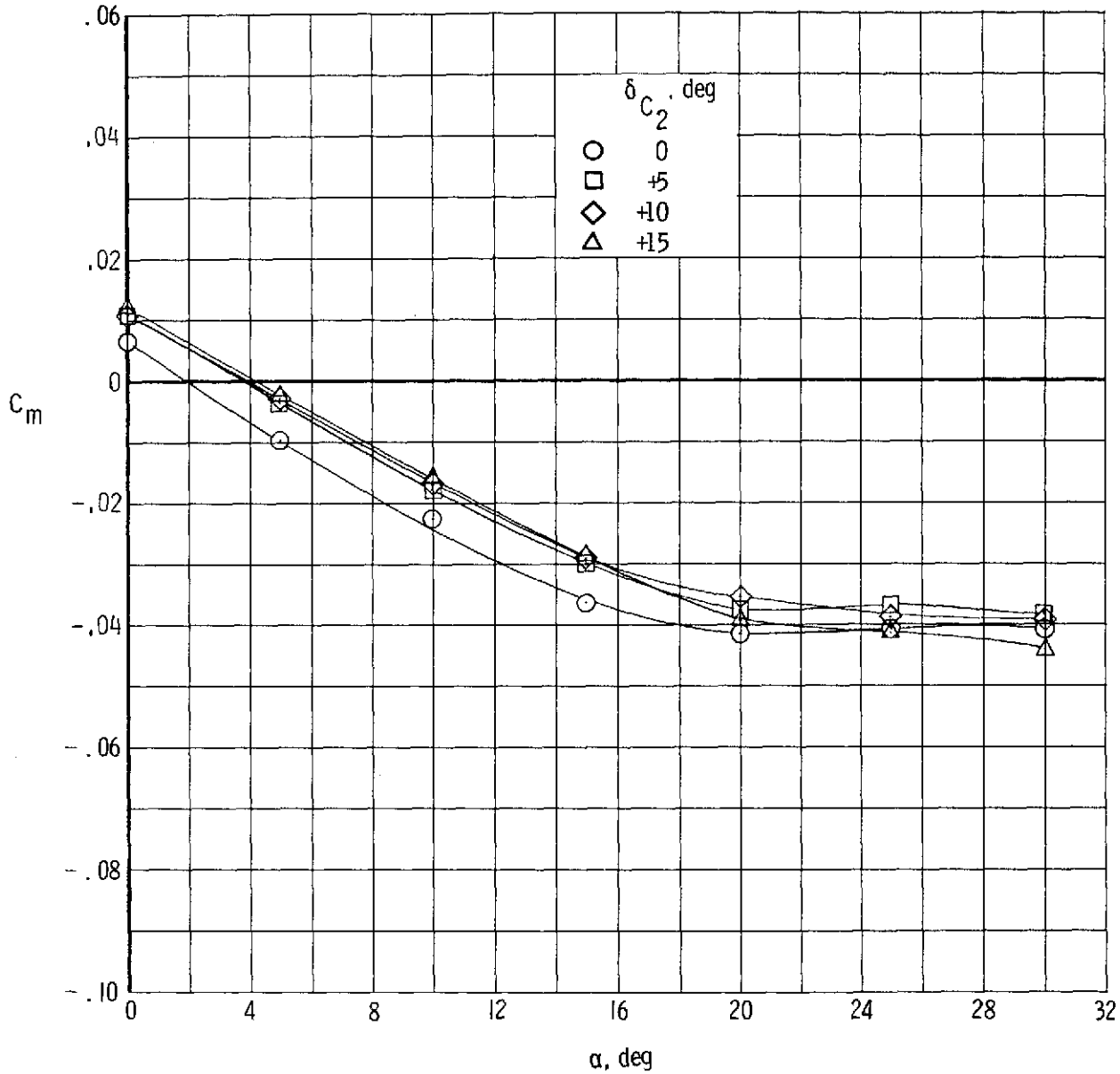

(d) Pitch.

Figure 10.- Continued.

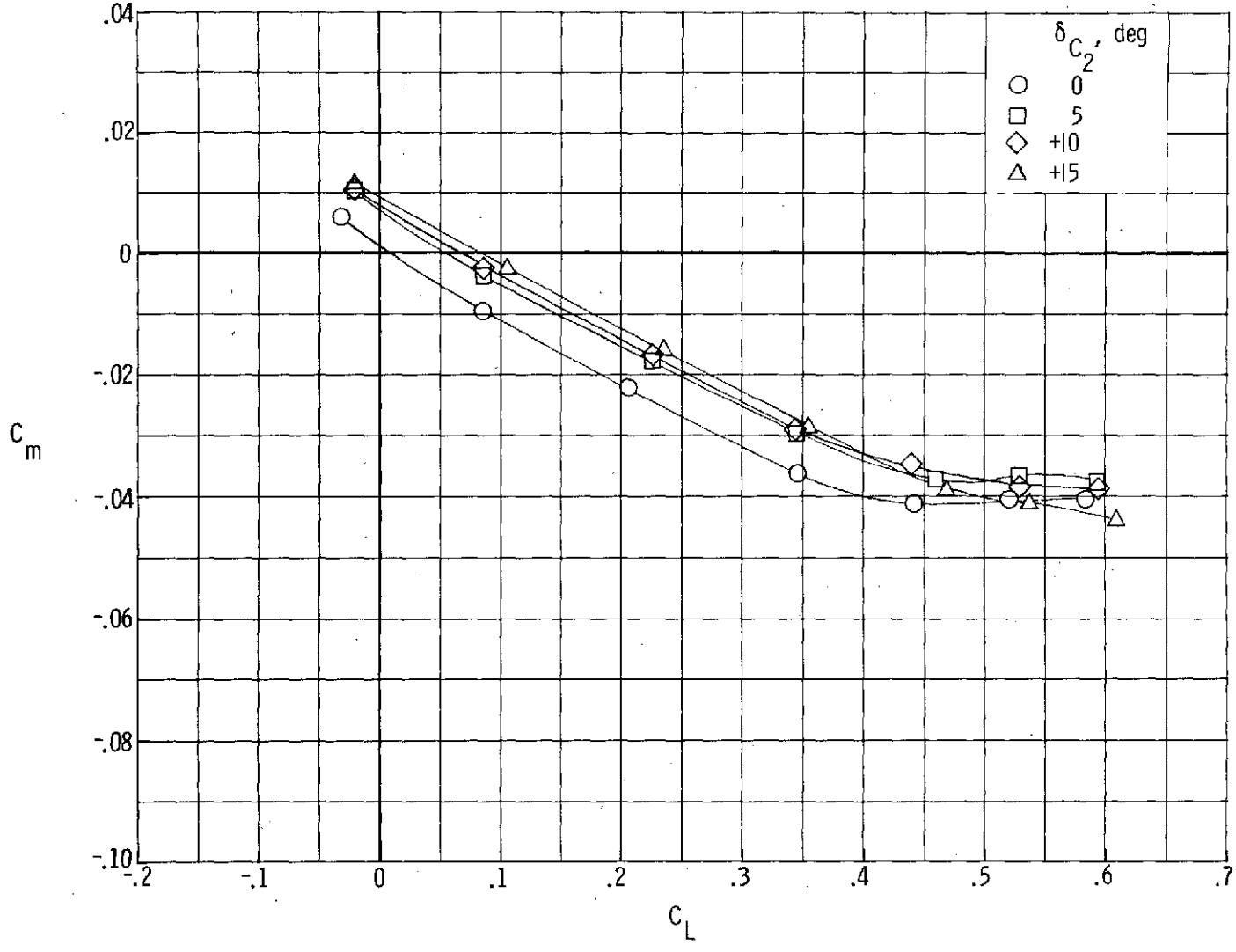

(e) Stability.

Figure 10.- Concluded.

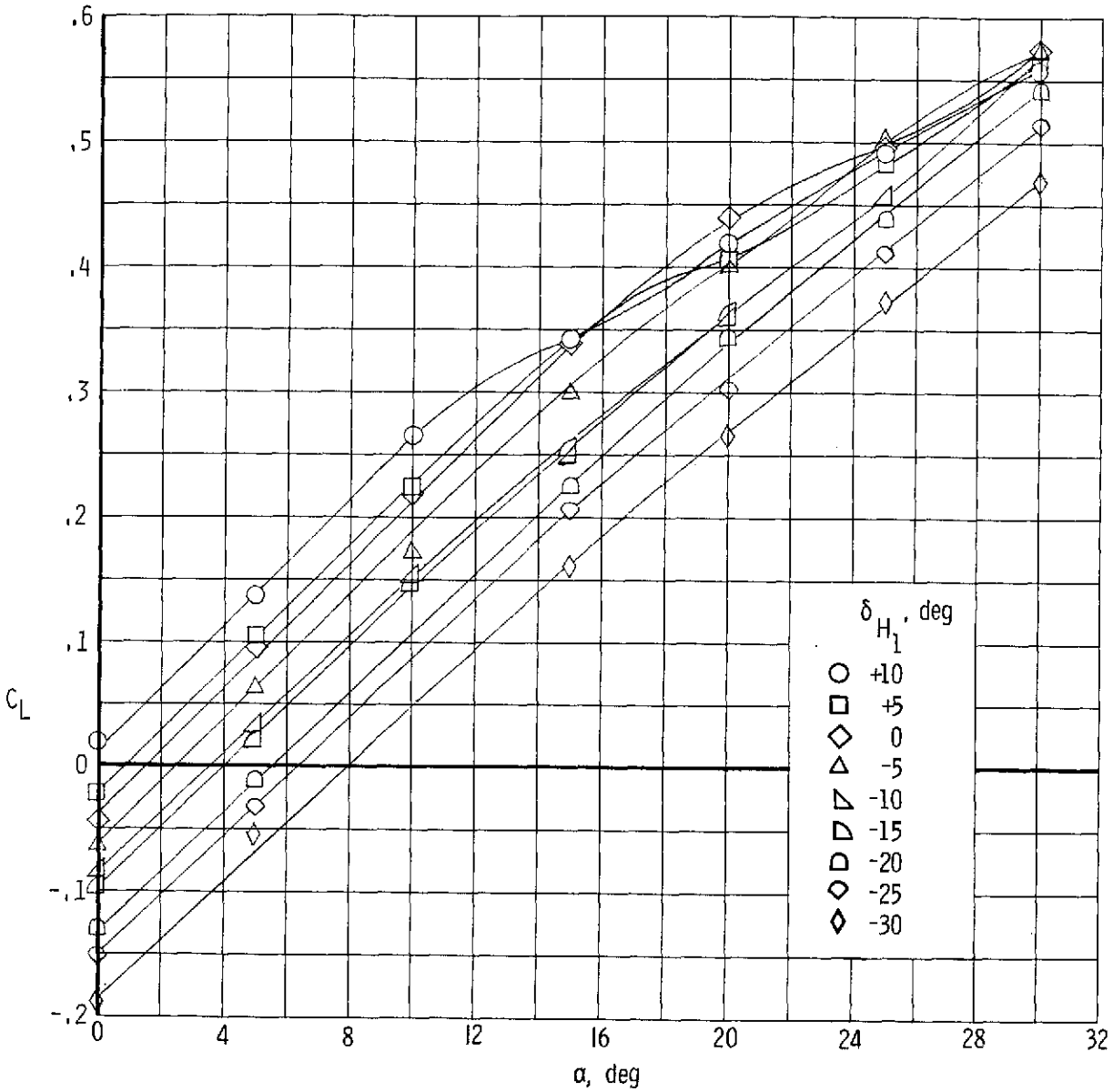

(a) Lift.

Figure 11.- Longitudinal characteristics of model $BH_1V_1E_RC_P$ (body, small tails, retracted engine, and canopy).

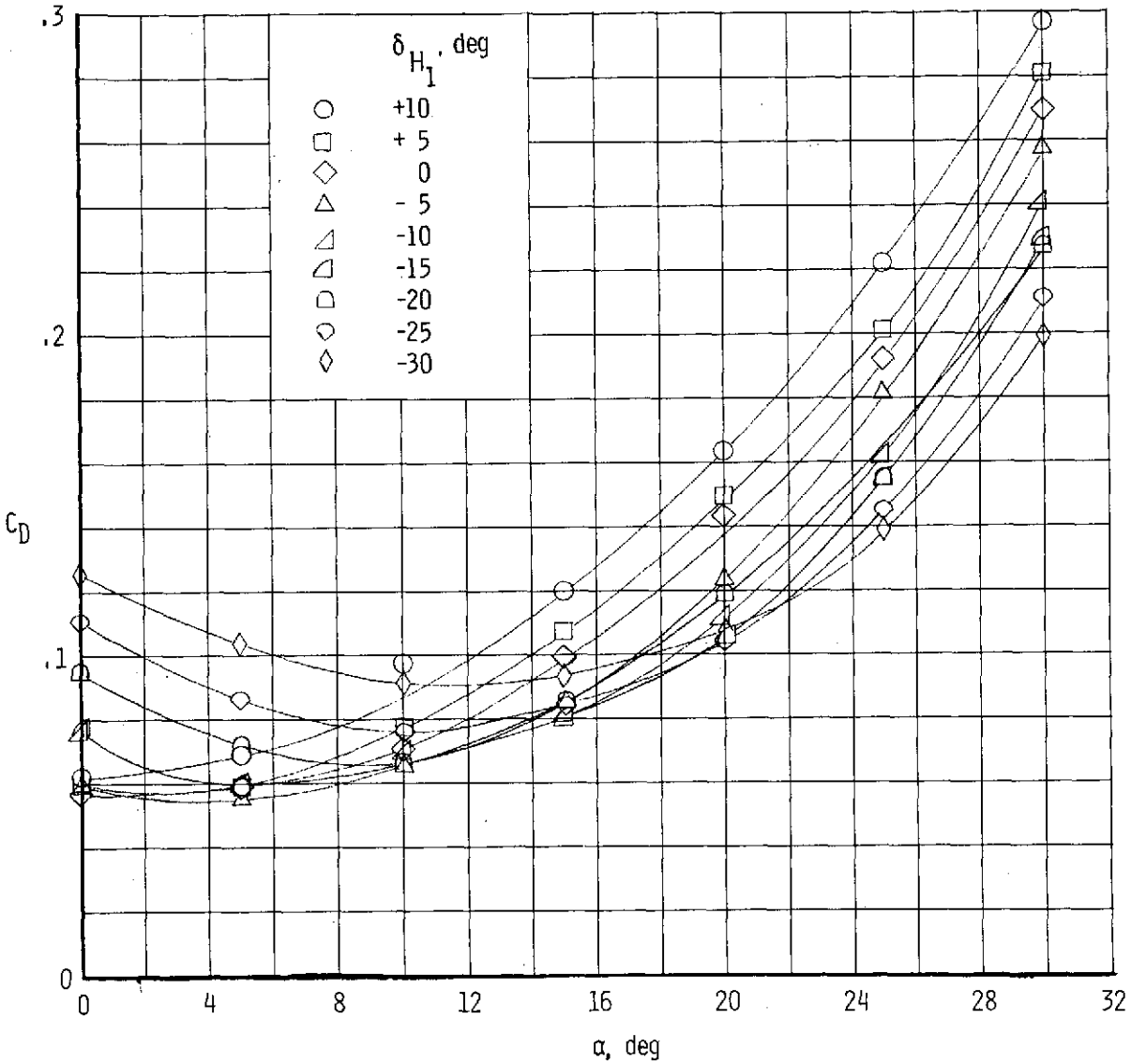

(b) Drag.

Figure 11.- Continued.

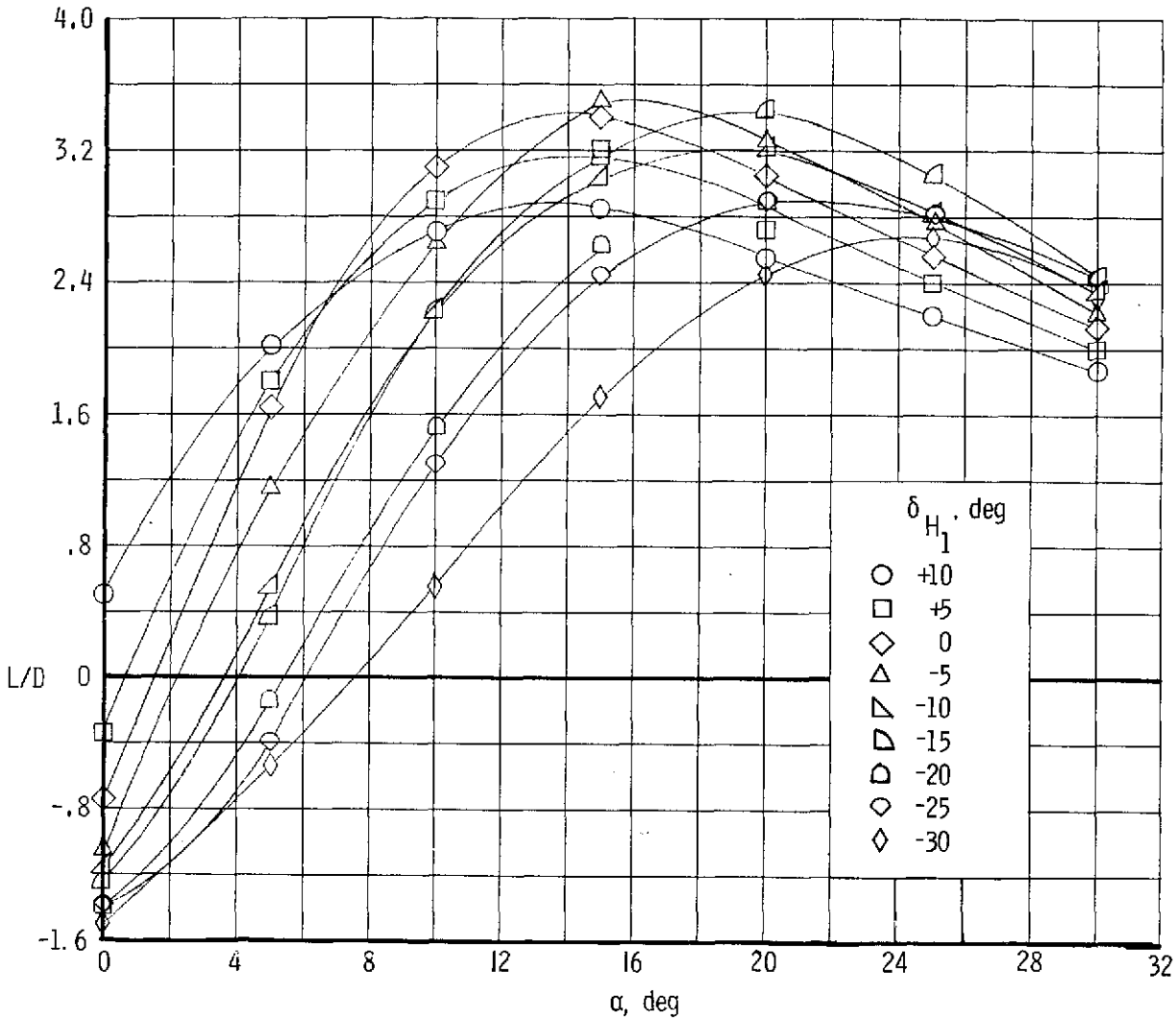

(c) Lift-drag ratio.

Figure 11.- Continued.

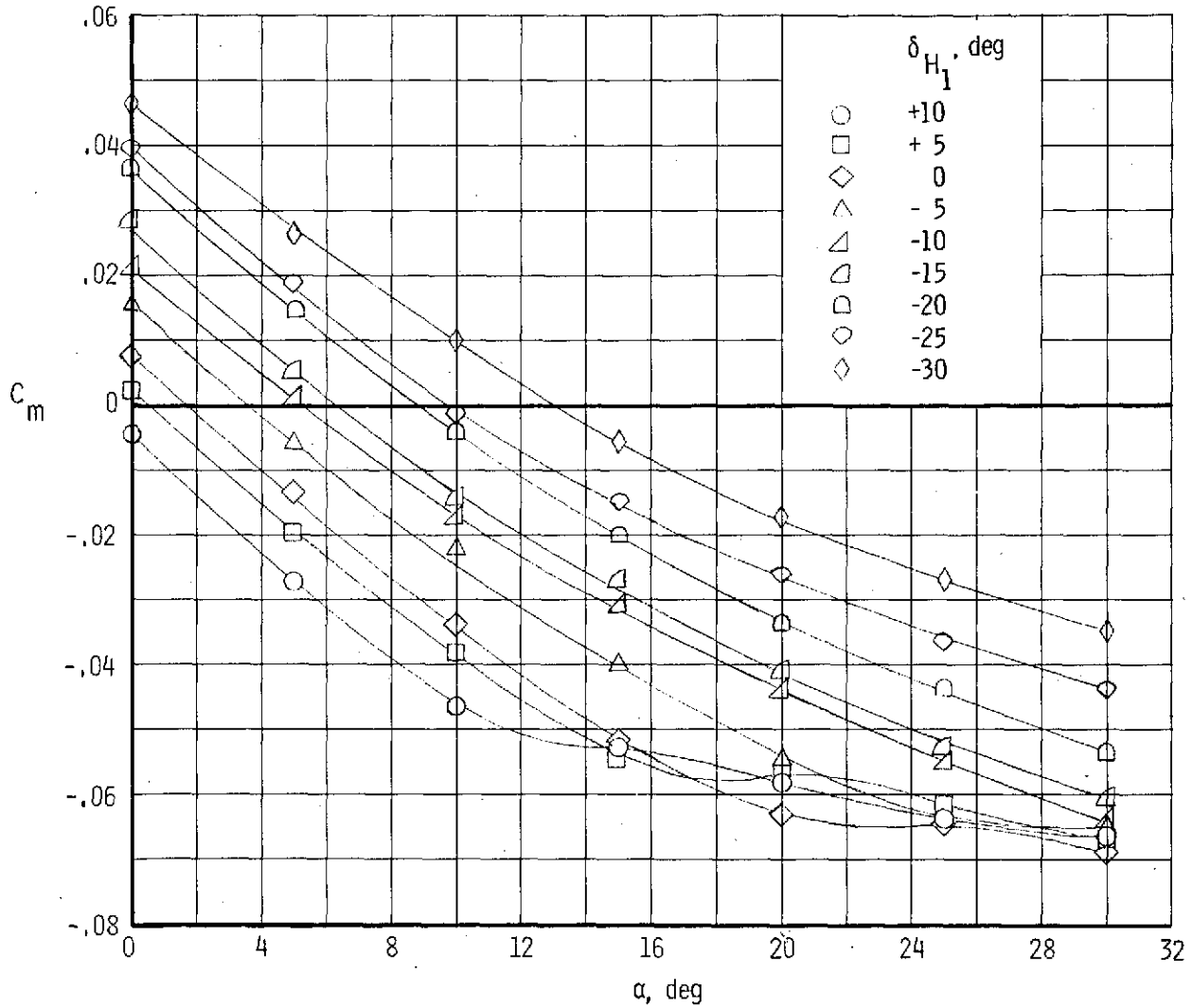

(d) Pitch.

Figure 11.- Continued.

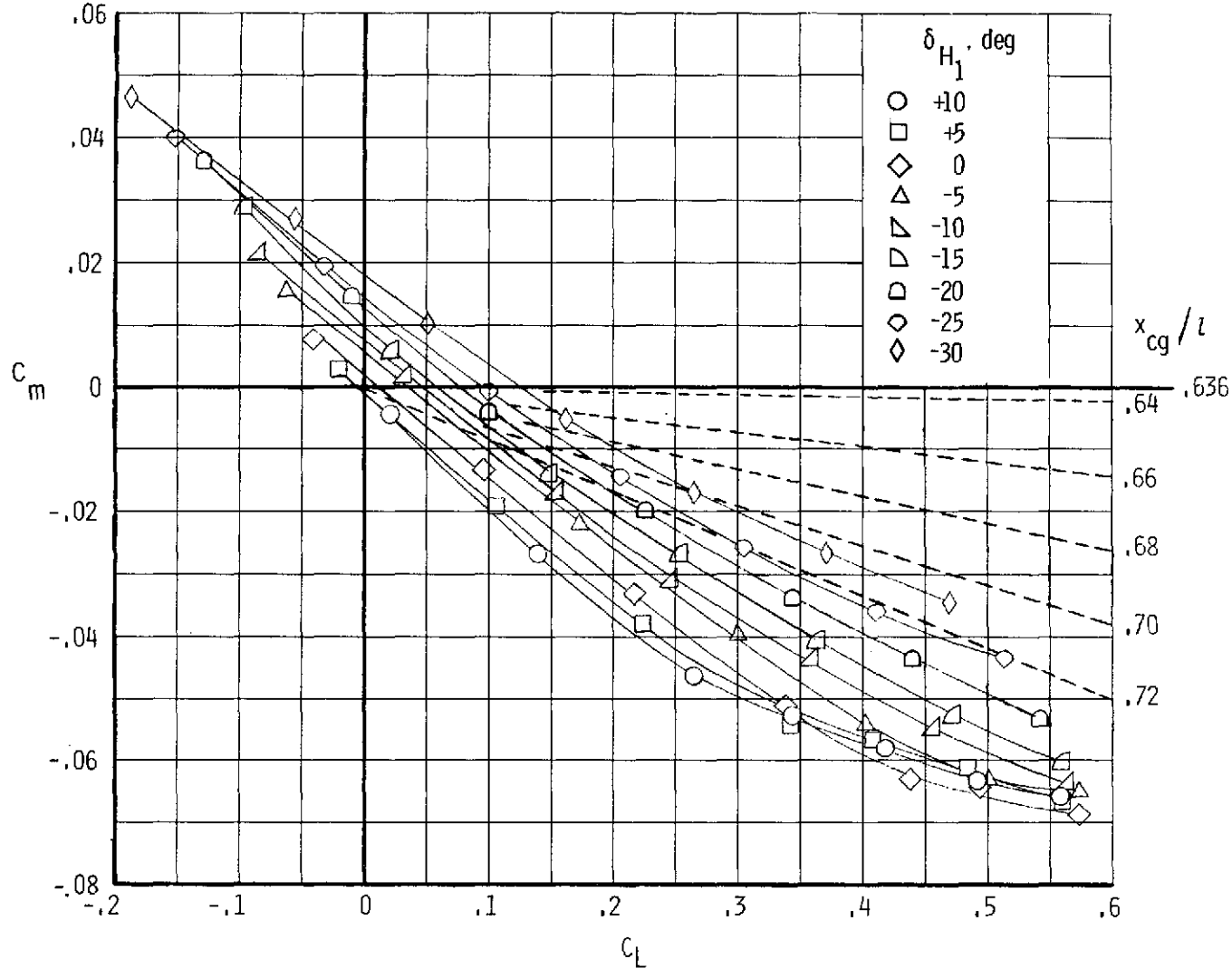

(e) Stability.

Figure 11.- Concluded.

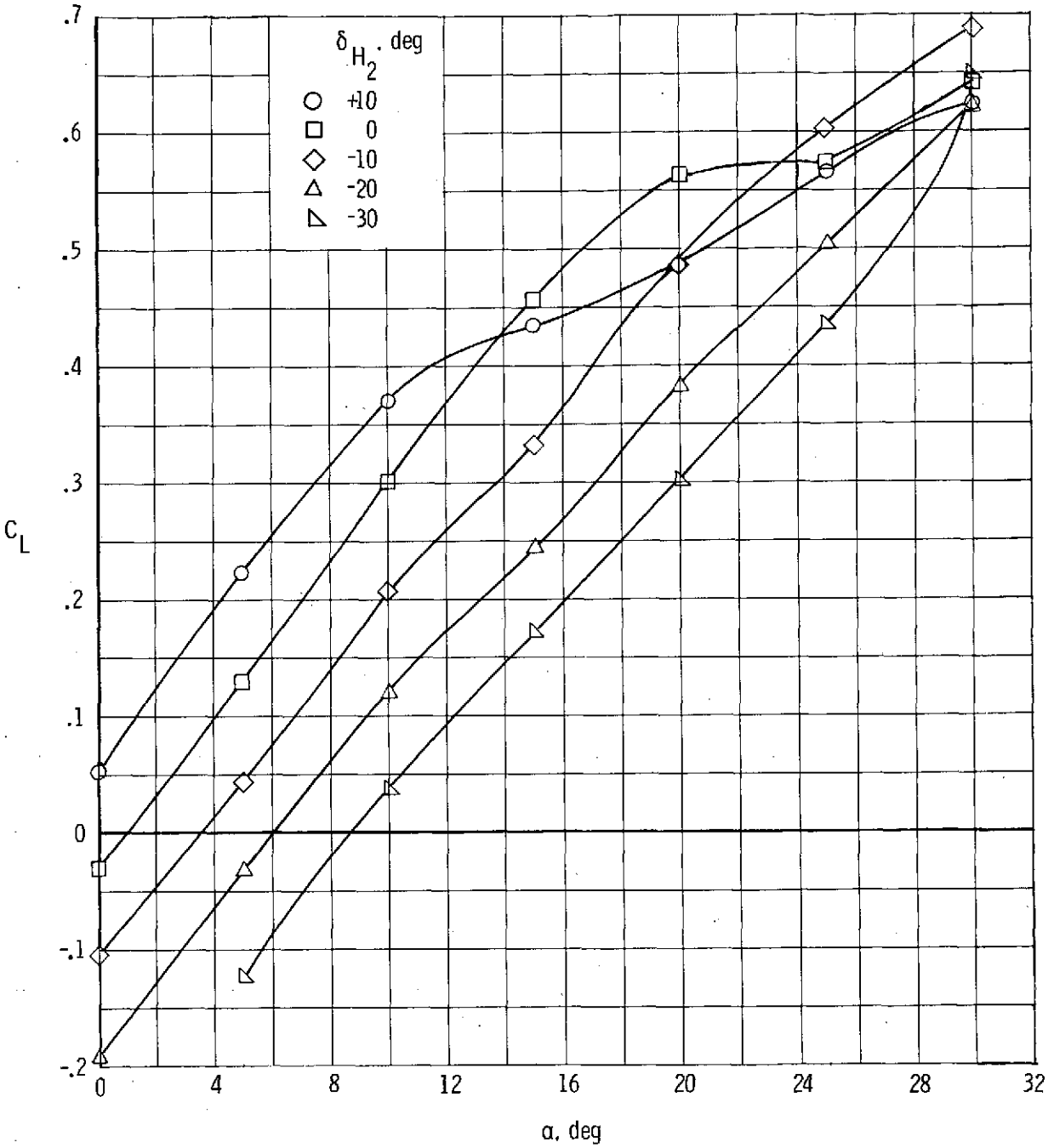

(a) Lift.

Figure 12.- Longitudinal characteristics of model $BH_2V_2E_RC_P$ (body, large tails, retracted engine, and canopy).

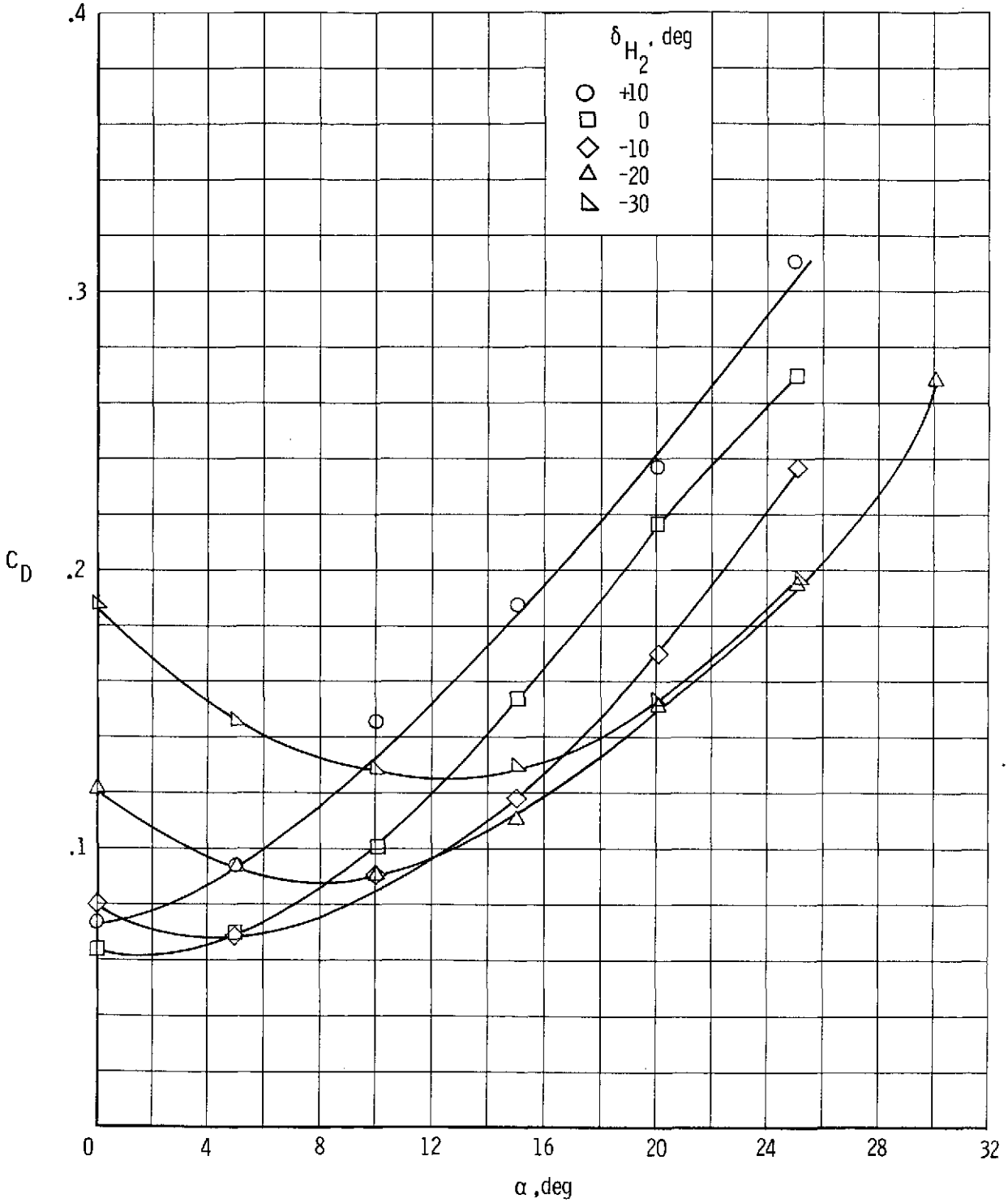

(b) Drag.

Figure 12.- Continued.

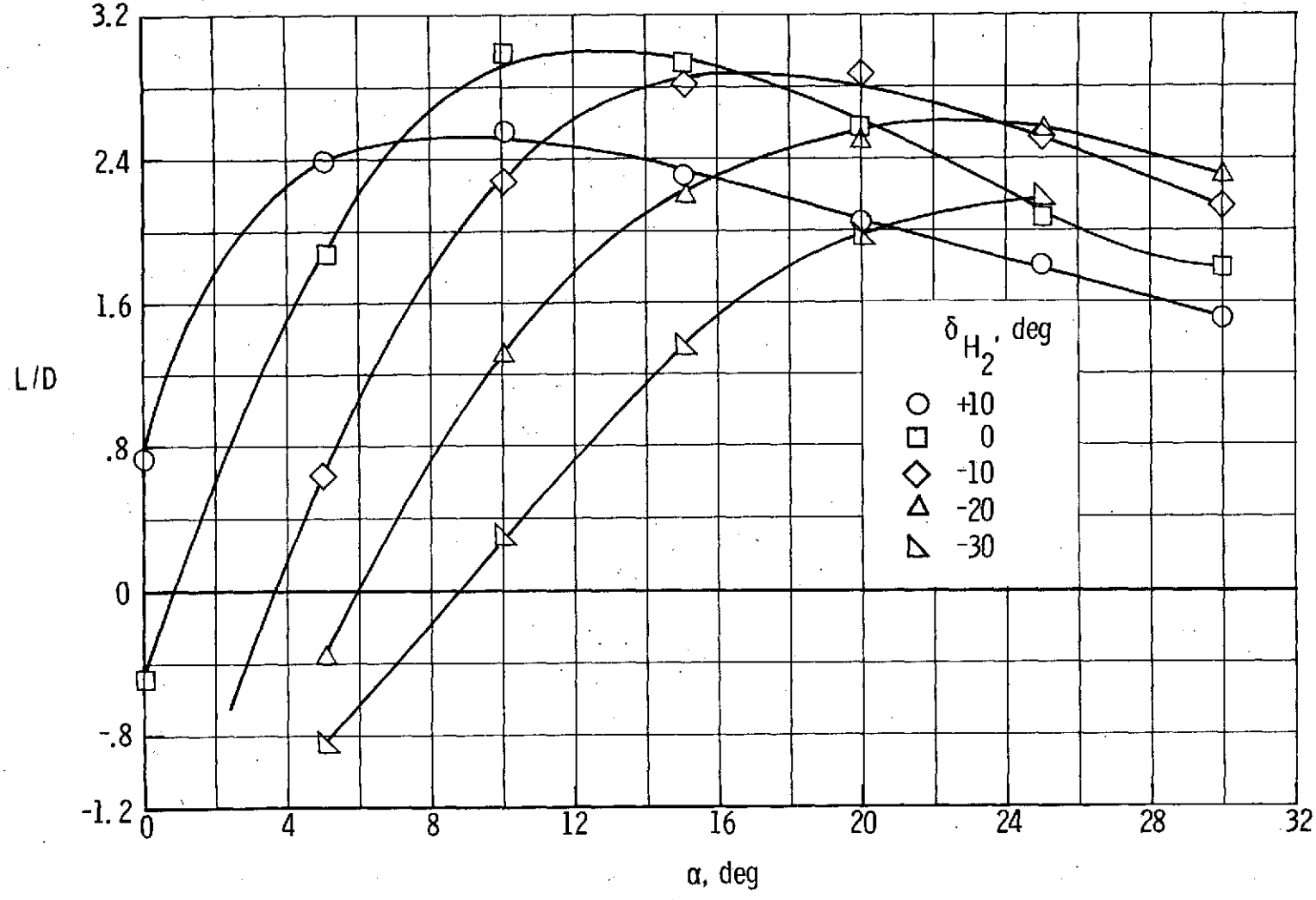

(c) Lift-drag ratio.

Figure 12.- Continued.

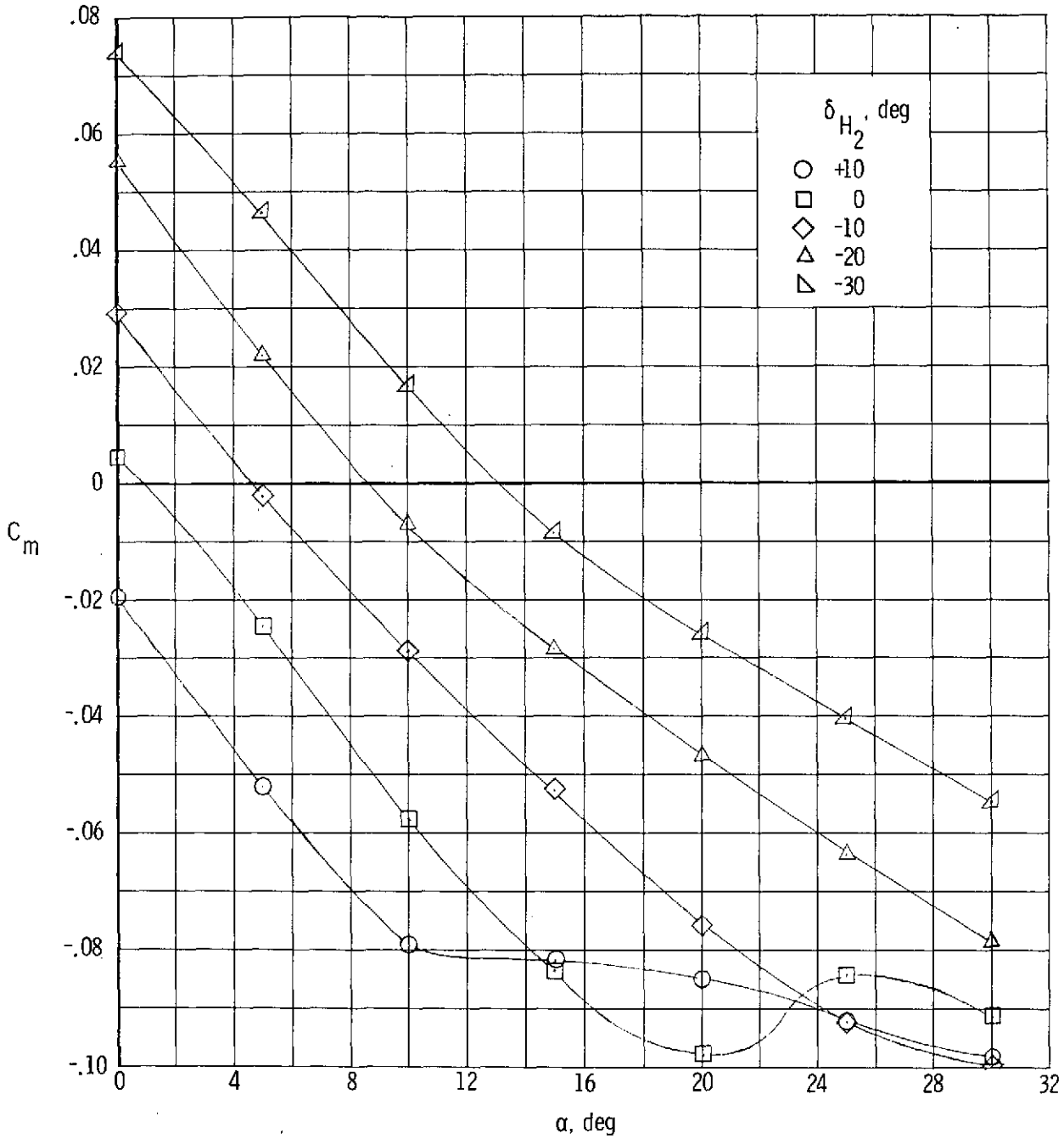

(d) Pitch.

Figure 12.- Continued.

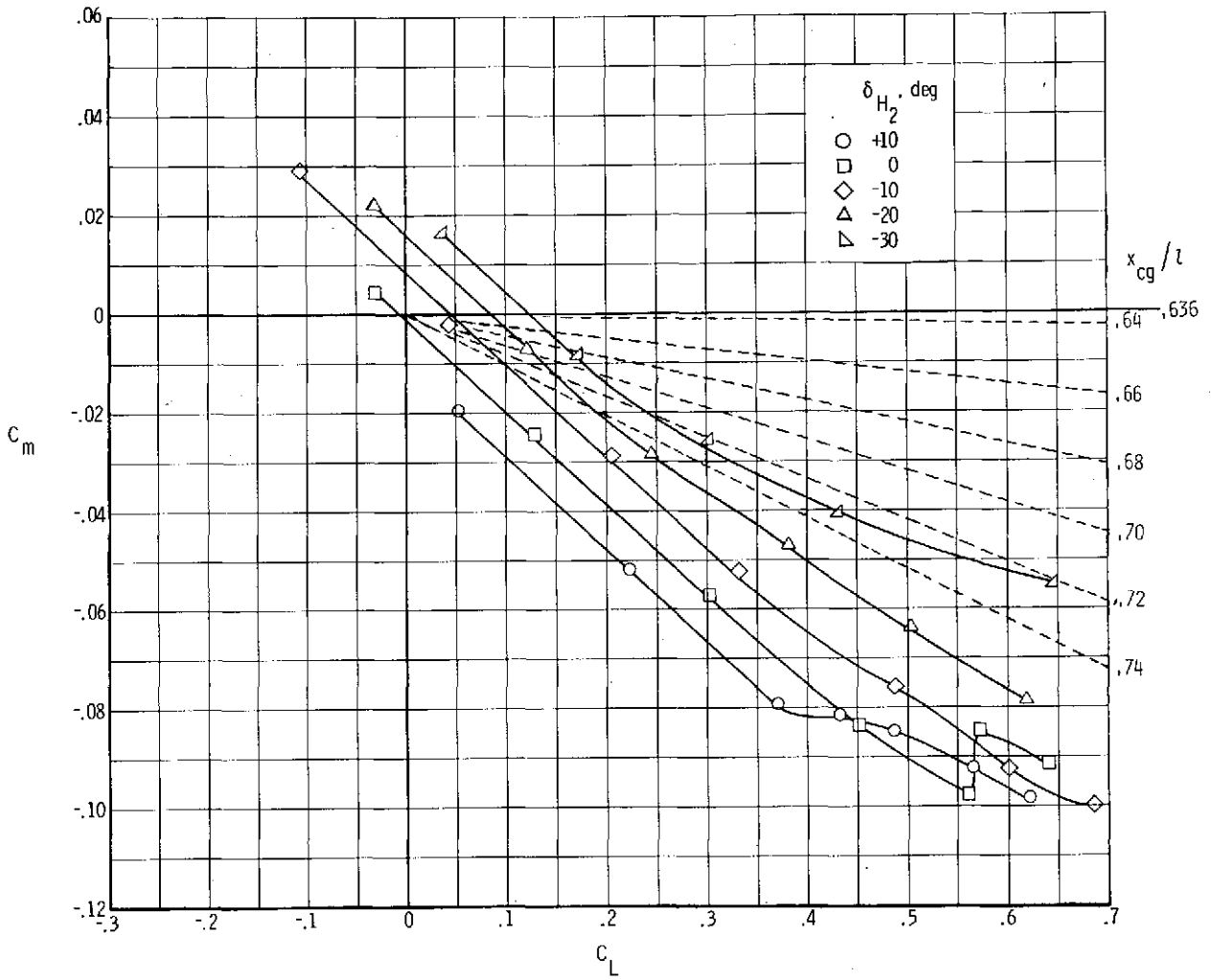

(e) Stability.

Figure 12.- Concluded.

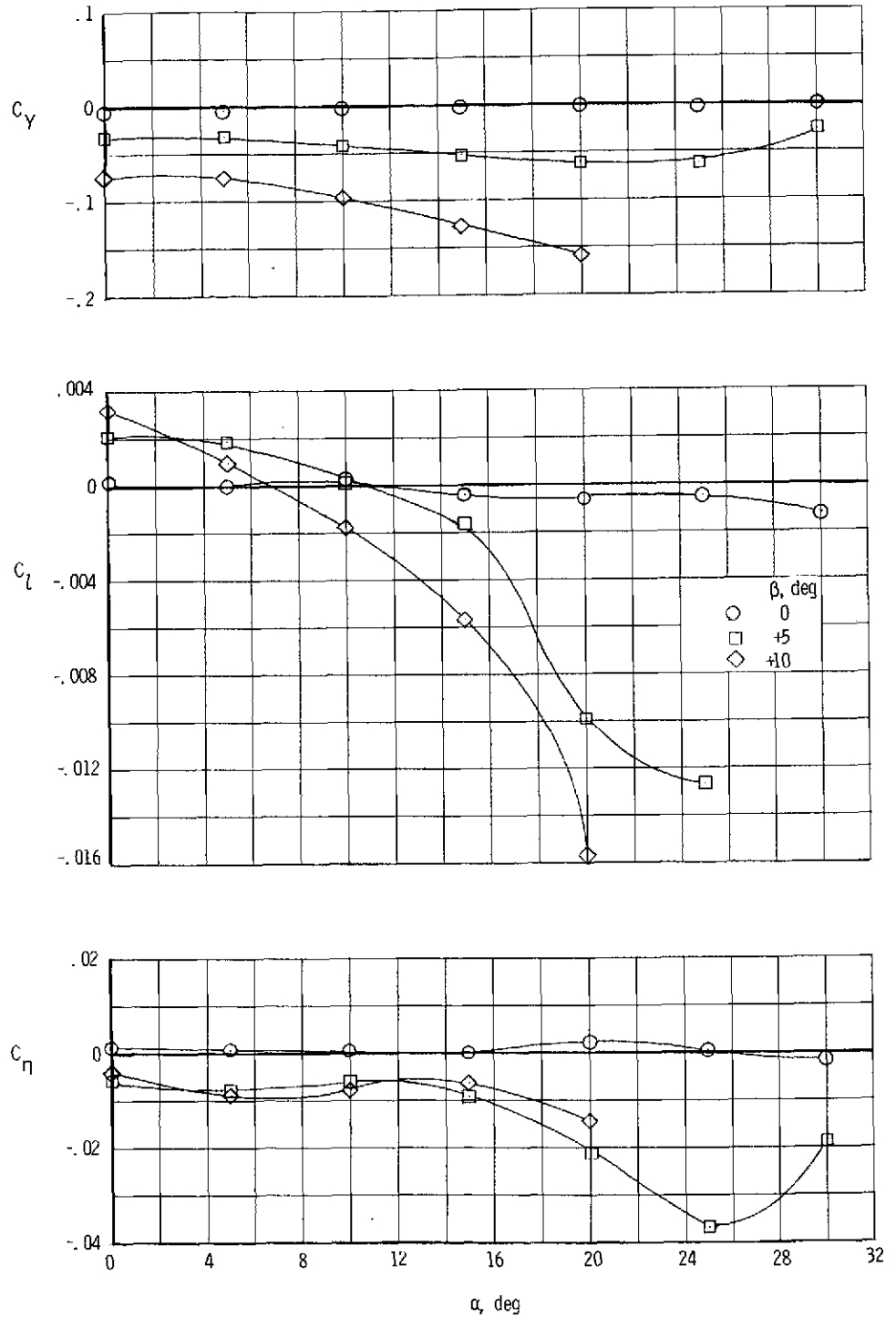

Figure 13.- Variation of side force and rolling and yawing moments with angle of attack at various angles of sideslip for $B_1H_1V_1E_RC_P$.

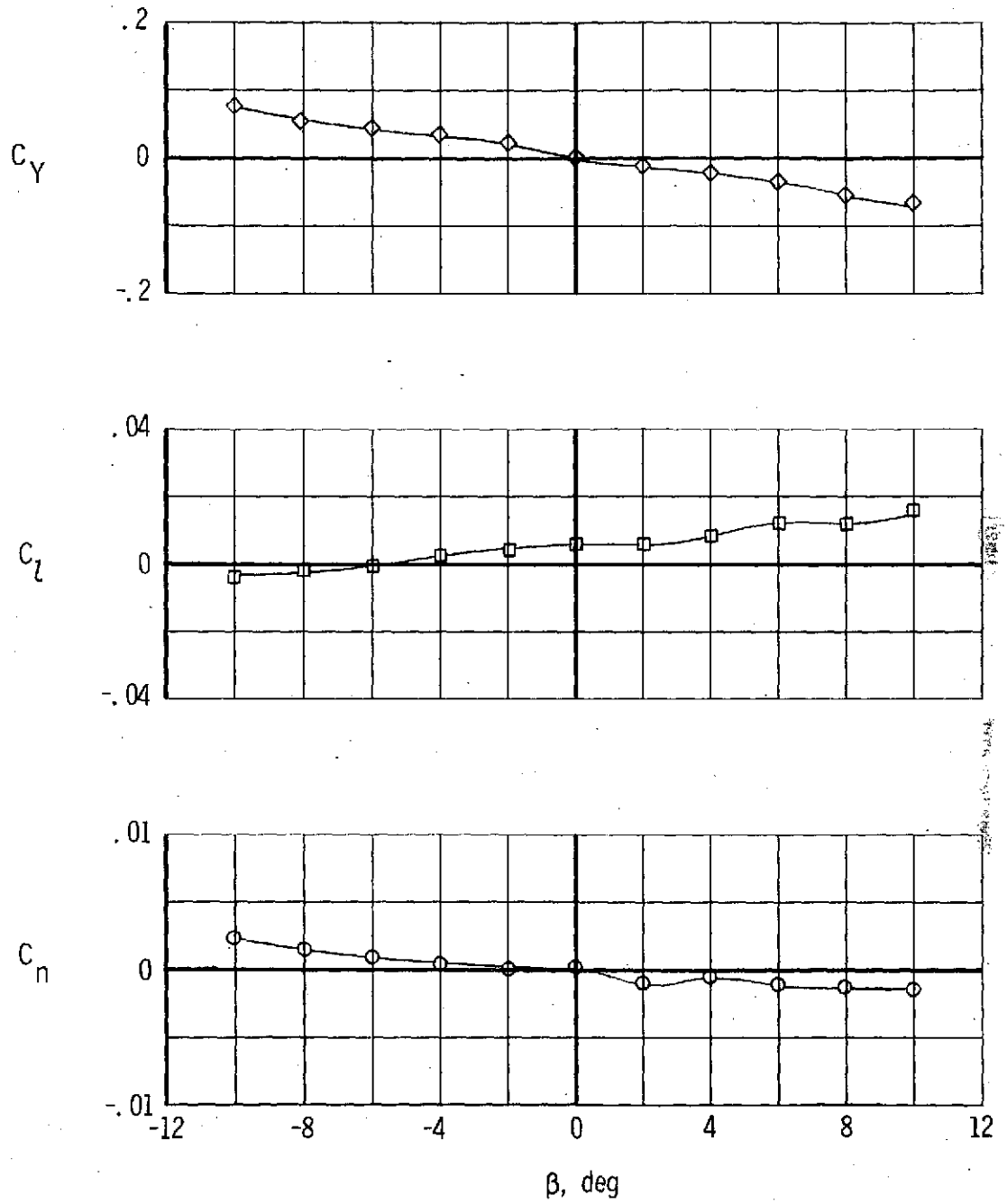

Figure 14.- Variation of side force and rolling and yawing moments with sideslip angle for $BH_1V_1E_RC_P$. $\alpha = 0^o$.

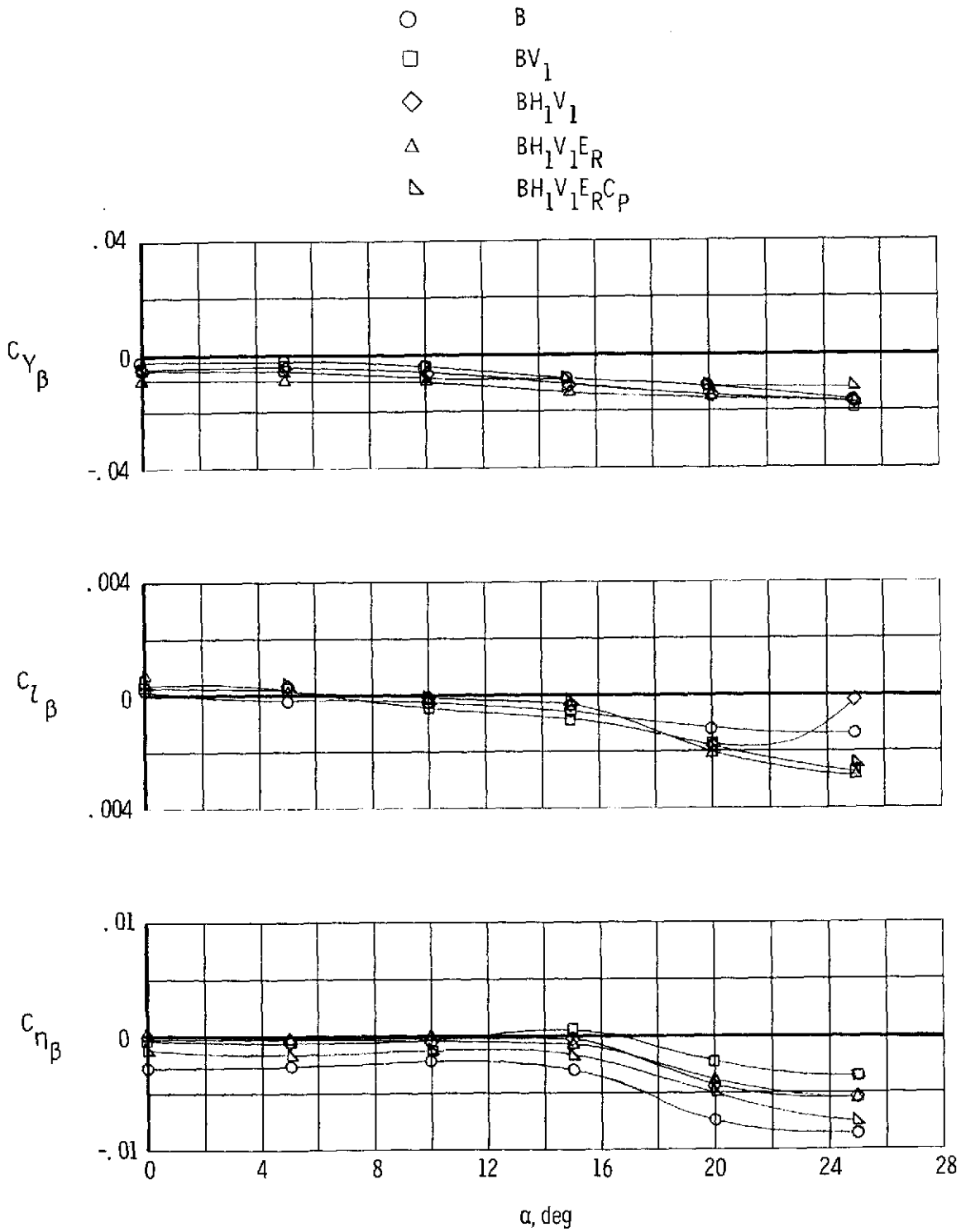

Figure 15.- Lateral and directional stability of the body alone and the body with small vertical and horizontal tails, retracted engine, and canopy.

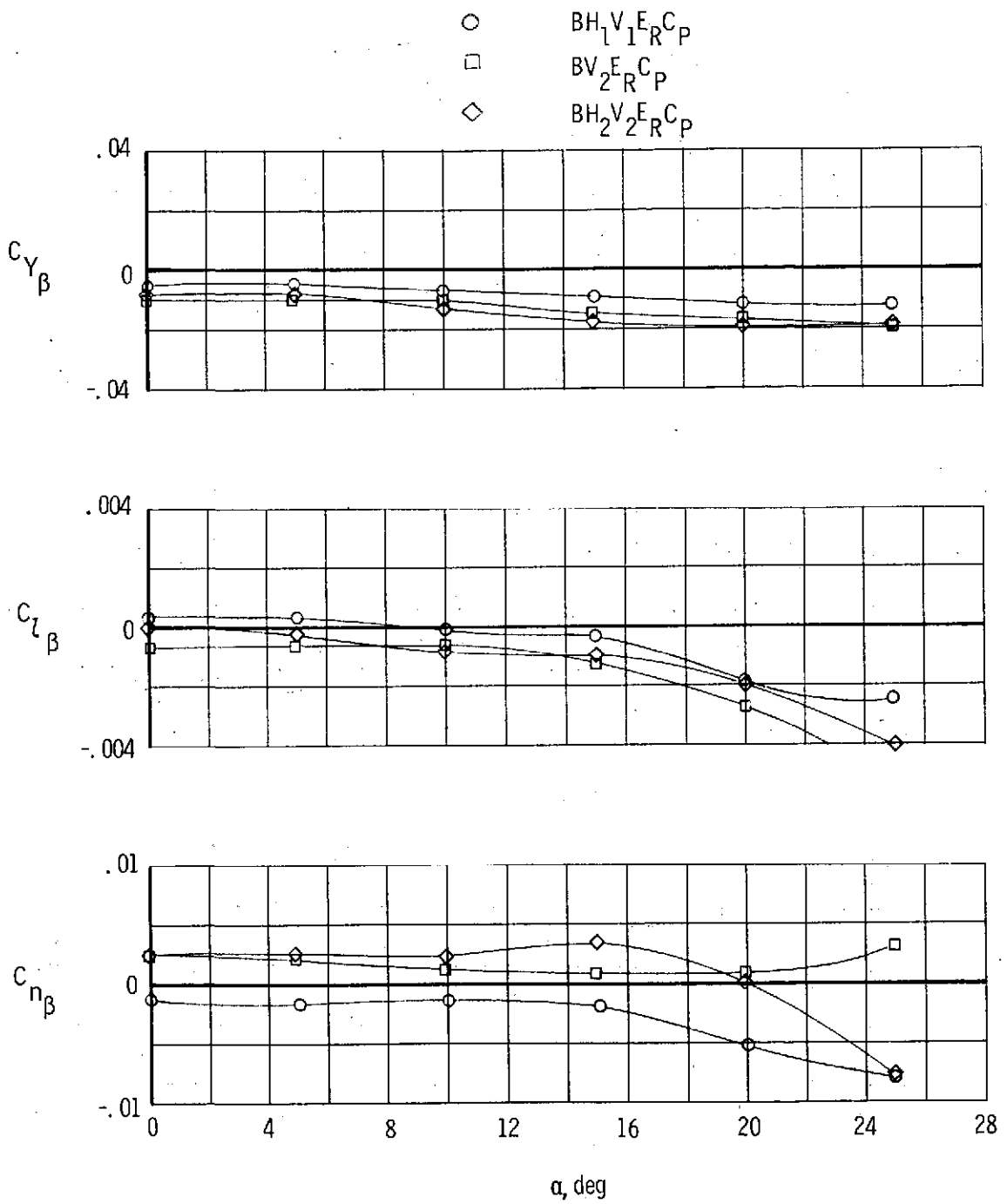

Figure 16.- A comparison of the lateral and directional stability of the model with small and large vertical tails. $\delta_H = 0^o$.

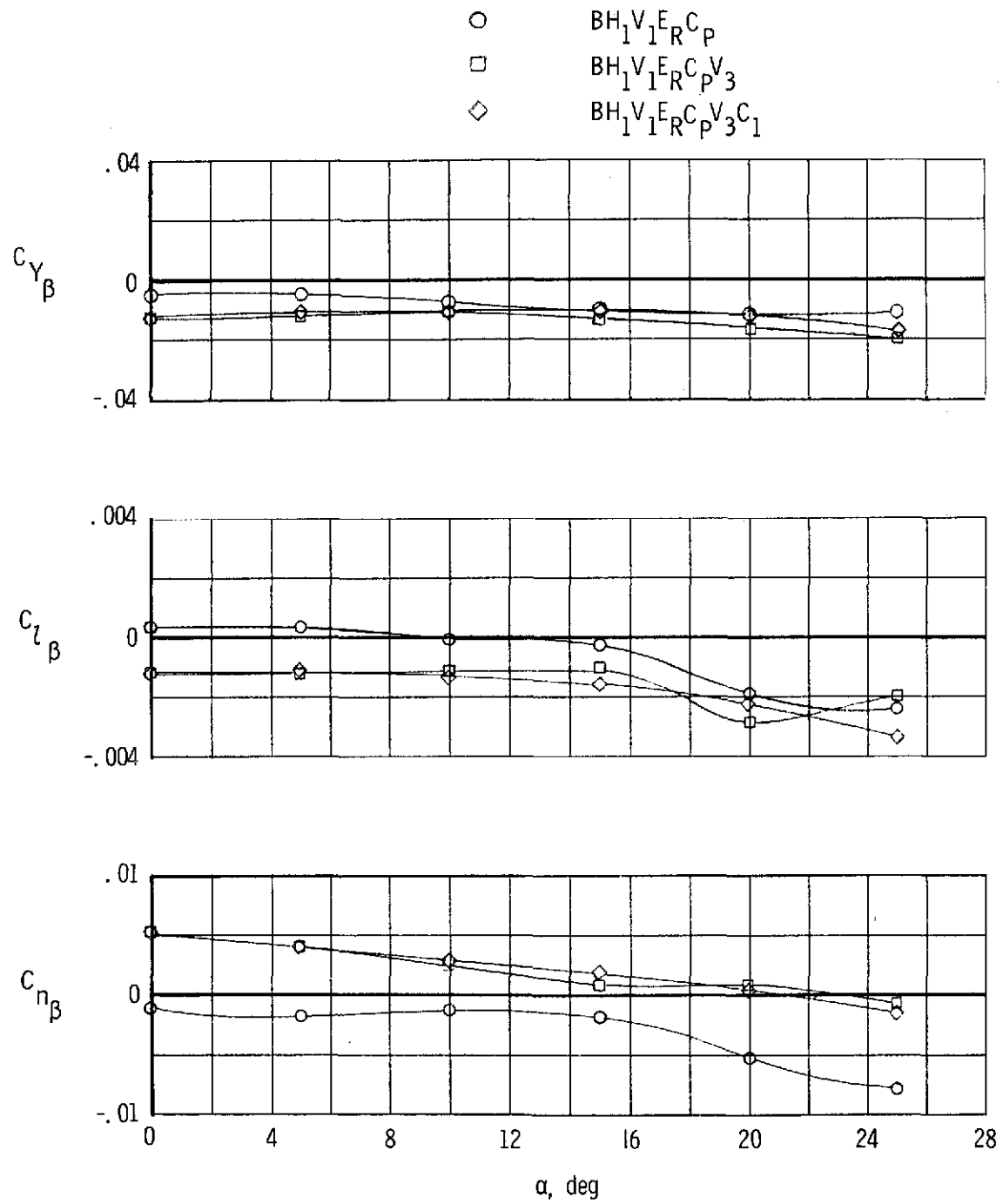

Figure 17.- Effect on lateral and directional stability of addition of a center vertical tail and canards to the basic complete configuration. $\delta_H = 0^o$.

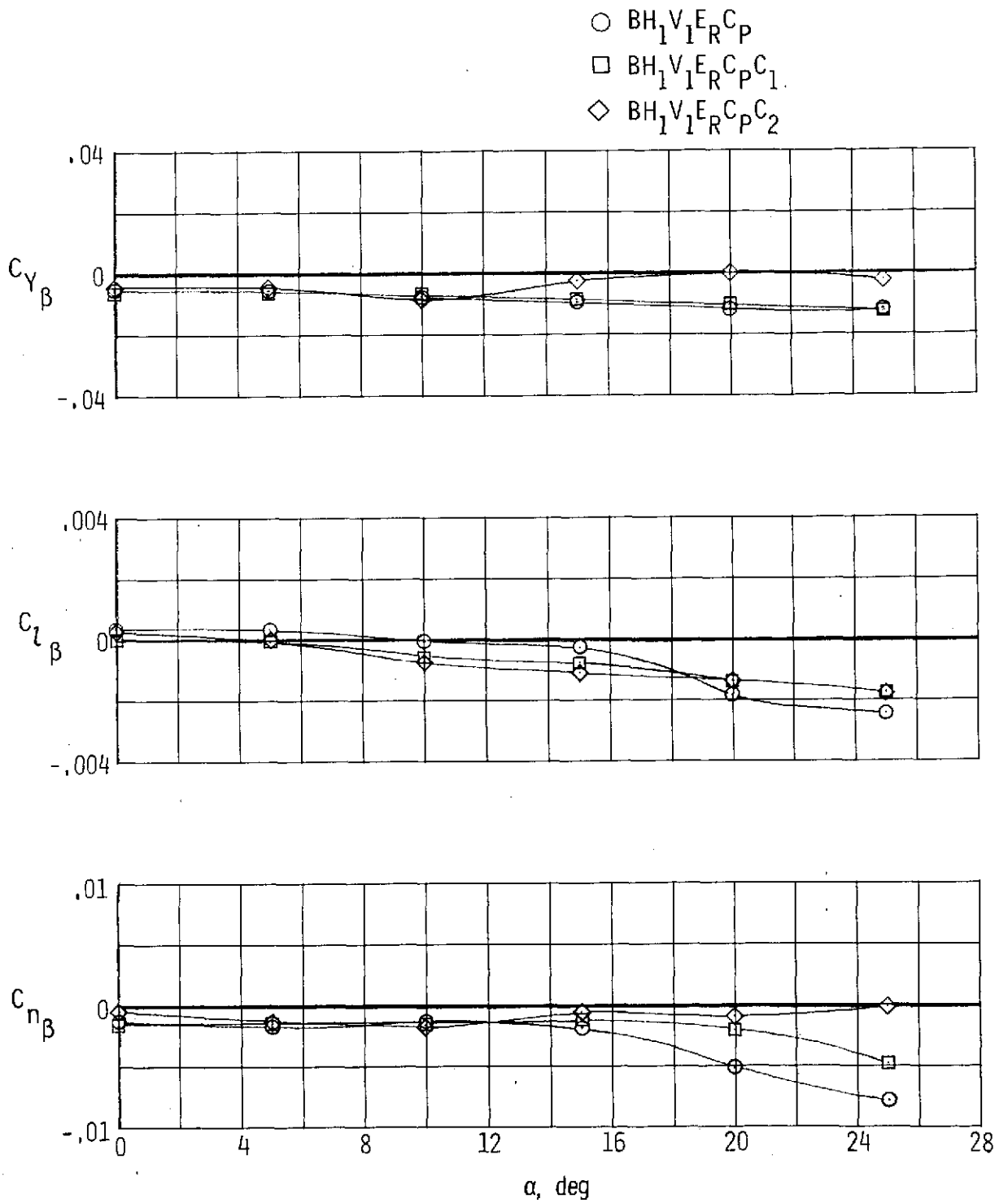

Figure 18.- Effect on lateral and directional stability of the basic configuration with the addition of small trapezoidal and delta canards. $\delta_H = \delta_C = 0^o$.

$$\frac{\text{Longitudinal aerodynamic center}}{l} = \frac{x_{cg}}{l} - \frac{\partial C_m}{\partial C_L}, \quad \alpha = 0°$$

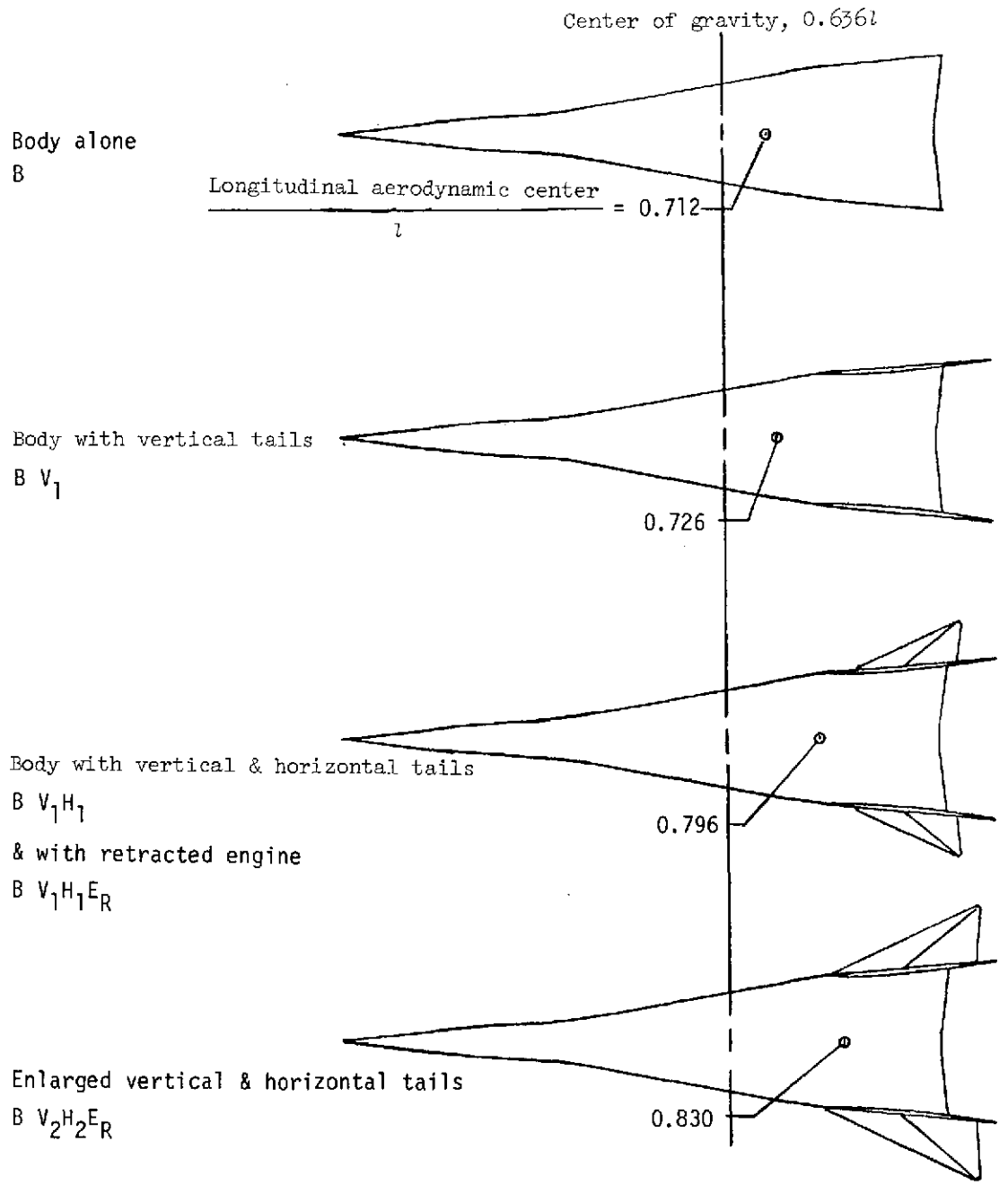

Figure 19.- Summary of longitudinal aerodynamic-center location for configuration buildup.

$$\frac{\text{Directional aerodynamic center}}{l} = \frac{x_{cg}}{l} - \left(\frac{\partial C_n}{\partial C_Y}\frac{b}{l}\right), \quad \alpha = 0°$$

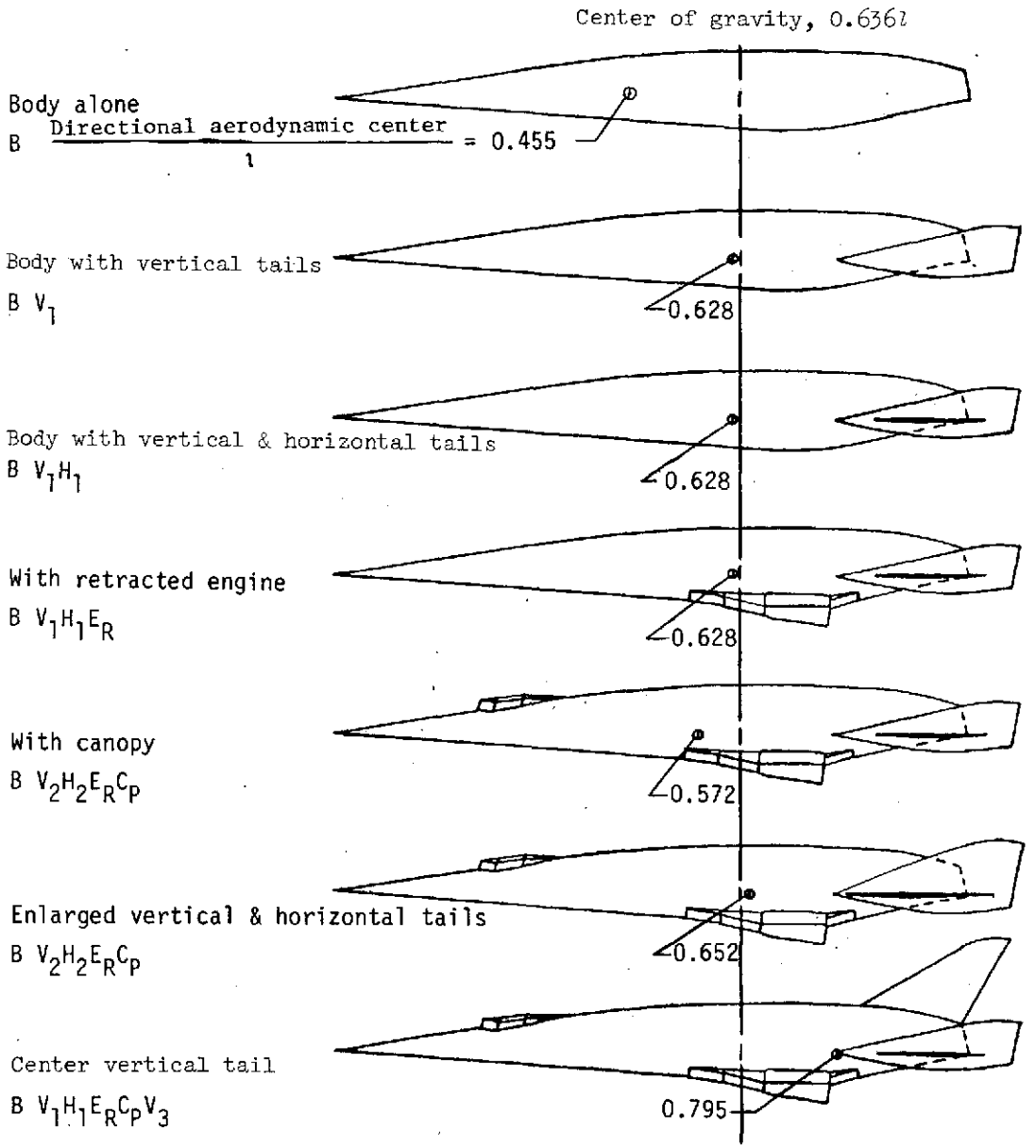

Figure 20.- Summary of directional aerodynamic-center location for configuration buildup.

N75-15611

ERRATA

NASA Technical Note D-7851

LOW-SPEED AERODYNAMIC CHARACTERISTICS OF A LIFTING-BODY HYPERSONIC RESEARCH AIRCRAFT CONFIGURATION

By Jim A. Penland and Theodore R. Creel, Jr.

February 1975

Page 17: Replace figure 2(a) with the attached figure 2(a).

Issued September 1975

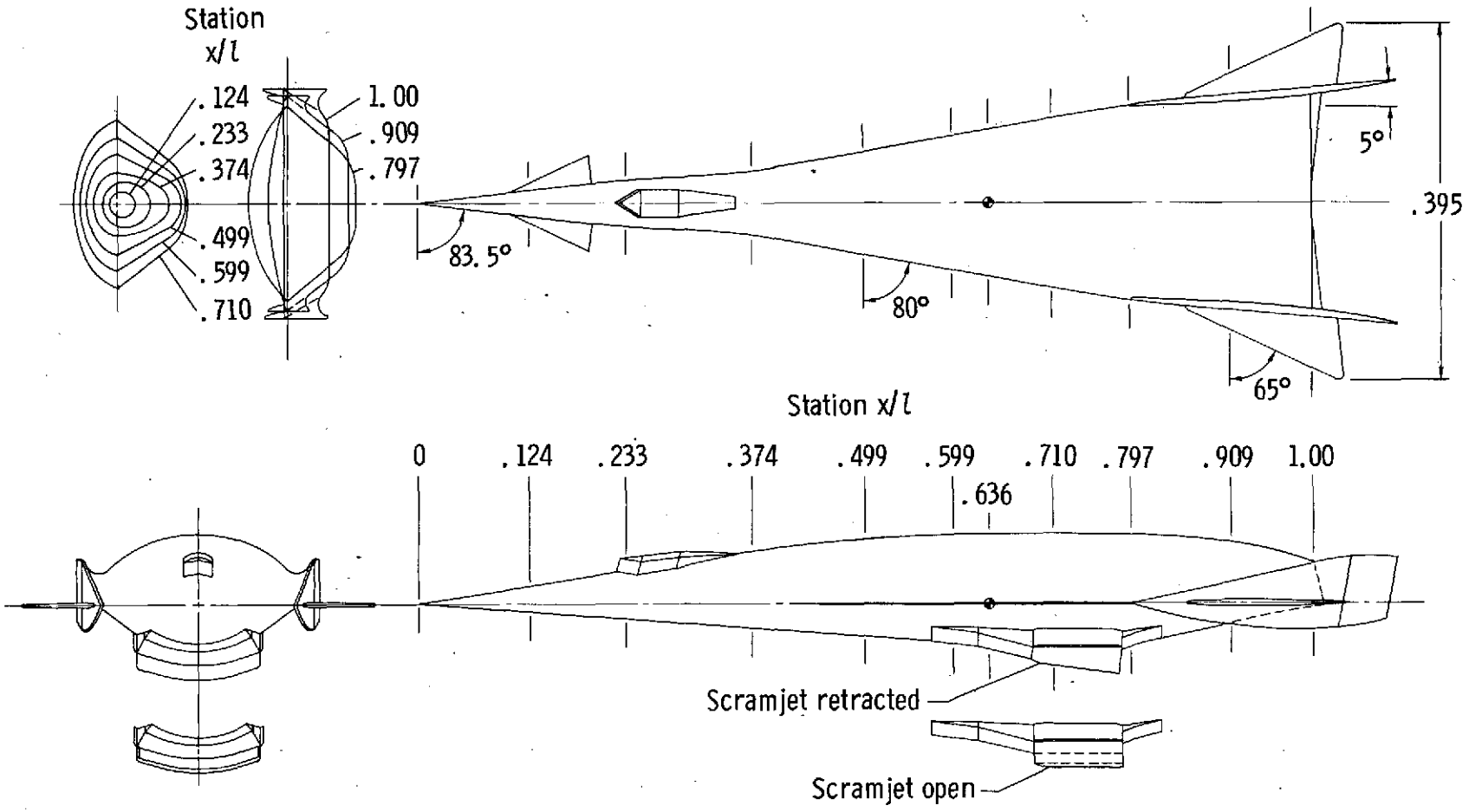

(a) Complete model.

Figure 2.- Details of wind-tunnel model. All dimensions are normalized by the fuselage length l.